Environmental sensitivities of coupled biogeochemical cycles in anoxic conditions: from soil batch experiments to a bioenergetics approach

by

Heather Rose Townsend

A thesis

presented to the University of Waterloo

in fulfilment of the

thesis requirement for the degree of

Master of Science

in

Earth Sciences (Water)

Waterloo, Ontario, Canada, 2021

Author's Declaration

This thesis consists of material all of which I authored or co-authored: see Statement of Contributions included in the thesis. This is a true copy of the thesis, including any required final revisions, as accepted by my examiners.

I understand that my thesis may be made electronically available to the public.

Statement of contributions

I am the sole author for Chapters 1, 3 and 4 of this thesis. Research contained within these chapters was conducted with supervision from Dr. Fereidoun Rezanezhad and Dr. Philippe Van Cappellen.

The second chapter of this thesis consists of a co-authored manuscript-format paper written for publication. As the first author, I was primarily responsible for conceptualizing and building the experimental design, executing the experimental methods, and drafting the manuscript. The manuscript presented in this chapter was written by me and has subsequently been reviewed by my co-authors. Additional contributions to the manuscript are as follows:

The experiment was designed by me with insight from Fereidoun Rezanezhad, Christina Smeaton, and Philippe Van Cappellen. All laboratory work was conducted by me with assistance from Stephanie Slowinski (Research Biogeochemist in the Ecohydrology Research Group) for gas, water and soil sampling and Marianne VanderGriendt (Research Technician in the Ecohydrology Research Group) for geochemical analyses. During the COVID-19 pandemic, while I was unable to work in the lab, Shuhuan Li conducted Scanning Electron Microscopy for solid soil samples. Applications of the energetics model was completed by myself with assistance from Stephanie Slowinski and Christina Smeaton.

Abstract

The ongoing displacement of climate zones has aggravated warming effects at regions from mid- to high-latitudes, affecting terrestrial organic carbon (C) stores. Amplified effects of warming occurring through the winter season within these regions are anticipated to alter physical and biogeochemical soil processes, thereby influencing greenhouse gas (GHG) emissions as well as dissolved organic carbon and nutrient concentrations during thaw events. Fluxes of GHGs, namely carbon dioxide (CO_2), methane (CH_4), and nitrous oxide (N_2O), and dissolved porewater species, are derivative of the energetic needs of the microorganisms who facilitate their production and consumption. Changes in the thermodynamic favourability of microbial reactions may vary seasonally and regionally with temperature and chemical energy availability (*e.g.*, reactant availability, pH), influencing the biogeochemical transformation of nutrients, associated products, and the rates of redox reactions. This thesis presents experimental and theoretical results that provide insight into the geomicrobial reaction network present in mid- and high-latitude ice-covered soils during the winter as well as environmental and thermodynamic controls the reactions.

In this thesis, Chapter 1 discusses how land-use management changes may influence anaerobic redox reactions mediated by microorganisms under warming climate conditions exacerbated during the winter season. The role of soils in a warmer world and land-use management changes are discussed under a bioenergetics lens regarding climate feedback (*e.g.*, GHG emissions) and changes to water quality for microbially mediated reactions. Specifically, the unique (hydro)biogeochemical environment of climate-vulnerable northern wetlands is examined with changes to soil-freezing processes. In Chapter 2, the effects of chemical energy availability on anaerobic biogeochemical cycles are explored using a factorial design sacrificial-batch experiment

that simulates the closed, low-temperature (non-frozen) winter subsurface environment. To simulate chemical fertilizer additions and the chemical effects of increasing freeze-thaw cycles, soil samples were amended with variable combinations of excess nitrate (NO_3^-), sulfate (SO_4^{2-}), and glucose ($C_6H_{12}O_6$). During the 50-day incubation period, temporal concentrations of headspace CO_2, N_2O, and CH_4 were measured in addition to changes in the porewater pH and concentrations of e^- acceptors and donors (*e.g.*, NO_3^-, SO_4^{2-}, ammonium, and acetate). Stable acetate concentrations were achieved after ~21 days of incubation producing peak CH_4 concentrations, which quickly diminished via oxidative consumption to CO_2. Anaerobic oxidation of methane and ammonium (AOM and anammox, respectively) reactions coincided with a significant increase in porewater pH and increasing concentrations of NO_3^- and nitrite (NO_2^-). Thermodynamic calculations combined with solid-phase data reveal a syntrophic relationship between dissimilatory denitrification, anammox, and AOM driven by manganese (Mn) oxides. The proposed reaction network renews the terminal electron acceptors (TEAs) iron (II), and SO_4^{2-} by NO_3^- produced in anammox. Thermodynamic calculations support these results for anammox and AOM reactions, which are more favourable under acidic and low-temperature conditions. These results highlight the importance of the duration of anoxia to biogeochemical soil cycles and the observed syntrophic relationship between C and N under close conditions, which may limit CH_4, reducing CO_2 emissions via autotrophy, and consume dissolved NO_3^-.

In Chapter 3, CH_4 was examined as a reducing agent under anoxic conditions and the rates of AOM in various freshwater and marine environments. Previously published rates of AOM were reviewed and utilized a bioenergetic approach to develop a linear free energy relationship capable of estimating anaerobic CH_4 consumption rates using different TEAs at variable temperatures. Then, the importance of climate-sensitive environmental parameters such as pH, temperature, and

salinity on microbial kinetics were explored. The bioenergetics informed framework for AOM rates presented therein is constructed using thermodynamic and kinetic factors, including an optimized temperature dependant kinetic factor, which relates the reaction rate to the microbial community's ideal temperature range, and normalizes the maximum estimated rates. The framework is used to derive the maximum rate constants for AOM by normalizing the observed rates by the kinetic and thermodynamic factors, which are related to the standard Gibbs energies of reaction to derive a linear free energy relationship. The review of published AOM rates highlights the ongoing knowledge gaps regarding AOM that should be addressed in future studies, including the role of Mn as an e^- acceptor during AOM and the understudied environments where AOM is likely occurring under unique environmental constraints: soda lakes, permafrost regions, and coastal wetlands impacted by sea-level rise. This framework emphasizes the critical link between the anaerobic C and N cycles via the syntrophic coupling of anammox and AOM and emphasizes that AOM rates are constrained by the energy of the electron acceptor, and thus that thermodynamics does influence kinetics. Despite the more considerable energy constraints of AOM, CH_4 oxidation in anoxic environments is possible, and the framework developed within this chapter can be used to predict AOM rates as a function of the TEA used (*e.g.*, temperature, pH, and CH_4 concentration). The framework can be extended in the future to account for the effects of salinity and toxicity. Observation of low AOM rates with NO_2^- amendments emphasize the critical link between anaerobic C and N cycles, utilizing low concentrations of NO_2^- derived from NO_3^- reduction or anammox for CH_4 consumption.

Overall, this thesis highlights the importance of inorganic e^- donors within the environment as well as the presence of Mn-oxides and their importance to syntrophic reaction networks under changing environmental conditions. Climate change sensitive parameters, pH and temperature,

were shown to have a strong influence over the energetic yield and reaction favourability for AOM and anammox, influencing the reaction rate in addition to its occurrence. Hence, in order to accurately monitor the influence of climate change and land-use management on GHG emissions and climate feedbacks, rates of AOM must be accounted for across diverse environments with variable chemical energy limitations (*e.g.*, TEA availability).

Acknowledgements

Foremost, I would like to thank my supervisors, Fereidoun Rezanezhad and Philippe Van Cappellen, who welcomed me into the Ecohydrology Group. I am deeply grateful for the countless invaluable experiences that have shaped my research and interests over the last four years. Thank you, Fereidoun, for the unlimited support and compassion you have given me since my undergraduate days. Philippe, thank you for your guidance and passion for science, providing me with energy above the maintenance level, and reminding me that research is like wine – better with time.

Thank you to my co-authors Stephanie Slowinski, Christina Smeaton, Kara Webster, and Chris Parsons, whose remote insights into biogeochemistry consistently answered my questions and shaped my research. Thank you, Steph, for your endless enthusiasm for bioenergetics as well as your assistance in the lab, which helped shape my research and graduate student experience. Many thanks to Christina for providing me with new ideas whenever I got stuck, stimulating discussions, pictures of ducks, and being an excellent role model for women in science. Thank you, Kara, for your assistance in the field and insights into the Turkey Lakes Watershed, without which my Master's research would not be the same. Chris, thank you for the breadth of knowledge and laughter you have brought me, in addition to your expertise in collecting solid phase data.

Thank my committee members and co-authors, Merrin Macrae and Scott Smith, for their support and invaluable guidance they have provided me. Additionally, thank you, Thai Phan, for joining my committee without hesitation.

I am deeply grateful to Marianne VanderGriendt, whose expertise and support in the lab provided me with the tools to succeed. Shuhuan Li, thank you for your assistance and perseverance

to continue assisting me in the lab throughout COVID-19. Thank you to former co-op students Carly Kemp and Alison Mao, without whom I could not undertake a rigorous experimental design.

I am unable to thank all the Ecohydrology Research Group members I have encountered over the past four years. Your thoughtful advice, assistance, and questions at group meetings and insightful research discussions have motivated me and providing me with research tools. Thank you, Bhaleka, Tatjana, Kunfu, Igor, Saru, Bijen, Bingjie, and Mehdi, for always making time to discuss my results and teach me something new. Thank you to my fellow graduate students and co-op students for innumerable impactful conversations and laughter shared. Thank you, Grant for your assistance with my genomics data, and Tyler for introducing me to the R interface of PHREEQC.

Many thanks to my close friends Linden, Tamara, Steph, Nady, and Konrad for providing me with some of the brightest moments of my graduate degree. Thank you for sharing in highs and lows with me, for some deep-ish conversations, and many bad puns. Your edits, support, and insights into my thesis writing have been invaluable to me.

I am deeply thankful to my siblings, Catherine, Liz, and Stephen, for their encouragement and a welcome distraction. Thank you, James, who believed in me and helped me find joy during my most challenging days. Lastly, thank you to my parents, Margaret and Bill, who've fostered my curiosity, seen me through every success and failure, and supported me in everything I do.

Table of Contents

List of Figures

List of Tables

List of Abbreviations

Anammox	Anaerobic oxidation of ammonium
AOM	Anaerobic oxidation of methane
ASV	Amplified sequence variant
ATP	Adenosine triphosphate
ADP	Adenosine diphosphate
C	Carbon
CEC	Cation exchange capacity
$C_2H_3O_2^-$	Acetate
$C_6H_{12}O_6$	Glucose
CH_4	Methane
CO_2	Carbon dioxide
DIC	Dissolved inorganic carbon
DNRA	Dissimilatory nitrate reduction to ammonia
DOC	Dissolved organic carbon
DOM	Dissolved organic matter
e^-	Electron
FWL	Freshwater lake

FWS	Freshwater sediment
Fe	Iron
Fe^{3+}	Ferric iron
Fe^{2+}	Ferrous iron
$Fe(OH)_3$	Goethite
GHG	Greenhouse gas
H_2	Dihydrogen gas
IPCC	International Panel on Climate Change
LFER	Linear free energy relationship
M	Marine
Mn	Manganese
Mn^{4+}	Manganese (IV)
Mn^{2+}	Manganese (II)
MnO_2	Pyrolusite
N	Nitrogen
NGS	Non-growing season
NH_4^+	Ammonium
NO_3^-	Nitrate

NO_2^-	Nitrite
N_2	Dinitrogen gas
N_2O	Nitrous oxide
NOM	Natural organic matter
O_2	Oxygen
PCR	Polymerase chain reaction
SL	Soda Lake
S	Sulfur
SO_4^{2-}	Sulfate
H_2S	Dihydrogen sulfide
SOC	Soil organic carbon
SOM	Soil organic matter
SON	Soil organic nitrogen
TEA	Terminal electron acceptor
TLW	Turkey Lakes Watershed
TN	Total Nitrogen
W	Wetland

List of Symbols

$C_{i,t}$	The concentration of compound *i* at time (*t*)	[mol L^{-1}]
f_{Temp}	Temperature correction function	[-]
F	Faraday's constant	[J V^{-1} mol^{-1} e^{-}]
F_K	Kinetic limitation factor	[-]
F_T	Thermodynamic limitation factor	[-]
k_{eff}	Effective thermal conductivity	[W m^{-1} K^{-1}]
$K_{H_{298}}$	Equilibrium constant at 25˚C and 1 bar	[mol L^{-1} atm^{-1}]
$K_{H_{obs}}$	Equilibrium constant at observation temperature	[mol L^{-1} atm^{-1}]
K_S^{ED}	Electron donor half-saturation constant	[mol L^{-1}]
K_S^{EA}	Electron donor half-saturation constant	[mol L^{-1}]
$K_S^{CH_4}$	Methane half-saturation constant	[mol L^{-1}]
$K_{S_{FW}}^{CH_4}$	Methane half-saturation constant in freshwater environments	[mol L^{-1}]
$K_{S_M}^{CH_4}$	Methane half-saturation constant in marine environments	[mol L^{-1}]
n	Molar ratio	[mol]
q	Heat flow	[W m^{-2}]

R	Gas constant	[J K^{-1} mol^{-1}] or [L atm K^{-1} mol^{-1}]
r	Substrate utilization rate	[mol L^{-1} s^{-1}]
$\bar{r}_{max}$	Maximum substrate utilization rate	[mol mol–C^{-1} s^{-1}]
T	Temperature	[K]
T_{max}	A microbial community's maximum temperature for growth	[˚C]
T_{min}	A microbial community's minimum temperature for growth	[˚C]
T_{opt}	A microbial community's optimum temperature for growth	[˚C]
T_{obs}	Temperature of observation	[˚C]
t	Time	[days]
X	Biomass concentration	[mol–C L^{-1}]
z	Depth	[m]
[ED]	Electron donor concentration	[mol L^{-1}]
[EA]	Electron acceptor concentration	[mol L^{-1}]
$\Delta G^{\circ}_{f,products}$	Standard state Gibbs energy of formation of a product	[J mol^{-1}]

$\Delta G^{\circ}_{f,reactants}$	Standard state Gibbs energy of formation of a reactant	[J mol^{-1}]
$\Delta G^{\circ}_{r_{298}}$	Standard state Gibbs energy of reaction at 25˚C and 1 bar	[J mol^{-1}]
ΔG°_{rT}	Standard state Gibbs energy of reaction at a specified temperature	[J mol^{-1}]
$\Delta G^{\circ}_{r_{opt}}$	Standard state Gibbs energy of the catabolic reaction at optimum temperature	[J mol^{-1}]
ΔG_r	Gibbs energy of the catabolic reaction	[J mol^{-1}]
ΔH°_{r298}	Standard state Enthalpy of reaction at 25˚C and 1 bar	[J mol^{-1}]
μ_{max}	A microbial communities maximum specific growth rate	[hr^{-1}]
$\Delta\Psi$	Membrane potential	[V]

1 Introduction

1.1 Climate Change in a Growing World

The ongoing displacement of climate zones has resulted in globally elevated air temperatures, leading to precipitation regime migration. The Intergovernmental Panel on Climate Change (IPCC) estimates global air temperatures to increase by 1.5˚C between 2030 and 2052. Their assessment of climate feedbacks attributes 0.8˚C to 1.2˚C of the increase above pre-industrial levels to anthropogenic activity (IPCC, 2014). The extent of global warming effects varies spatially across the globe and seasonally, particularly in the arctic and sub-arctic regions (Bintanja, 2018). High-latitude environments are particularly vulnerable to climate change with amplified temperature increases expected to occur during the winter (Cohen *et al*., 2014), jeopardizing relatively dormant carbon (C) stocks in perennially and annually frozen soils (Tarnocai, 2006; Natali *et al.*, 2019). Arctic amplification may result in a positive feedback cycle, furthering climate effects through increased C mineralization rates resulting in greenhouse gas (GHG) emissions (Tarnocai, 2009; Brooks *et al*., 2011).

The IPCC (2014) believes that carbon dioxide (CO_2) emissions are the largest climate change force alongside other GHGs. Soils represent the largest terrestrial reservoir of organic C on Earth and naturally contributes 75 Pg C per year (Schlesinger, 1977; Raich and Potter, 1995). Anthropogenic land use has directly contributed to increased CO_2 emissions, producing an additional 6.2 ± Gt CO_2-eq yr^{-1} from agriculture and 5.8 Gt CO_2-eq yr^{-1} from forestry and other land use (Jia *et al*., 2019). Increased mobilization of C from anthropogenic activity has degraded soil quality, altering the long-term steady-state capacity of soil organic carbon and nitrogen (SOC and SON, respectively) and decreasing agroecosystems' productivity for crop growth (Munoz *et al.*, 2010). Hence, the importance of sustainable agricultural practices in cold climate-vulnerable

regions is a pressing 21st-century issue. A balance between soil ecosystem services (*e.g.*, C sequestration) with agricultural activity is vital to global C and N biogeochemical cycles and climate warming.

1.1.1 Climate Change and Agricultural Expansion

By 2050, roughly 9.7 billion people will need food, requiring global food production to increase by 70% (Cole *et al*., 2018). As a result, the global fertilizer demand has risen, estimated to increase by roughly 9.6% over five years, reaching 201.66 million tonnes through to 2020 (FAO, 2017). Sustainable food production is a global problem; increases in fertilizer application to agroecosystems are linked to the eutrophication of surface waters, damaging downstream ecosystem health and endangering drinking water quality for human consumption (Davidson *et al.*, 2015). Designing agricultural best management practices to limit nutrient loads to freshwater systems has become a focal point in environmental research as 'soil health' continues to decline. In cold regions, agricultural soils have demonstrated their role as critical non-point sources of nutrients to freshwater bodies, governing water flow and quality within agricultural catchments, as discussed by Liu *et al.* (2019).

Amplified climate change effects are expected to occur at mid and high latitudes, particularly during the winter or non-growing season (Screen, 2014). Predicted shifts in precipitation patterns during the fall and early winter seasons may decrease the snow-covered season up to 30 days (Wuebbles *et al.*, 2010; Byun *et al.*, 2018), potentially extending the growing season's duration. Additionally, elevated temperatures may facilitate the expansion of agriculture into traditionally colder climates, furthering positive climate change effects in the agricultural sector. King *et al.* (2018) estimated 76% of the boreal region would reach temperatures capable of supporting crop

growth by 2099. A northward shift in agriculture, and associated nutrient inputs, may alter soil biogeochemical processes. In a pristine or nutrient-limited environment, such as wetlands, chemical energy availability changes could have significant cascading effects to water quality and greenhouse gas emissions. Hence, increases in chemical energy (*e.g.*, from anthropogenic fertilizer input) in climate-vulnerable seasonally snow-covered regions may perturb the natural C and N cycles with ramifications to C stores, GHG emissions, and water quality.

1.1.2 Climate Change and Wetlands

Northern peatlands in boreal and subarctic environments represent less than 3% (~4 million km^2) of Earth's terrestrial surface (Rydin and Jeglum, 2006; Yu *et al*., 2010); however, they hold 455-600 Gt C, or roughly 30% of the world's terrestrial C (Gorham, 1991; Yu *et al.*, 2010; Yu, 2011). In Canada, peatlands cover approximately 12% of land area (1.1 million km^2 landmass), holding 56% of the country's terrestrial organic C (Tarnocai *et al*., 2011). Effects of climate change, particularly winter warming, are of great importance to cold region peatland soils, holding 147 Gt of SOC in Canada (Tarnocai, 2006). 37% of Canadian peatland currently experience perennial freezing and are the most vulnerable to climate action (Tarnocai, 2009). As temperatures rise in Canada's boreal region to levels suitable for crop growth and soil health declines (Figure 1.1), the conversion of organic-rich peatlands into agricultural fields to achieve food security becomes more attractive (King *et al*., 2018), potentially compromising C stores (Chapman *et al*., 2003).

The drainage of peatlands for agriculture results in altered hydrophysical properties (Liu *et al*., 2020), closely linked to biogeochemical cycles in peatlands (Rezanezhad *et al*., 2016). Shifts in microbial activity resultant of peatland drainage are estimated to contribute ~6% of anthropogenic

CO_2 per year (Joosten *et al.*, 2012), jeopardizing peatlands as a CO_2 sink. Under natural conditions, low temperatures and reduced oxygen (O_2) concentrations limit soil organic matter (SOM) degradation in northern peatlands and create an ideal C- assimilating setting. Peatlands are estimated to accumulate C at a rate of 76 Tg C per year (Gorham, 1991). However, these natural conditions promote methane (CH_4) production, a potent GHG with a global warming potential 25 times greater than that of CO_2 on a centennial-scale (Forster *et al.*, 2007). Peatlands and wetlands are the largest single source of CH_4 to the atmosphere, contributing an average of 164 Tg CH_4 each year (Bridgham *et al.*, 2013). Intuitively, small fluctuations in natural wetland physical or biogeochemical processes may have significant long-term global consequences and climate feedbacks.

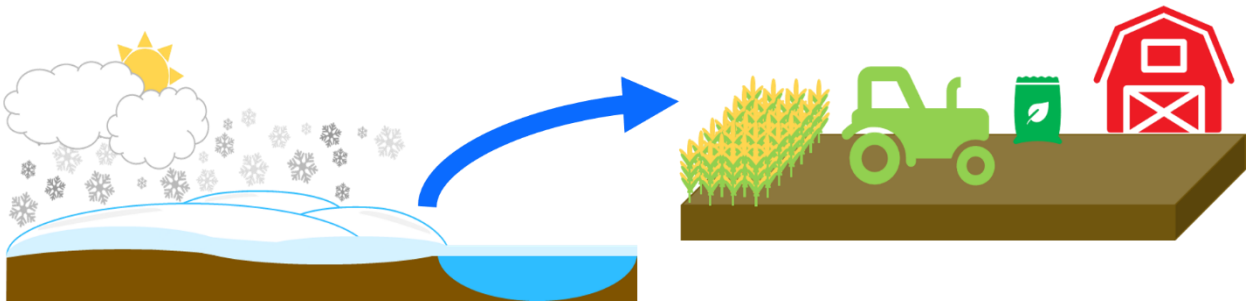

Figure 1.1: Climate change is expected to result in air temperatures suitable for crop growth in the boreal region. As a result, wetland soils may be converted to agricultural landscapes altering soil hydrobiogeochemistry.

Under anaerobic conditions, CH_4 is produced by microbes (methanogens) that yield energy through methanogenesis. Traditionally, the consumption of terminal electron acceptors (TEAs) occurs in order of energy yield, where the most potent oxidants are consumed in sequential order, beginning with nitrate (NO_3^-) in the absence of O_2. Peatlands are typically considered nutrient and metal-poor, a characteristic which quickly advances them to methanogenesis in the absence of O_2. Hence, nutrient-poor peatlands' conversion to agroecosystems introduces an additional layer of uncertainty in future climate scenarios wherein fertilizer application to a nutrient-poor ecosystem

may significantly shift microbial metabolism. In turn, microbial metabolic shifts may alter GHG emissions, damage water quality, and cascade to other biogeochemical cycles. Additions of nitrogen to peat in saturated systems may result in increased rates of denitrification during periods of anoxia, causing soils to produce larger quantities of nitrous oxide (N_2O) than CH_4, as observed in a two year *in situ* study conducted by Luan *et al*. (2019) in Newfoundland, Canada. N_2O is a long-lived GHG with a global warming potential 298 times higher than CO_2 over one hundred years (Forster *et al*., 2007). Indirect and direct emissions stemming from agricultural N are estimated to have contributed 52% to total anthropogenic emissions between 2007 and 2016 (Tian *et al*., 2020). Since N_2O is a significantly more potent and long-lived GHG, it is crucial to understand how peatland conversion may alter biogeochemical cycles in peatlands under future climate scenarios for sustainability, the effects of which may be heightened through on-going climate change.

1.1.3 Climate Change and Winter Soil Processes

Climate projections suggest intensified warming effects during the winter season of cold regions (Screen, 2014). For example, in Canada's eastern Boreal Shield ecozone, winter minima air temperatures are predicted to increase by 4 to 7˚C by 2100 (Price *et al*., 2011). Associated increases in temperature will alter the precipitation ratio, thereby decreasing the spatial and temporal distribution of seasonal snow cover (Hayhoe *et al*., 2007). Projected shifts in precipitation regimes may reduce insulating snowpack volume, expose soils to colder temperatures in turn, and affect seasonal freezing (Hayashi, 2013). Changes in snow-cover conditions may affect the porewaters present beneath the Earth's surface with cascading effects to biogeochemical processes and nearby reservoirs (Jonasson *et al*., 1999; Grogan *et al*., 2004; Henry, 2007; Matzner and

Borken, 2008; Joseph and Henry, 2008; Hayashi, 2013; Kurylyk *et al.*, 2014). Therefore, the presence of snow can significantly impact the nature of C and nutrient cycling during the fall, winter, and spring (*e.g.*, non-growing season; NGS) through soil freezing.

More than half of all surficial soils in the northern Hemisphere experience seasonal freezing each year, implicating their hydrological and biogeochemical functions (Hayashi, 2013). Hence, small perturbations in snow cover and soil freezing may produce long-term and widespread effects on global C and N biogeochemical cycles.

1.2 Winter Wetland Hydro(bio)geochemistry

1.2.1 Importance of Snow-cover

The presence of snow- and ice cover on the surface of wetlands exerts an essential control over soil hydrology, which is closely linked to wetland biogeochemistry. Water storage in snow and ice limits precipitation inputs to the subsurface until thaw events occur (Ireson *et al.*, 2013). Hence, snowmelt events are arguably the most critical hydrologic events to occur in seasonally snow-covered landscapes, representing an extensive water input that may infiltrate into the vadose zone or create an over-land flow to neighbouring surface water. Subsequent spring melt events may then rapidly export solutes and products of over-winter chemical reactions in the porewater to the adjacent ground- or surface water reservoirs. In turn, winter soil biogeochemical processes may dominate the speciation of dissolved C and N exported during snowmelt, impacting cold region water quality (Creed *et al*., 1996; Heuer *et al.*, 1999; Finlay *et al*., 2006).

In ombrotrophic or isolated wetland settings, soils experience limited groundwater exchange and gain water inputs primarily through precipitation (Winter, 2000). The presence of snow throughout the winter can prolong static hydrologic conditions in these systems by delaying

precipitation inputs within the snowpack until melt events occur. As a result, build-ups of chemical end-products produced from over-winter nutrient transformations can occur, increasing dissolved species concentrations, such as mercury and dissolved organic carbon (DOC) (Schelker *et al.*, 2011). Ombrotrophic wetlands' dependency toward precipitation as their input increases their vulnerability to climatic changes in total precipitation and the precipitation ratio (Winter, 2000).

Snow represents a vital control on overwinter soil processes through a combination of its optical, chemical, and physical properties. During the winter, the accumulated snowpack separates the soil from the atmosphere, which creates a barrier to soil-atmosphere interactions and influences the surface energy balance. The high albedo of snow (0.65 to 0.9) reflects incoming solar radiation away from the Earth's surface, forcing radiative and turbulent fluxes (sensible and latent) to interact at the surface of the snowpack rather than the underlying soil (Hayashi, 2013). Perovich (2007) observed that a 10 cm deep layer of snow could reduce visible light transmittance to less than 5% of incident irradiance and 5 cm of snow was sufficient to reach an albedo of 0.9. In turn, the presence of snow may suppress photosynthetic activity within the subsurface and decrease nutrient uptake by plants throughout the winter (Lee *et al.*, 2013).

The low thermal conductivity of snow further decouples winter soils from the atmosphere by insulating the underlying soil from low winter air temperatures (<0˚C). The flow of heat in one direction (*e.g.*, through the snow into the subsurface) can be described by adapting Fourier's equation:

$$\boldsymbol{q = -k_{eff}\frac{dT}{dz}} \tag{1.1}$$

where the flow of heat (q) [W m^{-2}] is dependant on the effective thermal conductivity (k_{eff}) [W m^{-1} K^{-1}] and temperature (T) gradient over a depth (z) [m] (Sturm *et al.*, 1997). Here, k_{eff} represents heat transport through the ice lattice, air-filled pore spaces, and latent heat, which can be affected

by the snowpack density; values typically range from 0.1 to 0.5 W m^{-1} K^{-1} (Sturm *et al.*, 1997). In non-permafrost regions, as little as 20 cm of snow cover can decouple air and soil temperatures (Hirota *et al*., 2006). Moore (1986) theorized that organic soil's high thermal diffusivity should increase frost depth without snow-cover. Hence, changes in the depth and duration of snow cover over the winter may influence soil temperature, altering soil freezing depth and time.

1.2.2 Soil Freezing

The loss of insulating snowpack throughout the winter by climate warming may alter soil freeze-thaw cycles' frequency and duration (Henry, 2007; Hayashi, 2013). However, the snowpack loss might also affect the depth and time of soil freezing over the winter months when air temperature remains below 0˚C for extended periods. Heat is carried throughout the subsurface by porewater, intertwining subsurface thermal and hydrologic regimes. In organic soils (*e.g.,* peat), with characteristically low bulk density and high porosity (Rezanezhad *et al*., 2016), thermal and hydrologic regimes vary significantly with soil moisture content (Nagare *et al.*, 2011). In soils with less connected pores or lower saturated hydraulic conductivity, the amount of time required for soil freezing will increase. As a result, in hetero- and anisotropic landscapes such as peatlands, the coupled transport of moisture and heat may vary significantly with physical properties influenced by the degree of decomposition (Rezanezhad *et al*., 2016). Younger organic soils located at the top of the soil profile and in contact with the atmosphere typically have a lower degree of degradation and contain larger, more conductive pores than older, deeper peats (Rezanezhad *et al*., 2016), which could enable soil freezing (Nagare *et al.*, 2011). *In situ* observations by Patel *et al.* (2018) indicated that snow removal and increased winter rain-on-soil events resulted in more concrete frost formation within the soil O-horizon. Some unfrozen water has been demonstrated

to persist within the frozen soil layer in small pores and around soil grains even at temperatures well below freezing (Eberling and Brandt, 2003; Brooks *et al.*, 2004; Oquist *et al.*, 2004, 2007, 2009).

As soil freezes, the liquid water content decreases, and water potential becomes more negative in a process similar to soil drying (Flerchinger *et al.*, 2006). The decrease in pressure induces a reversal in the water flow direction, forcing porewater to migrate towards the freezing front, further promoting ice lens formation (Peppin and Style, 2012). The total potential is a function of both matric and osmotic potential, which can be influenced by the SOM water holding capacity (Harryson Drotz *et al*., 2009). The matric and osmotic potentials, as well as grain size and rate of cooling, have been observed to influence the freezing point of soil (Kozlowski, 2009) and the thickness of the unfrozen film surrounding soil grains (Edwards and Cresser, 1992; Harryson Drotz *et al.*, 2009; Tian *et al.*, 2014). Under normal environmental conditions, the cooling rate is slow and dissolved species are rejected from the ice lattice formation, increasing impurities concentrations within the residual liquid phase (Rempel, 2012).

Unfrozen water can provide a habitat for microbes to continue C and N mineralization in the frozen layer at temperatures well below freezing (Eberling and Brandt, 2003; Brooks *et al.*, 2004; Oquist *et al.*, 2004, 2007, 2009). Observations of respiration in the frozen layer indicate that ice acts as a barrier to gas exchange during the winter, trapping biogenic GHG until thaw events (Eberling and Brandt, 2003). Nyameogo *et al.* (2018) developed a model exploring the diffusion coefficient of O_2 in variably saturated frozen soil. Model and experimental results indicated that freezing reduced O_2 diffusion rates, with more significant reductions in gas-diffusion occurring in soil with less air-filled pore space. The presence of ice in soil may therefore induce a seasonal redox gradient, where limited atmospheric exchange can result in O_2 depletion (Yanai *et al*., 2011),

shifting metabolic pathways and forming a 'closed system' in both the frozen layer as well as the underlying unfrozen soil (Figure 1.2).

Additionally, mechanical weathering of soils caused by the expansion of water through freezing may result in macropore networks forming within the subsurface, decreasing the transport time of solutes produced during the winter (Mohammed *et al*., 2018). These macropore networks may also facilitate the rapid expulsion of gas from deeper soil layers observed after snowmelt events, delivering increased fluxes of GHGs and decreasing soil's ability to hold gaseous C and N.

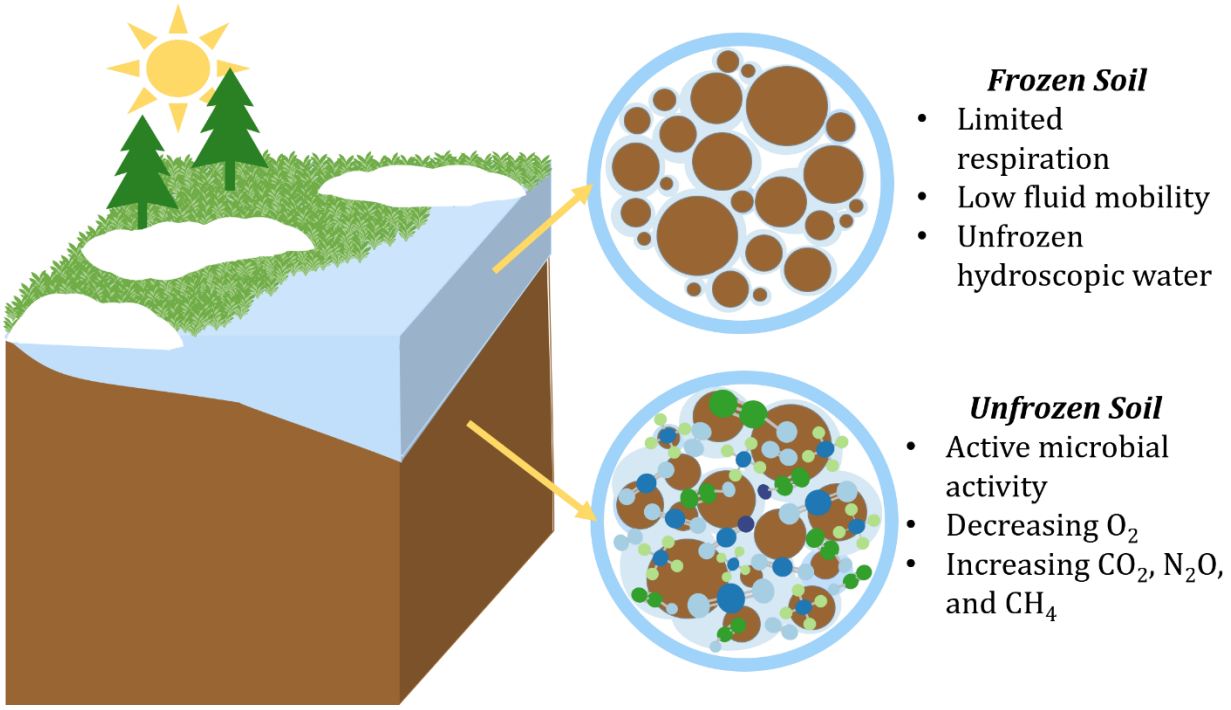

Figure 1.2: Schematic showing the presence of ice in the soil during the winter, which can induce seasonally cold and anoxic conditions, creating unique environments for soil microbes in both the frozen and underlying unfrozen layers.

1.3 Winter Soil Respiration

1.3.1 Soil Organic Matter Mineralization

Approximately 75 Pg C are reportedly released each year from terrestrial ecosystems globally as a natural by-product of SOM degradation through a process generally referred to as 'soil respiration' (Schlesinger, 1977; Raich and Potter, 1995). Here, progressively smaller molecules are generated from the hydrolysis and fermentation of complex polymers in SOM, resulting in short-chained organic acids (*e.g.*, acetate and lactate). The resultant DOC (generally denoted as CH_2O) is later oxidized to CO_2 by organisms who gain energy from the redox reaction as:

$$CH_2O + H_2O \rightarrow CO_2 + 4H^+ + 4e^- \quad (1.2)$$

There are a variety of metabolic pathways for DOC oxidation to occur using different e^- acceptors. In the absence of O_2, other common e^- accepters, such as NO_3^-, sulfate (SO_4^{2-}), and oxidized manganese and iron (Mn^{4+} and Fe^{3+}, respectively), are commonly used (Bethke *et al.*, 2011) (see Table 1.1). The reductive consumption of terminal electron acceptors (TEAs) results in different chemical species' uptake and production, affecting GHG emissions and water quality. For instance, denitrification paired with organic carbon oxidation would remove dissolved NO_3^- but could result in N_2O and CO_2 production – two potent GHGs. Hence, the microbial community's activity dictates water quality and GHG effects resultant of their energy needs and the availability of e^- acceptors (and donors) in the environment.

Table 1.1: Microbial metabolisms involved in soil organic matter decomposition.

Process	Reactants/e^- acceptor	Potential Products
Aerobic respiration	O_2	CO_2
Fermentation	Organic matter	CH_4, H_2, short-chain organic acids
Denitrification	NO_3^-	N_2O, N_2, NH_4^+
Iron/manganese reduction	Fe^{3+}, Mn^{4+}	Fe^{2+}, Mn^{2+}
Sulfate reduction	SO_4^{2-}	H_2S
Methanogenesis	CO_2, H_2, acetate	CH_4

Rates of microbial respiration are dependent on soil moisture content and temperature in the subsurface environment. Elevated respiration rates have been observed in soils stored between 25 and 40˚C; however, there is some discrepancy in how temperature impacts respiration at a mechanistic level (Trumbore, 2006). Respiration rates may also increase with soil moisture up to an optimal value; when exceeded, rates decrease again (Moyano *et al.*, 2013; Fairbairn, 2020). Temperature increases associated with climate warming have drawn concern to the arctic, sub-arctic, and boreal regions where large C stores exist in permafrost and peatlands (Tarnocai, 2006; Natali *et al*., 2019). Similarly, changes in precipitation patterns may alter soil moisture with implications for C respiration rates (Moyano *et al.*, 2013). Anticipated changes to temperature and precipitation patterns may enable elevated soil respiration rates, increasing current CO_2 fluxes (Schlesinger and Andrews, 2000). However, the exact impacts and amplification of climate feedback on soil respiration are unknown (Davidson and Janssens, 2006; Schlindlbacher *et al.*, 2012).

1.3.2 Winter Microbial Activity

Previously, soil respiration has been assumed negligible at low temperatures, and therefore, winter soil respiration has historically been disregarded. However, recent studies indicate that respiration continues to occur throughout the NGS, as discussed by Brooks *et al*. (2011) in both

the frozen and underlying unfrozen soil layers. An active microbial community persists under the winter snowpack performing at reduced activity rates (Alster *et al.*, 2016). In one study, soil microbial biomass reached its annual peak under the winter snowpack (Sorenson *et al*., 2020). The microbial community present is capable of distinct biogeochemical functions that are not apparent during adjacent periods, including the period immediately following snowmelt (Schmidt *et al*., 2007; Sorenson *et al*., 2020). Additionally, the suppression of photosynthetic activity by ice and snow enables chemosynthetic microbes to be the dominant organisms controlling soil geochemistry, particularly C and N speciations (Brooks *et al.*, 1998; Schmidt *et al*., 2007).

Gases produced through either aerobic and anaerobic activity during the NGS are often trapped under the winter ice layer, contributing to spring gas pulses of CO_2 and N_2O at thaw events (Burton and Beauchamp, 1994). This effect has been observed in several *in situ* snow manipulation experiments (Groffman *et al*., 2001, 2006; Yanai *et al*., 2011; Aanderud *et al.*, 2013; Wertz *et al*., 2013; Risk *et al*., 2014; Wagner-Riddle *et al*., 2017; Brin *et al*., 2018). An *in situ* study by Brooks *et al.* (2011) observed increased rates of C mineralization in snow-covered soil amended with glucose, sustained over 30 days (62 to 70% or higher). Unfortunately, the reliability of snow manipulation experiments is low, as discussed by Henry (2007). The removal of snow may expose soil to unrealistic temperatures and contribute to weathering and alter moisture content.

The presence of ice in soil and the associated trapping of biogenic CO_2, N_2O, and CH_4 indicate that frozen soil may behave as a barrier to soil-atmosphere gas exchange, restricting the diffusion of atmospheric O_2 into the subsurface throughout the winter. Seasonal redox fluctuations may then force active microbes to rely on other e^- acceptors (Table 1.1), such as NO_3^- (De Bruijn *et al*., 2009). This hypothesis is consistent with findings from Wagner-Riddle *et al.* (2017), who linked the magnitude of observed N_2O fluxes at thawing events to freezing duration. Other studies

have related winter subsurface concentrations of CO_2 and N_2O to the timing of snowfall, frost depth, soil moisture, and O_2 availability (Risk *et al*., 2014; Brin *et al*., 2018).

O_2 limitations developed throughout the winter may also implicate water quality as less energetic TEAs, such as SO_4^{2-} or ferric iron (Fe^{3+}), become favourable. Microbial activity may be promoted further during the winter from increased DOC and ammonium (NH_4^+) concentrations resultant of winter cell and roots damage (Scott-Denton *et al*., 2005; Patel *et al*., 2018). Ivarson and Sowden (1970) theorized that substrate existing in porewater is extruded from the ice phase during freezing resulting in increased concentrations in unfrozen water, stimulating microbial activity within and below the frozen layer. Ultimately, the impact of snow-cover and a physical ice barrier on soil biogeochemical cycling under winter conditions and its implications (*e.g.*, water quality, GHG emissions) are primarily unknown (Brooks *et al*., 2011).

1.4 Chemical Limits in the Subsurface: Bioenergetics

1.4.1 Microbial Activity: Chemotrophic Metabolisms

Frozen conditions and decreased light availability throughout the winter suppress plant activity (Brooks *et al.*, 2011) and, conceptually, result in increased nutrient availability for chemotrophic microorganisms who derive energy by catalyzing chemical reduction-oxidation (redox) reactions. Microbial activity dictates the speciation and mobility of nutrients year-round, including during the winter months. Therefore, it is imperative to understand the chemical transformations catalyzed by soil microorganisms under frozen soil to accurately predict water quality effects from spring porewater exports and GHG eruptions occurring at thaw.

Redox reactions are defined as chemical reactions involving the exchange of electrons wherein an e^- acceptor oxidizes an inorganic (*e.g.*, NH_4^+) or organic e^- donor. Organic e^- donors consist

primarily of short-chain organic acids (*e.g.*, lactate) formed from the hydrolysis of polymeric compounds in SOM. Inorganic e^- donors include species such as iron (II) (Fe^{2+}), manganese (II) (Mn^{2+}), dihydrogen sulfide (H_2S), or dihydrogen (H_2). Some inorganic e^- donors in the subsurface include species thought to be the 'end products' of anaerobic metabolisms, including NH_4^+ and CH_4 (Zhu *et al.*, 2010).

Where O_2 availability is limited naturally or from winter conditions, other common e^- accepters, such as NO_3^-, SO_4^{2-}, and Mn- and Fe- oxides, would be used (Bethke *et al*., 2011; Burgin *et al.*, 2011). Traditionally, TEAs are consumed in energetic order, beginning with reactions that will produce the most energy for uptake by their catalyzing microorganism. This idea, deemed the 'redox ladder' in geochemistry, results in redox cascades or zonations over spatial and temporal scales (Bethke *et al.*, 2011). However, observation of overlaps in successive redox zonations exists. Changes in the environment, such as pH, can influence energetic competition between metabolisms (Marquarat *et al*., 2018). Additionally, syntrophic relationships exist in various environmental settings for different nutrient cycles (Handley *et al*., 2013; Jiang *et al*., 2013) including the anaerobic oxidation of methane (AOM) (Iverson and Jorgensen, 1985; Pernthaler *et al*., 2008).

In closed systems, the reduction of oxidized species results in inorganic e^- donors' production, which may be used in future redox reactions if kinetic and thermodynamic constraints are favourable. For instance, SO_4^{2-} may be reduced to H_2S but then recycled to its oxidized form through coupled denitrification-sulphur-oxidation reactions performed by chemoautotrophs (Cardoso *et al*., 2006; Burgin and Hamilton, 2008). A similar reaction network has been observed between Fe and NO_3^- (Haaijer *et al.*, 2007), and in an AOM pathway using Fe-oxides as a TEA (Egger *et al*., 2016). The recycling of inorganic e^- donors further entangles C, N, S, Fe and Mn's

coupled biogeochemical cycles and perpetuates so-called 'cryptic cycles' or hidden anaerobic networks (Burgin *et al.*, 2011).

1.4.2 Bioenergetics and Thermodynamic Constraints

Chemotrophic organisms harness their energy (catabolic reaction) from the transfer of e^- and simultaneously uptake C to create biomass (anabolic reaction). Thus, microorganisms preferentially use e^- acceptors and donors in energetic order to gain the most energy possible, a phenomenon known as the redox ladder (Bethke *et al.*, 2011). The Gibbs energy of a reaction represents the amount of chemical energy available for work under constant pressure. For reactions where the change in Gibbs energy is negative (exergonic), a reaction is considered energetically favourable as energy is released into its surroundings and available for uptake by the catalyzing microorganism. The standard state Gibbs energy of a redox reaction (ΔG_r°) [J mol^{-1}] can be calculated by subtracting the sum of the Gibbs energy of formations for the reactants ($\Delta G_{f,reactants}^\circ$) [J mol^{-1}] from the products ($\Delta G_{f,products}^\circ$) [J mol^{-1}] (Eq. 1.3). The standard state Gibbs energy of formation for each product and reactant is multiplied by its molar ratio (n) for the balanced catabolic reaction.

$$\Delta G_{r298}^\circ = \sum n\Delta G_{f,products}^\circ - \sum n\Delta G_{f,reactants}^\circ \quad (1.3)$$

The standard state Gibbs energy of reaction can be transformed for a reaction occurring at different temperatures using the Gibbs-Helmholtz equation (Eq. 1.4). Where ΔG_{rT}° is the standard state Gibbs energy at temperature T [K], ΔG_{r298}° is the standard state Gibbs energy of a reaction at 25˚C and 1 bar [J mol^{-1}], and ΔH_{r298}° [J mol^{-1}] is the standard state enthalpy of the reaction.

$$\Delta G^{\circ}_{rT} = \Delta G^{\circ}_{r298}\left(\frac{T}{298.15}\right) + \Delta H^{\circ}_{r298}\left(\frac{298.15 - T}{298.15}\right) \quad (1.4)$$

The Gibbs energy can be transformed further to reflect conditions of a non-standard state using the reaction quotient, Q [-] (Eq. 1.5), which is dependant on the activities of the products and reactants available.

$$\Delta G_r = \Delta G^{\circ}_{rT} + RTlnQ \quad (1.5)$$

For soil microbes to perform nutrient transformations, reactions must be exergonic, and a threshold of energy must be met for ATP synthesis, the currency of the energy economy. Schink (1997) determined that the minimum energy yield for microorganisms was roughly -20 kJ mol^{-1}; more recently, a smaller energy requirement ($\Delta G' \cong 0$ kJ mol^{-1}) has been idealized for microorganisms adapted to low-energy or oligotrophic environments executing only maintenance metabolism using syntrophic associations (Jackson and McInerney, 2002). Therefore, microbial activity is limited by the availability of chemical energy in an environment, reflected in the *in situ* concentrations of available e^- donors and acceptors.

The standard state Gibbs energies of formation for common e^- donors and acceptors at 25˚C and 1 bar are provided in Table 1.2 in the relative order of thermodynamic favourability. In environments with low chemical energy, like wetlands, TEA such as NO_3^-, SO_4^{2-} and Fe- and Mn-oxides are often absent or present in concentrations too low to meet thermal and kinetic constraints. Hence, soil organisms may progress quickly through the redox ladder, resulting in methanogenesis and fermentation reactions.

Table 1.2: Balanced half-reactions of common e^- donating and accepting processes, presented with their calculated standard Gibbs energies. Reactions are written in energetic order, beginning in each section with the most energetically favourable process.

e^- Donating Reactions	
Balanced Half Reaction	**ΔG°_{rHalf} [kJ mol^{-1} e^-]**
$H_2 \rightarrow 2H^+ + 2e^-$	-8.79
$CH_4 + 3H_2O \rightarrow H_2CO_3 + 8H^+ + 8e^-$	15.35
$H_2S + 4H_2O \rightarrow SO_4^{2-} + 10H^+ + 8e^-$	29.01
$Fe^{2+} + 3H_2O \rightarrow Fe(OH)_3 + 3H^+ + e^-$	78.38
$NH_4^+ + 2H_2O \rightarrow NO_2^- + 8H^+ + 6e^-$	86.07
e^- Accepting Reactions	
Balanced Half Reaction	**ΔG°_{rHalf} [kJ mol^{-1} e^-]**
$NO_3^- + 6H^+ + 5e^- \rightarrow 0.5N_2 + 3H_2O$	-120.3
$MnO_2 + 4H^+ + 2e^- \rightarrow Mn^{2+} + 2H_2O$	-118.6
$Fe(OH)_3 + 3H^+ + e^- \rightarrow Fe^{2+} + 3H_2O$	-78.38
$SO_4^{2-} + 10H^+ + 8e^- \rightarrow H_2S + 4H_2O$	-29.01
$H_2CO_3 + 8H^+ + 8e^- \rightarrow CH_4 + 3H_2O$	-15.35
Disproportionation Reactions	
Balanced Half Reaction	**ΔG°_{rHalf} [kJ mol^{-1} e^-]**
$0.5C_2H_3O_2^- + 2H_2O \rightarrow H_2CO_3 + 3.5H^+ + 4e^-$	8.98
$0.5C_2H_3O_2^- + 4.5H^+ + 4e^- \rightarrow CH_4 + H_2O$	-29.01

1.4.3 Thermo-Kinetic Models

A thermodynamic minimum must be met for a microbially mediated reaction to proceed; however, the reaction rate depends on both thermodynamic and kinetic factors. Within biogeochemical systems, Monod type kinetics are used to predict the maximal growth of a singular culture. The Dual Monod equation (Eq. 1.6) is limited in that it can only account for one-directional reactions and does not consider the thermodynamic energy requirements of soil microorganisms (Jin and Bethke, 2005).

$$r = \bar{r}_{max} \cdot \frac{[ED]}{K_S^{ED} + [ED]} \cdot \frac{[EA]}{K_S^{EA} + [EA]} \cdot X = \bar{r}_{max} \cdot F_K \cdot X = \bar{r} \cdot X \tag{1.6}$$

Where r [mol L^{-1} s^{-1}] is the substrate utilization rate, $\bar{r}_{max}$ [mol mol–C^{-1} s^{-1}] is the maximum substrate utilization rate per unit biomass, X [mol – C L^{-1}] is biomass concentration, $[ED]$ and $[EA]$ are the molar concentrations of the e^- donor and acceptor [mol L^{-1}], respectively, and K_m^{ED} and K_m^{EA} are their related half-saturation constants [mol L^{-1}]. The equation can be simplified using a unitless kinetic limitation factor, F_K, and $\bar{r}$ which combines $\bar{r}_{max}$ and F_K as the substrate utilization rate per unit biomass [mol mol–C^{-1} s^{-1}]. The Monod equation can account for nutrient-poor environments through the dimensionless thermodynamic limitation factor, F_T using Eq. 1.7:

$$R = \bar{r}_{max} \cdot F_K \cdot F_T \cdot X \tag{1.7}$$

The thermodynamic limitation is defined using several approaches as discussed by Thullner and Regnier (2019), which have previously used the energetic minimum for ATP synthesis from ADP. However, in nutrient-poor environmental settings where microorganisms function approaches the thermodynamic limit, maintenance metabolisms prevail, and the standard equation becomes inappropriate as reaction rates susceptibility to F_T is heightened (Thullner *et al.*,

2007). An equation (Eq. 1.8) proposed by LaRowe *et al*. (2012) minimizes this effect by using the energy requirements for maintaining membrane potential for low energy environments:

$$F_T = \begin{cases} \dfrac{1}{exp\left(\dfrac{\Delta G_{cat} + F\Delta\Psi}{RT}\right) + 1} & for\ \Delta G_{cat} \leq 0 \\ 0 & for\ \Delta G_{cat} \geq 0 \end{cases} \quad (1.8)$$

where ΔG_{cat} [J mol^{-1}] is the Gibbs energy of the catabolic reaction, F [J V^{-1} mol^{-1} e^-] is Faraday's constant, and $\Delta\Psi$ [V] is the membrane potential. When the catabolic reaction is endergonic ($\Delta G_{cat} \geq 0$), and energetic constraints are unmatched, the thermodynamic factor is equal to zero. As a result, the anticipated rate of microbial respiration for the metabolic pathway would be zero as well.

1.5 Thesis Objectives

The main objective of this thesis is to advance the mechanistic understanding of winter soil biogeochemical cycles concerning chemical energy availability over a temporal scale for C and N mineralization purposes.

The specific objectives of Chapter 2 include:

- Assess the changes in C and N speciation under prolonged cold, oxygen-limited, and cold conditions,
- Understand how high concentrations of chemical end products influence subsequent reactions in closed conditions,
- Utilize bioenergetics to predict the thermodynamic favourability of reduction-oxidation reactions for nutrient transformations in wetland soils under winter conditions,
- Examine how winter soil biogeochemistry impacts wetlands as a source of biogenic CH_4 to the atmosphere.

In Chapter 3 of this thesis, the specific objectives are to:

- Review the current understanding of anaerobic methane oxidation rates in freshwater and marine ecosystems,
- Develop a framework for estimating rates of anaerobic methane oxidation rates in various environmental settings using published observations.

1.6 Thesis Outline

This thesis comprises four chapters that explore the biogeochemical processes of wetland soils under a frozen layer. Chapter 1 provides a general introduction and relevant background information on climate change, hydrological and chemical conditions experienced by wetland soils throughout the winter, SOM degradation, and bioenergetics as a tool to understand thermodynamic limitations and reaction rates. Chapter 2 includes a co-authored manuscript, for which I am the first author. This manuscript has been prepared for submission to Frontiers in Environmental Science – Biogeochemical Dynamics. The formatting of manuscript figures, tables, equations, and sections have been updated for consistency with the overall thesis. The manuscript in Chapter 2 depicts a soil incubation experiment wherein a sacrificial sampling technique and factorial design allowed for the decoupling of e^- acceptor and e^- donor availability by allowing the soil system to develop without disruption from removing chemical end products, such as CH_4. Chapter 3 is composed of a literature review and data analyses of anaerobic methane oxidation rates for freshwater and marine environments. In Chapter 4, overall conclusions are presented in addition to recommendations for future research. Finally, Appendix A contains supplementary materials for the manuscript presented in Chapter 2, including additional results and laboratory methods.

Anammox and manganese oxides as drivers of anaerobic methane oxidation in cold wetland soils

Heather Townsend[1], Fereidoun Rezanezhad[1], Stephanie Slowinski[1], Christina Smeaton[2], Kara Webster[3], Scott Smith[4], Merrin Macrae[5], Chris Parsons[1], Philippe Van Cappellen[1]

[1] Ecohydrology Research Group, Department of Earth and Environmental Sciences and Water Institute, University of Waterloo, Waterloo, Canada
[2] School of Science and the Environment, Grenfell Campus, Memorial University of Newfoundland, Corner Brook, Canada
[3] Canadian Forest Service Great Lakes Forestry Centre - Natural Resources Canada, Sault Ste Marie, Canada
[4] Department of Chemistry and Biochemistry, Wilfrid Laurier University, Waterloo, Canada
[5] Department of Geography and Environmental Management, University of Waterloo, Waterloo, Canada

*Corresponding author: Heather Townsend

Ecohydrology Research Group, Department of Earth and Environmental Sciences and Water Institute, University of Waterloo, 200 University Avenue West, Waterloo, Canada N2L 3G1

Email: heather.townsend@uwaterloo.ca

This chapter will be modified for submission to *Frontiers in Environmental Science – Biogeochemical Dynamics*.

2 Anammox and manganese oxides as drivers of anaerobic methane oxidation in cold wetland soils

2.1 Abstract

Accelerated temperature increases during the winter season at mid- and high latitude cold regions and altered precipitation regimes are expected to mobilize terrestrial organic carbon (C) from organic-rich wetland-dominated landscapes. Winter warming may have positive implications for the agricultural sector in mid-latitude regions where the elevated temperatures enable the expansion of agriculture into colder climates, resulting in the cultivation of organic-rich wetlands. Therefore, climate-driven shifts in precipitation may further mobilize soil C and nitrogen (N) through changes in the duration and frequency of freezing and thawing cycles in soils. Soil freezing has been linked to decreased oxygen concentrations and the accumulation of greenhouse gases in soil pore spaces, affecting C and N cycling and affecting water quality through the prevalence of anaerobic microbial metabolisms. In this study, a series of sacrificial batch experiments simulated the impact of winter ice barrier conditions on subsurface organic soil. Soil samples were collected from a swamp in the Turkey Lakes Watershed near Sault Ste. Marie, Ontario, treated with input solutions containing variable quantities of labile organic C and e^- acceptors (nitrate and sulfate) and were incubated under anaerobic conditions at 5˚C over a 50-day sacrificial sampling period. Time series data collected at 6 time-points included headspace carbon dioxide (CO_2), methane (CH_4) and nitrous oxide (N_2O) as well as porewater chemistry such as pH, major cations and anions, organic and inorganic C, total N, and ammonium (NH_4^+). The results indicate that up to 9 mM of acetate and 1.5 mM of NH_4^+ were consumed throughout the experiment, resulting in CO_2, CH_4, and N_2O production, and a decrease in porewater from pH 6.7 to 5.3 within the first week of incubation. CH_4 concentrations peaked at 100 µM between days 28 and 35 before decreasing, and

the observed oxidation of CH_4 coincides with an increase in pH from 5.3 to 6.2, despite small changes in nitrate or sulfate concentrations. Thermodynamic calculations support our observations of chemolithoautotrophic reactions, including anaerobic NH_4^+ and CH_4 oxidation, which were energetically favourable under the experimental conditions.

Keywords: climate change, winter soil processes, greenhouse gas emissions, wetlands, methane, ammonium, anaerobic oxidation of methane, anammox, bioenergetics

2.2 Introduction

Global increases in air temperature are anticipated to have amplified effects in cold regions (Cohen *et al*., 2014; Screen, 2014), where the eastern Boreal Shield ecozone is predicted to experience a 4 to 7˚C increase in winter minima temperatures by 2100 (Price *et al*., 2011). Resultant shifts in winter temperature and precipitation are expected to alter the accumulation and melt of insulating snow cover significantly, thereby exposing soils to cold air temperatures (Wuebbles *et al.*, 2010; Hayashi, 2013). As a result, non-trivial consequences for biogeochemical cycling in northern organic-rich soils are predicted (Groffman *et al.*, 2006; Tarnocai, 2006; Henry, 2007; Brooks *et al.*, 2011), including increased dissolved organic matter (DOM), dissolved organic carbon (DOC), and ammonium (NH_4^+) leaching (Reyes and Lougheed, 2015; Fouché *et al*., 2020), increased carbon dioxide (CO_2) (Natali *et al*., 2019) and nitrous oxide (N_2O) emissions (Voigt *et al.*, 2020), and changes in oxygen (O_2) availability.

Warmer annual air temperatures may have positive implications for the agricultural sector in boreal and temperate regions, where warmer temperatures and an extended growing season for plants could enable the expansion of agricultural landscapes into traditionally colder climate regions (Chapman *et al.*, 2003; Maracchi *et al.*, 2005; Olesen *et al*., 2007; Tuck *et al.*, 2006; King *et al*., 2018; Ceglar *et al.*, 2019). However, the conversion of pristine organic soils into cropland could introduce excess nutrients into low-energy environments, disturbing natural soil biogeochemical function (Gilbert *et al.*, 1998; Lai, 2009). The consequent increase in chemical energy sources for chemosynthetic microbes could induce shifts in carbon (C) and nitrogen (N) cycling. Changes in microbially-driven C and N cycles ultimately modify soil greenhouse gas (GHG) emissions and the export of dissolved C and N species to aquatic ecosystems, impacting water quality (Thullner and Regnier, 2019).

Winter snow cover exerts essential control over winter soil processes and the annual cycling and budgets of C and N in cold region watersheds (Aanderud *et al.*, 2013; Brooks *et al*., 2011). The optical and thermal properties of snow limit photosynthetic plants' activity and, through soil freezing, can limit gas exchange with the atmosphere (Warren, 1982; Brooks *et al*., 2011; Gobel *et al.*, 2019). The reduction in photosynthetic activity throughout the snow-covered season enables chemosynthetic microbes to be the dominant organisms controlling soil geochemistry, including C and N speciation (Brooks *et al.*, 1998; Schmidt *et al*., 2007). Despite cold temperatures, an active microbial community persists under the winter snowpack, performing geochemical reactions at reduced rates due to decreased temperature (Alster *et al.*, 2016). Throughout the snow-covered season, the microbial community may reach peak biomass and is capable of distinct biogeochemical functions that are not apparent during adjacent periods, including the period immediately following snowmelt (Schmidt *et al*., 2007; Sorenson *et al*., 2020). Snowmelt is a significant driver of hydrology and biogeochemistry in seasonally snow-covered landscapes; rapid infiltration of meltwater into the subsurface exports porewater to the neighbouring ground- and surface water (Hayashi, 2013). Hence, over-winter soil biogeochemical processes are the dominant control on the porewater composition, and the speciation of dissolved C and N exported during snowmelt, when the export to aquatic ecosystems occurs on a short temporal scale (Creed *et al*., 1996; Heuer *et al.*, 1999; Finlay *et al*., 2006; Raymond *et al.*, 2016).

The absence of insulating snowpack decreases soil temperature and increases soil freezing depth during the winter (Groffman *et al*., 2001, 2006). Emissions of microbially-produced GHGs such as carbon dioxide (CO_2), methane (CH_4), and nitrous oxide (N_2O) from soils are associated with the seasonal thaw events in agricultural soils (Wagner-Riddle *et al*., 2017; Brin *et al*., 2018). Although there is some debate regarding the magnitude of N_2O and other GHGs produced under

the frozen soil layer throughout the winter versus rapidly during thaw conditions, some studies indicate that frozen soil may act as a barrier to gas exchange, trapping biogenic gases produced in underlying unfrozen layers (Wagner-Riddle *et al.*, 2008; Wertz *et al.*, 2013). The observed emissions of gases produced by anaerobic microbial reactions (N_2O and CH_4) imply that the presence of a physical ice barrier at the soil surface inhibits atmospheric gas exchange, decreasing oxygen gas (O_2) diffusion into the subsurface (Nyameogo *et al.*, 2018) while trapping belowground biogenic gases (van Bochove *et al.*, 2001). The associated depletion of O_2 throughout the winter, induced by soil freezing conditions, would shift microbial metabolisms to alternative e^- acceptors, including nitrate (NO_3^-), iron (Fe^{3+}), manganese (Mn^{4+}), and sulfate (SO_4^{2-}) reduction as well as fermentative pathways (*e.g.*, methanogenesis).

On a global scale, the largest source of methane (CH_4) to the atmosphere is natural wetlands (Denman *et al.*, 2007). Biogenic CH_4 production is the final stage of organic C decomposition in anoxic environments. However, the extent to which CH_4 produced in these anoxic environments is consumed (*i.e.*, oxidized as an e^- donor) anaerobically is still unclear (Smemo and Yavitt, 2011; Segarra *et al.*, 2015). Aerobic CH_4 oxidation is often considered the dominant sink of CH_4 in soils wherein gas produced in deep anoxic layers of soil is transported upwards and oxidized in the oxic layer (Dean *et al.*, 2018). Anaerobic oxidation of methane (AOM) is identified as a significant control on CH_4 release from marine sediments (Valentine, 2002), limiting CH_4 emissions by up to 90% in marine environments (Dale *et al.*, 2006). Syntrophic association between CH_4 and SO_4^{2-} resulted in AOM near the base of the SO_4^{2-}-reducing interface (Iverson and Jorgensen, 1985).

Lower concentrations of SO_4^{2-} in freshwater systems had previously resulted in an assumption of thermodynamically unfavourable AOM pathways in wetland and lacustrine environments (Smemo and Yavitt, 2011; Segarra *et al.*, 2015). Yet, recent studies have identified microbes

capable of AOM in freshwater wetland sediments (Segarra *et al.*, 2015), lake water columns and sediments (Deutzman and Schink, 2011; Deutzmann *et al.*, 2014; Cabrol *et al*., 2020), and under lake ice, using a variety or combination of terminal electron acceptors (TEAs) (Smemo and Yavitt, 2007; Martinez-Cruz *et al.*, 2017). In both freshwater and marine sediments (Beal *et al*., 2009), Fe- and Mn- oxides have been found to play a crucial role in oxidizing CH_4 either directly as TEAs (Egger *et al*., 2015; Leu *et al*., 2020) or through e^- shuttling to SO_4^{2-} (Sivan *et al.*, 2014). Recently, denitrification-driven AOM has been observed in the presence of excess nitrite (NO_2^-) (Raghoebarsing *et al.*, 2006) and NO_3^- as well as anaerobic ammonium oxidation (anammox) (Haroon *et al*., 2013). Anammox facilitates AOM by regenerating the oxidized N species, NO_2^- and NO_3^-, which are subsequently consumed as TEAs by AOM (Zhu *et al.*, 2010). High concentrations of trapped CH_4 accumulated under frozen soil may increase the thermodynamic and kinetic favourability of AOM throughout the winter, pending the availability of TEAs (Smemo and Yavitt, 2011).

As the most reduced N species, NH_4^+ is used for energy by microbial reactions as an e^- donor and serves as a source of nutrient N for biomass growth. The relatively recent discovery of combined anammox and AOM processes has shifted the perspective of how the soil C and N cycles are coupled (Thamdrup 2012). The oxidative consumption of NH_4^+ to N_2 coupled to either NO_3^- or NO_2^- reduction is widely recognized; more recently, NH_4^+ oxidation to NO_2^- by SO_4^{2-} or Fe-oxides (Ding *et al.*, 2017; Rios-Del Toro *et al*., 2018; Liu *et al*., 2021; Yang *et al.*, 2021) and NO_3^- by Mn-oxides were reported (Fernandes *et al*., 2014) demonstrating the complex nature of autotrophic anammox bacteria. Thus, with sufficient NH_4^+ present alongside favourable TEA concentrations, it may be thermodynamically and kinetically possible for anammox to produce NO_2^- or NO_3^-, creating TEA for the oxidation of other reduced species, such as CH_4 in AOM. By

extension, in soils where there are sufficient concentrations of NH_4^+ or NO_2^- from fertilizer, AOM may remove both N from the porewater and CH_4 from the gas phases, thereby improving water quality and limiting the release of a potent GHG.

In this study, to investigate the effects of potential land use management changes on the over-winter geomicrobial reaction network in organic soils, time-series data of GHG and nutrient concentrations were collected from organic soils incubated under temperature-controlled, anaerobic, and closed system conditions. Soil treatments were incubated at 5˚C for up to 50 days with variable added quantities of NO_3^-, SO_4^{2-}, and glucose ($C_6H_{12}O_6$) to simulate the addition of excess e^- acceptors from fertilizer addition and increased winter labile organic carbon (e^- donors) derived from soil freezing-induced cell lysis (Patel *et al*., 2018) and autumn leaf litter decay. The experiment's sacrificial sampling and factorial design allowed for the de-coupling of e^- acceptor and e^- donor availability by allowing the soil system to develop without disruption from removing chemical end products, such as CH_4. As a result, measurements of (bio)geochemical end products and nutrient transformations can occur on a temporal scale for soil incubations. This study's objective was to investigate the changes in C and N speciation and reaction rates under prolonged low temperature, oxygen-limited and closed system (*i.e.*, no exchange of gases with the atmosphere) conditions with different quantities of e^- acceptors and e^- donors (*i.e.*, chemical energy). The experiment's goal is to advance our understanding of the effects of chemical energy availability on the soil C and N cycling functions controlling GHG emissions and the export of dissolved nutrients during the spring thaw.

2.3 Materials and Methods

2.3.1 Field Site and Sample Collection

Soil samples were collected from a hardwood swamp within the experimental Turkey Lakes Watershed (TLW) in central Ontario, Canada (47° 03'N, 84° 25'W). The TLW drains into Lake Superior and historically experiences a mean annual air temperature and precipitation of 4.6˚C and 1,189 mm per year, respectively (data from 1981 to 2010; Semkin *et al*., 2012). Within this watershed, snow cover persists typically from November to April, resulting in major snowmelt-driven hydrologic events through late May (Characteristics of the Turkey Lakes Watershed Study Site, 2014). The mean daily snow depth was reported as lowest in November and maximal in February with depths of ~28.5 cm and 90 cm, respectively (Semkin *et al.*, 2012). During the snow-covered period (November to April) the mean daily temperature (1980 to 2010) is reported as -4.5˚C (Semkin *et al.*, 2012).

Saturated soil samples were collected from a depth of 5 to 15 cm at the field site from the peat layer. The top 5 cm of soil was removed to minimize plant debris, and intact block samples were collected using a wide-toothed saw. Collected soil samples were stored in a cooler and transported to the Ecohydrology Research Group laboratory at the University of Waterloo. Upon arrival, the soil samples were moved into an anaerobic chamber (Mandel Scientific Anaerobic Chamber, AC11-074) and allowed to dry uncovered in anoxic and room temperature conditions (22 ± 2˚C) for 35 days while being hand-mixed at regular daily intervals.

2.3.2 Soil Incubation Experiment

A series of static incubation experiments were conducted for five different treatments. The dried soil samples were sieved to 2 mm, homogenized, and divided evenly by mass into five

groups. Each soil group was re-wetted with equal amounts of its designated N_2-purged input solution and mixed by hand to achieve an approximate gravimetric water content of 75% (± 3%), consistent with field observations of the field site by Webster *et al*. (2008). Treatment groups were then subdivided into 16 samples of equal mass and inserted into the air-tight 250 mL widemouthed septa jars (Fisher Scientific, S321-0250), leaving approximately 150 mL of headspace. An additional 30 g sample from each group was massed into beakers and oven-dried at 80˚C to determine the initial gravimetric moisture content and bulk density per soil group. Additional moisture content calculations were determined for each soil jar at every time point using the same methodology with 10 g of soil. For these measurements, soil was taken for oven-drying following the collection of headspace gas samples and porewater analysis (Section *2.3*).

Four defined sample groups of 'Natural', '+Electron Acceptors', '+Glucose', and '+Electron Acceptors +Glucose' were designed to isolate the relative amounts of e^- donors and acceptors available to soil microbes under low energy conditions through their associated artificial input solutions (Table 2.1). The Natural treatment group received only background concentrations of e^- acceptors, including NO_3^- and SO_4^{2-}, while the +Electron Acceptor treatment received elevated concentrations. The +Glucose treatment group received a similar input solution as the Natural group; however, 1,000 µM of glucose was added as an extra e^- donor. Likewise, the +Electron Acceptor +Glucose treatment group received a similar input solution as the +Electron Acceptor group with the addition of 1,000 µM $C_6H_{12}O_6$. Exact concentrations of NO_3^- and SO_4^{2-} were measured using the same method outlined in *2.3.2*. Each treatment group consisted of 16 samples, and the assembled soil jars were tightly sealed, removed from the anoxic chamber, and placed into an environmental chamber (Percival Scientific INTELLUS Control System) to

incubate at a constant temperature of 5˚C under low light conditions and were sacrificed over 8 weeks at 6 time points.

A smaller abiotic control group consisting of autoclaved soil was measured in duplicate over 4 time points. 500 g of dried soil and its input solution were removed from the anaerobic chamber and autoclaved (Tuttnauer Electronic Tabletop Autoclave) for sterilization the day before soil re-wetting. This sample group was re-wetted with an autoclaved artificial porewater solution with the same N_2-purged input water as the Natural treatment group. The autoclaved group's soil jars were prepared using the same method outlined for the other treatments.

Table 2.1: Input solution concentrations of added e^- acceptors and glucose for each treatment group.

Treatment	Input Solution Concentration [µM]		
	NO_3^-	SO_4^{2-}	$C_6H_{12}O_6$
Natural	9.92	22.11	0
+Electron Acceptors	528	59.50	0
+ Glucose	12.10	21.94	1,000
+ Electron Acceptors + Glucose	616.69	56.76	1,000
Abiotic Control	9.92	22.11	0

Geochemical Analysis

Time series data of porewater chemistry and headspace gas concentration were collected using sacrificial sampling. Upon sampling, soil jars were removed from the environmental chamber and brought into the anaerobic chamber. First, headspace gas samples were extracted, then solid soil samples were collected, and finally, the remaining soil was removed for centrifugation. A

sacrificial sampling of porewater, soil, and gases and their respective analyses occurred every 1 to 2 weeks following the same sample extraction methods, preparation, and analysis described below.

Gas Phase Analysis

After moving the samples to the anaerobic chamber, 2 to 5 mL gas phase samples were collected from the jars' headspaces using a plastic 50 mL syringe inserted through the septa lid of each jar. 45 to 48 mL of helium was added to the gas samples and allowed to mix for at least thirty minutes to equilibrate before analysis. Analysis of the gas phase for concentrations of CO_2, CH_4, N_2O, and H_2 was conducted using a Shimadzu Gas Chromatograph (Model GC-2014) equipped with Electron Capture, Flame Ionization, and Thermal Conductivity Detector technologies (ECD, FID, and TCD, respectively). CO_2 and CH_4 were measured by FID, H_2, O_2 and N_2 were measured by TCD, and N_2O was measured by ECD. At time points 3 and 4, a second dilution of the extracted headspace gas was required to meet the CO_2 detection limit, where ~10 mL of the initial dilution was mixed with an additional ~40 mL of helium.

Porewater Analysis

Following the extraction of headspace gas, the soil jars were opened inside the anaerobic chamber and prepared for porewater extraction. Approximately 80 g of soil was removed from each jar and divided into two tightly sealed and sterile 50 mL centrifuge tubes. Soil samples were centrifuged (Avanti® J-E Centrifuge) at 5˚C and 4,800 RPM for 30 to 60 minutes outside of the anaerobic chamber. Afterwards, the centrifuge tubes were returned to the anaerobic chamber to extract the separated water phase for sub-sampling.

10 mL of porewater sample was collected from each centrifuged soil sample inside the anaerobic chamber, filtered through a 0.45 μm membrane filter (Thermo Scientific Polysulfone filter) and then sub-sampled for porewater chemical analyses. The porewater analyses included pH measurements and the concentrations of dissolved organic carbon (DOC), dissolved inorganic carbon (DIC), total nitrogen (TN), major cations and anions, organic acids, and NH_4^+. Porewater pH of the filtered samples was measured using a calibrated electrode (Thermo-Fisher Scientific Versa Star Meter using an Orion Triode-3 in 1 pH/Automatic temperature compensation gel probe). The DOC, DIC, and TN samples were analyzed using a total organic carbon analyzer (Shimadzu TOC-LCPH/CPN). Major cations (sodium, calcium, magnesium, potassium, and total sulfur) were measured using inductively coupled plasma optical emission spectrometry (Thermo Fisher Scientific ICP-OES 6000). Concentrations of major anions and organic acids were measured using ion chromatography (IC, Dionex ICS-5000 with a capillary IonPac® AS18 column; ± 3.0% error and ± 1.6% precision) where, for organic acids, an additional 1 mL of porewater filtered through a 0.2 μm membrane filter (Thermo Scientific Polysulfone filter) and treated with 20 μL of a 500 ppm CrO_4^{2-} solution. Measured organic acids and anions included acetate, butyrate, propionate, lactate, citrate, nitrate (NO_3^-), nitrite (NO_2^-), sulfate (SO_4^{2-}), and phosphate (PO_4^{3-}). For porewater analysis of NH_4^+ concentration, 1mL of porewater was collected during sampling in sterile vials and frozen for storage. Upon thawing, concentrations of reactive NH_4^+ were measured using the indophenol blue colourimetric technique via Berthelot's reaction described by Ringuet *et al.* (2011) for a microplate reader (Molecular Devices, Flexstation 3, Multi-Detection Reader with Integrated Fluid Transfer).

Net production rates were calculated for porewater species using Eq. 2.1, where $\frac{dC_i}{dt}$ is the net production rate at time (t), $C_{i,t}$ is the concentration measured at time (t), and $\overline{C}_{i,t-1}$ is the

average concentration at from the previous timestep. Calculated net production values were plotted at the midpoint of Δt.

$$\frac{dC_{i,t}}{dt} = \frac{C_{i,t} - \overline{C}_{i,t-1}}{\Delta t} \quad (2.1)$$

Solid phase analysis

The remaining soil from each incubation (following porewater extraction) was resealed in its jar and stored at 5˚C for solid-phase analysis using a Scanning Electron Microscope (SEM TM-3000, Bruker QUANTAX 70 Energy Dispersive X-Ray Spectrophotometer). Roughly 12 months after the experiment began, additional soil samples were extracted from the field site using the same methods outlined in Section *2.3.1* and couriered to the University of Waterloo for further solid-phase analysis, including cation exchange capacity (CEC) determination and Fe- and Mn-extractions. The freshly delivered soil was dried within the anaerobic chamber and sieved for analysis.

CEC was determined using the methods of Hendershot and Duquette (1986). Ten tubes containing 0.5 g of the freshly delivered dry soil were mixed with 30 mL of N_2-purged 0.1 M barium chloride ($BaCl_2$) solution end-over-end for 2 hours, then centrifuged 700*g* for 15 minutes. The well-mixed samples were filtered through Whatman No. 41 filter paper and subsequently prepared for ICP major cation analysis using the methods previously outlined in Section *2.3.2*. Calibration standards and QCs were prepared in the $BaCl_2$ solution to eliminate matrix artifacts.

Soil Mn and non-crystalline inorganic Fe pools were quantified using a hydroxylamine extraction modified by Rosso *et al.* (1985) and Wang *et al.* (1987). The fresh dry soil was crushed in the anaerobic chamber to pass through a 100 mesh sieve. Ten preparations containing 0.1 g of the crushed soil were re-wetted with 25 mL of N_2-purge hydroxylamine hydrochloride-

hydrochloric acid (0.25M $NH_2OH{\cdot}HCl$, 0.25M HCl) in the anaerobic chamber and mixed end-over-end for 16 hours. Extraction samples were centrifuged at 510*g* for 20 minutes, filtered and prepared for Fe and Mn analysis using ICP-OES. Similar to CEC measurements, the ICP calibration was validated using spiked matrix samples containing the extractant solution.

2.3.3 Gibbs Energy Calculations

The Gibbs energies of the catabolic reduction-oxidation reactions of interest were calculated for the *in situ*, non-standard conditions in the incubations at each time point using the approach described by Smeaton and Van Cappellen (2018). The Gibbs-Helmholtz equation (Eq. 1.4) was used to adjust the standard Gibbs energy for the incubation temperature, and Eq. (1.5) was used to account for the non-standard activities of the reactants and products. The reaction quotient was calculated using the reactants' and products' activities calculated in R interface (version 3.6.3, Charlton *et al*. (2020)) of PHREEQC (Version 3, USGS) from each soil incubations' unique aqueous and gas-phase chemistry, which are described in *2.2.2*. The balanced catabolic reactions of interest are listed in Table 2.2. These reactions include denitrification coupled to iron oxidation, anaerobic NH_4^+ oxidation coupled to Mn^{4+}, Fe^{3+} and SO_4^{2-} reduction, and anaerobic CH_4 oxidation coupled to NO_3^-, Mn^{4+}, Fe^{3+} and SO_4^{2-} reduction.

The relationship between the Gibbs energy of each NH_4^+ and CH_4 reaction with pH, and temperature for anammox and AOM was explored further by calculating the Gibbs energy over a range of temperatures (-5 to 30˚C) and pH (4 to 8). The effect of temperature on the Gibbs energies was imposed via the Gibbs-Helmholtz equation (Eq. 1.4), while the effect of pH was accounted for via the reaction quotient (Eq. 1.5). Activities used for the remaining products and reactants were imposed as constant values that were selected by averaging the calculated activities of the products and reactants at each treatment's CH_4 peak.

Table 2.2: Balanced catabolic reactions for anoxic conditions with their associated standard Gibbs energy.

e^- Donor	Reaction Number	Balanced Catabolic Reaction	ΔG°_{r298} [kJ / mol e^-]
Fe^{2+}	1	$0.2NO_3^- + Fe^{2+} + 2.4H_2O \rightarrow 0.1N_2 + Fe(OH)_3 + 1.7H^+$	-41.65
H_2S	2	$NO_3^- + 0.25H_2S + H_2O \rightarrow NH_4^+ + 0.25SO_4^{2-}$	-55.92
NH_4^+	3	$NH_4^+ + 6Fe(OH)_{3(s)} + 10H^+ \rightarrow NO_2^- + 6Fe^{2+} + 16H_2O$	7.69
	4	$NH_4^+ + 0.75SO_4^{2-} \rightarrow NO_2^- + 0.75H_2S + H_2O + 0.5H^+$	57.06
	5	$NH_4^+ + 4MnO_{2(s)} + 6H^+ \rightarrow NO_3^- + 4Mn^{2+} + 5H_2O$	-44.92
$CH_{4(aq)}$	6	$CH_{4(aq)} + 1.6NO_3^- + 1.6H^+ \rightarrow H_2CO_3 + 0.8N_{2(g)} + 1.8H_2O$	-104.68
	7	$CH_{4(aq)} + 8Fe(OH)_{3(s)} + 16H^+ \rightarrow H_2CO_3 + 8Fe^{2+} + 21H_2O$	-63.03
	8	$CH_{4(aq)} + SO_4^{2-} + 2H^+ \rightarrow H_2CO_3 + H_2S + H_2O$	-13.66
	9	$CH_{4(aq)} + 4MnO_{2(s)} + 8H^+ \rightarrow H_2CO_3 + 4Mn^{2+} + 5H_2O$	-103.27

2.4 Results

2.4.1 Dissolved and Gas Phase Biogeochemical Trends

Figure 2.1 shows the temporal data of porewater pH, NO_3^-, NO_2^-, SO_4^{2-}, Mn and Fe concentrations as well as headspace concentrations of N_2O and CH_4 gas. The grey shading highlights three distinct phases in biogeochemical species and their associated trends: denitrification (Phase I; day 1 to 8), SO_4^{2-} reduction and methanogenesis (Phase II; day 8 to 29), and AOM (Phase III; day 29 to 50). These three phases were observed throughout the soil incubation for all treatments.

Phase I occurs from re-wetting to day 8 and is defined by the initial decrease in pH and the simultaneous consumption of NO_3^- producing headspace N_2O. The magnitude of N_2O produced was treatment dependent with much smaller peaks occurring in the treatments without additional NO_3^-. Porewater pH decreased from days 1 to 8 for all treatments, stabilizing at an average value of 5.43 ± 0.02. A similar porewater pH change was observed in the abiotic control group (Figure S1 in Appendix A) during this Phase, suggesting that the initial decrease from the input solution is an abiotic process as the solution and soil reach equilibrium. Denitrification in Phase I consumed 452.84 and 587.27 µM NO_3^- in the +Electron Acceptor and +Electron Acceptor + Glucose treatments, respectively. Rates of denitrification appeared to be the fastest in the treatments which received excess NO_3^-, where the greatest net rate (-587 µM day^{-1}) occurred in the treatment amended with both NO_3^- and $C_6H_{12}O_6$ (+Electron Acceptor +Glucose). NO_3^- consumptions led to the production and subsequent reduction of headspace N_2O to N_2 during Phases I and II in all treatments. The rate of net N_2O reduction was notably slower in the latter part of Phase II (Net N_2O reduction rates days 14 to 28 = -0.1318 µM day^{-1} for the +Electron Acceptor +Glucose

treatment) than in the beginning (Net N_2O reduction rates days 14 to 28 = -0.8702 μM day^{-1} for the +Electron Acceptor +Glucose treatment), where the reduction rate slowed as headspace N_2O decreased in both the +Electron Acceptor and +Electron Acceptor +Glucose treatments.

NO_3^- and SO_4^{2-} concentrations measured at the first time point were greater than the input solution value for the Natural and +Glucose treatment groups (Figure 2.1, Table 2.1). Although some SO_4^{2-} reduction occurred alongside the initial NO_3^- consumption, most SO_4^{2-} reduction overlapped with methanogenesis during Phase II (days 8 to 29), reducing SO_4^{2-} concentrations and producing headspace CH_4 (Figure 2.1). SO_4^{2-} concentrations reached a minimum value by day 28 in all treatments. In Phase II, NO_3^- concentrations began to increase from their minimum values as remnant N_2O disappeared for all treatments. Additionally, porewater pH began to increase from its minimum values at the end of Phase II.

In Phase III, porewater pH increased significantly to an average value of 6.53 ± 0.25 for all treatments. Simultaneously, NO_3^- and SO_4^{2-} concentrations increased, reaching steady concentrations by days 36 to 50 in all treatments except for the +Electron Acceptor treatment. In the +Electron Acceptor treatment group, SO_4^{2-} reduction continued to occur more slowly throughout the entire incubation. A small increase in NO_2^- occurred in each treatment group during days 35 to 50 (Phase III), with the largest increase occurring in the Natural treatment.

Headspace CH_4 concentrations decreased from their peak values throughout Phase III in most treatment groups except the treatment, +Electron Acceptor +Glucose, which experiences CH_4 consumption between days 28 and 35; however, a new CH_4 peak develops by Day 49. Despite the consumption of CH_4 in all treatments throughout Phase III, final headspace concentrations of CH_4 values are stable and non-zero. The addition of $C_6H_{12}O_6$ to the soil jars resulted in an extended period of methanogenesis, particularly in the +Glucose treatment, which did not receive excess e^-

acceptors. The Natural and +Electron Acceptor treatment groups followed similar temporal trends and recorded similar peak CH_4 values despite the SO_4^{2-} reduction experienced in the +Electron Acceptor treatment group. The period of CH_4 oxidation was coupled with an increase in porewater pH, which was not observed in the abiotic control group (Figure S1 in Appendix A). Unlike the other treatments, the +Electron Acceptor +Glucose treatment group, which experienced a secondary CH_4 peak on day 50, the pH did not continue to increase between the last two time points and instead stabilized at a lower value (pH = 6.26 ± 0.4). The Natural treatment group experienced the largest increase in pH throughout Phase III, measured as 6.74 ± 0.09.

Concentrations of dissolved Fe and Mn fluctuate alongside each other during incubation, generally decreasing over the 50-day incubation. Saturation index calculations performed in PHREEQC indicate favourable conditions for FeS mineral precipitation in all treatments; however, stagnant concentrations of Fe and Mn in the Abiotic Control group suggest that the changes in Mn and Fe observed trends are resultant of increasing CEC with pH or biotic FeS mineral precipitation facilitated by Fe-oxide and sulfate reduction (Appendix A).

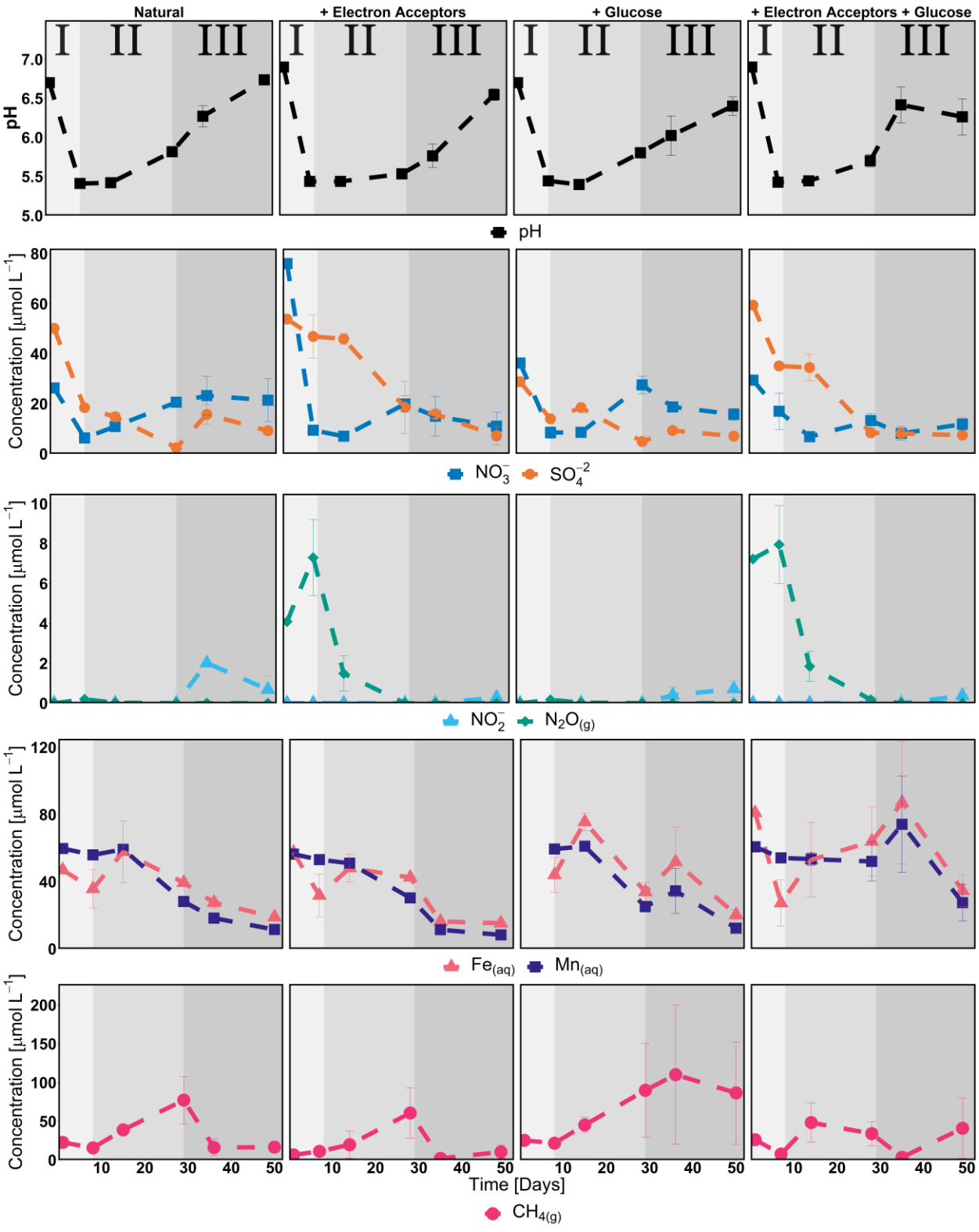

Figure 2.1: Concentrations of biogeochemical species overtime. Three distinct phases are observed: denitrification (Phase I), sulfate reduction and methanogenesis (Phase II), and AOM (Phase III).

Figure 2.2 outlines the net rates of production for the major e^- donors present in the soil, NH_4^+, and $C_2H_3O_2^-$. Calculated rates for the other measured low molecular weight organic carbon are available in the Supplementary Materials Figure 2.2. The majority of $C_2H_3O_2^-$ oxidation and fermentation occurred during Phase II alongside methanogenesis and the major period of SO_4^{2-} reduction, resulting in the net consumption of 7.35 ± 1.14 mM over 14 days (Figure 2.2). A small fluctuation in $C_2H_3O_2^-$concentration occurred during Phase I, which is attributed to the production and consumption of H_2 (see Figure S2 in Appendix A). In all treatment groups, the rate of acetate consumption approached 0 in Phase III, suggesting that $C_2H_3O_2^-$ had come to equilibrium (final concentration of 1.18 ± 0.6 mM) or that another e^- donor was being consumed.

Overall, NH_4^+ concentrations decreased over time in all treatment groups (net consumption); however, the consumption rates were more steady relative to $C_2H_3O_2^-$ trends. Rates of NH_4^+ production were more variable in treatment groups amended with e^- acceptors and/or donors (Figure 2.2). In the +Electron Acceptor and +Glucose treatments, NH_4^+ consumption was close to zero during denitrification (Phase I), suggesting that NO_3^- reduction was likely using another e^- donor. Similar $C_2H_3O_2^-$ to net rates of NH_4^+ approached zero in all treatments during Phase III.

Low rates of organic acid and NH_4^+ oxidation occur in Phases I and III of the soil incubation, despite NO_3^- and SO_4^{2-} reduction occurring in these phases, indicating that other unmeasured or hidden consumption e^- donors (*e.g.*, Fe^{2+}, H_2S) may be used at these times. This effect is particularly notable in the +Electron Acceptor treatment group, which received excess NO_3^- and SO_4^{2-}, but appears to have the lowest organic acid and NH_4^+ consumption during these time points. Energetically-favourable dissimilatory denitrification to ammonia (DNRA) coupled to Fe, or S oxidation may explain the prolonged period of SO_4^{2-} reduction experienced by the

+Electron Acceptor treatment. Concentrations of NH_4^+ and $C_2H_3O_2^-$ remained constant in the abiotic control group (1.76 ± 0.1 mM and 7.8 ± 1.3 mM, respectively; Figure S2 Appendix A), suggesting that the consumption and production of the e^- donors are biotic.

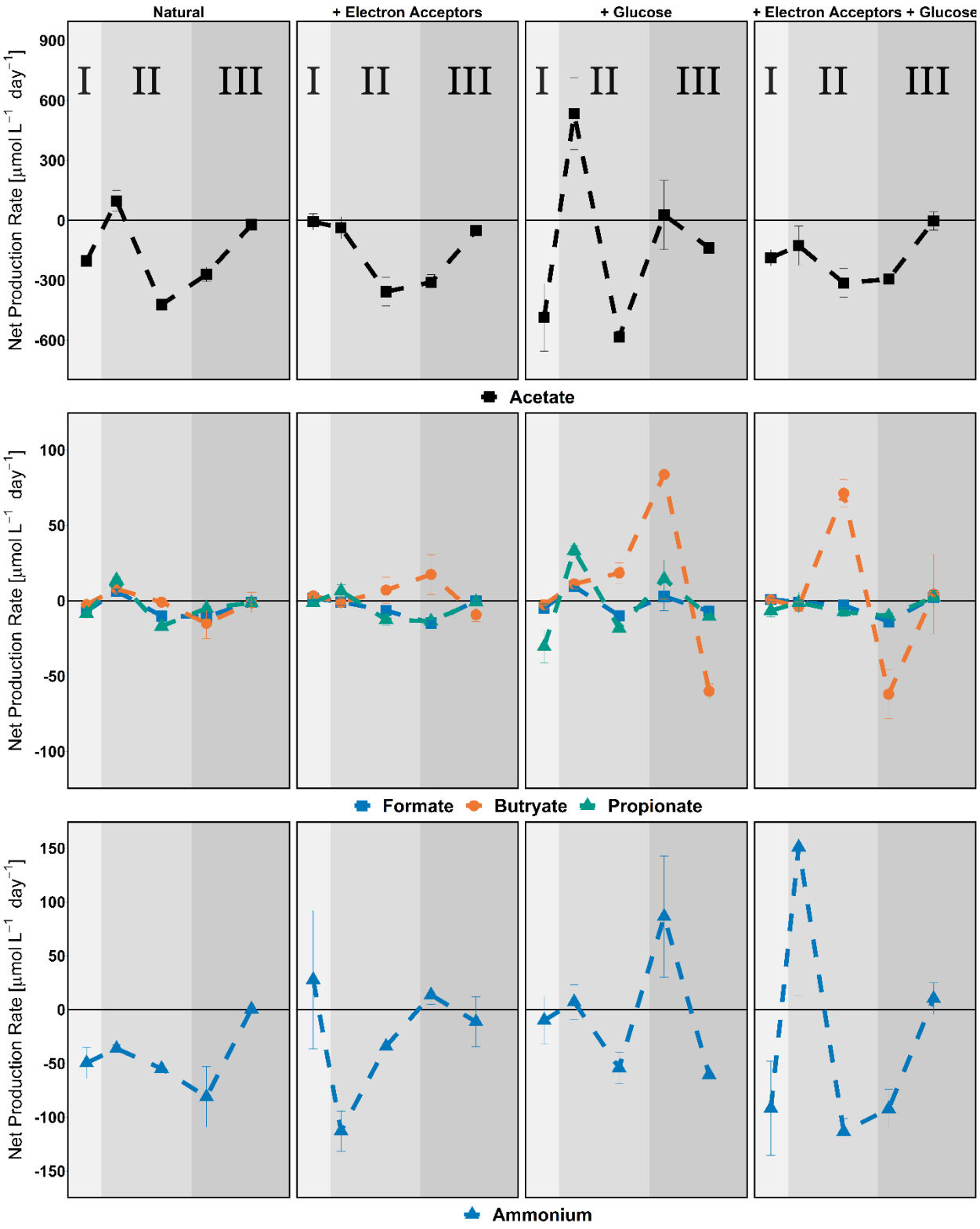

Figure 2.2: Net production rates of organic acids and ammonium throughout the incubation. Rates are calculated as the difference in concentration between two times points and plotted at the time mid-point for their calculation.

2.4.2 Solid Phase Analysis

SEM images reveal relevant concentrations of redox-active Mn and Fe as well as small scale minerals, including Fe and Mn associated with oxygen, and framboidal FeS minerals (Figure 2.3), providing indirect evidence of Fe^{3+} and SO_4^{2-} reduction. These minerals appear to be associated with plant debris, appearing within and around organic structures.

Average results from the 10 samples used in the hydroxylamine extraction indicate 19.96 µmol poorly crystalline Fe and 7.92 µmol Mn per gram dry soil. These quantities amount to 503.8 ± 66.4 and 200.1 ± 26.4 µmol Fe^{3+} and Mn^{4+}, respectively. The total CEC was determined to be 0.7331 meq g^{-1} at a pH 4.8, consistent with the published range of peat (Rezanezhad *et al*., 2016). Calcium was the dominant exchangeable cation with an exchangeable concentration of 0.679 meq g^{-1}. However, an increase in CEC is expected as pH climbs during Phases II and III, potentially masking Fe and Mn precipitation, reduction or oxidation reactions (see Appendix A).

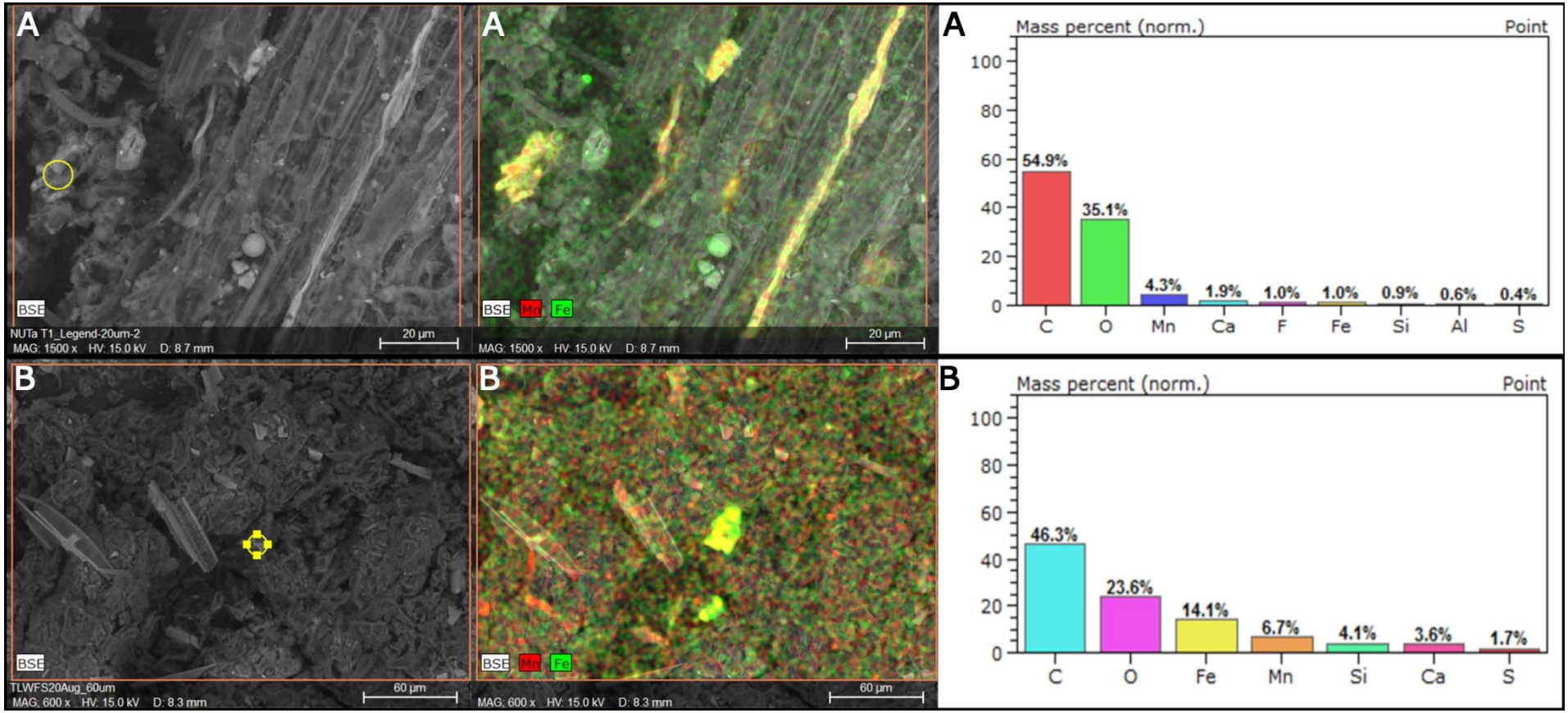

Figure 2.3: SEM images of the incubated soil samples indicating the presence of Mn-oxides and FeS minerals (A), and Fe- and Mn-oxides (B).

2.4.3 Energetics Calculations

Average calculated Gibbs energy values for the favourable catabolic reactions are presented in Table 2.3 for each identified Phase. For reactions where the change in Gibbs energy is negative, the reaction is considered energetically favourable, releasing energy to its surroundings and the catalyzing microorganisms if it proceeds. The calculated Gibbs energies indicate that denitrification coupled to Fe or S oxidation reactions (reactions 1 and 2, Table 2.3) are thermodynamically favourable at all points of the incubation period for each treatment. The most negative Gibbs energy values occurred during Phases I and III, where NO_3^- and NO_2^- concentrations were highest.

Calculations for Gibbs energy yielded negative values for anammox reactions where MnO_2 is the e^- acceptor and positive values for $Fe(OH)_3$ and SO_4^{2-} reduction reactions. AOM Gibbs energy values were negative for all e^- acceptors (NO_3^-, NO_2^-, MnO_2, $Fe(OH)_3$, and SO_4^{2-}) throughout the incubation period. For anammox and AOM reaction pathways utilizing N, Mn and Fe, the Gibbs energy values were the most favourable for anammox, and AOM reaction pathways during Phase II, where pH was the lowest and CH_4 was the highest (Figure 2.1). This relationship is extrapolated in Figures 2.4 and 2.5, where average activities from all treatments at peak CH_4 concentration were used to calculate ΔG_{cat} over a range of pH (4 to 8) and temperature (-5 to 30˚C). Figures 2.4 and 2.5 demonstrate the relationship between the ΔG_{cat}, pH, and temperature for anammox and AOM, respectively. In both figures, the reactions' Gibbs energies decrease (*i.e.*, energetic favourability increases) as pH and temperature decrease, or in other words, under acidic and cold conditions. Endothermic SO_4^{2-} reduction based anammox is the only exception to this trend. AOM paired to NO_3^-, NO_2^- or SO_4^{2-} reduction appeared to be less dependent on porewater pH spanning only a range of 5 kJ mol^{-1} e^- compared to the 20 to 40 kJ mol^{-1} e^- range of reactions with $Fe(OH)_3$ and

MnO_2. For AOM paired to either SO_4^{2-} or $Fe(OH)_3$ reduction, the calculated Gibbs energy was found to exceed the equilibrium point, reaching energetically unfavourable (positive) values under warm and alkaline conditions.

Table 2.3: Calculated ranges of Gibbs Energies calculated for experimental conditions throughout the incubation period.

e^- Donor	Reaction Number	Balanced Catabolic Reaction	$\Delta\overline{G}_r$ [kJ / mol e^-]		
			Phase I	**Phase II**	**Phase III**
Fe^{2+}	1	$0.2NO_3^- + Fe^{2+} + 2.4H_2O \rightarrow 0.1N_2 + Fe(OH)_3 + 1.7H^+$	-68.18	-64.34	-69.36
H_2S	2	$NO_3^- + 0.25H_2S + H_2O \rightarrow NH_4^+ + 0.25SO_4^{2-}$	-55.37	-55.63	-55.66
NH_4^+	3	$NH_4^+ + 6Fe(OH)_{3(s)} + 10H^+ \rightarrow NO_2^- + 6Fe^{2+} + 16H_2O$	+32.71	+29.56	+34.33
	4	$NH_4^+ + 0.75SO_4^{2-} \rightarrow NO_2^- + 0.75H_2S + H_2O + 0.5H^+$	+52.44	+52.81	+53.17
	5	$NH_4^+ + 4MnO_{2(s)} + 6H^+ \rightarrow NO_3^- + 4Mn^{2+} + 5H_2O$	-21.17	-22.11	-20.3
$CH_{4(aq)}$	6	$CH_{4(aq)} + 1.6NO_3^- + 1.6H^+ \rightarrow H_2CO_3 + 0.8N_{2(g)} + 1.8H_2O$	-110.81	-111.10	-110.02
	7	$CH_{4(aq)} + 8Fe(OH)_{3(s)} + 16H^+ \rightarrow H_2CO_3 + 8Fe^{2+} + 21H_2O$	-24.60	-28.10	-22.28
	8	$CH_{4(aq)} + SO_4^{2-} + 2H^+ \rightarrow H_2CO_3 + H_2S + H_2O$	-4.04	-3.72	-2.82
	9	$CH_{4(aq)} + 4MnO_{2(s)} + 8H^+ \rightarrow H_2CO_3 + 4Mn^{2+} + 5H_2O$	-82.72	-84.73	-81.98

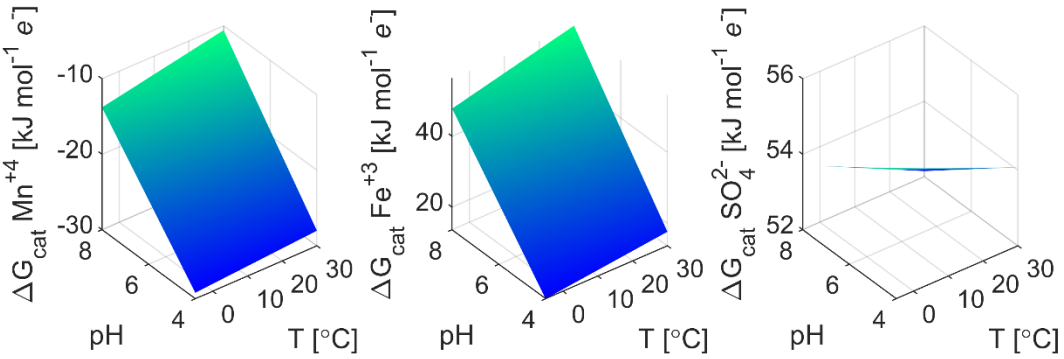

Figure 2.4: Surface area plots for the Gibbs Energy of catabolic anammox reactions. Values are calculated using averaged activity data from each soil treatments methane peak time-point.

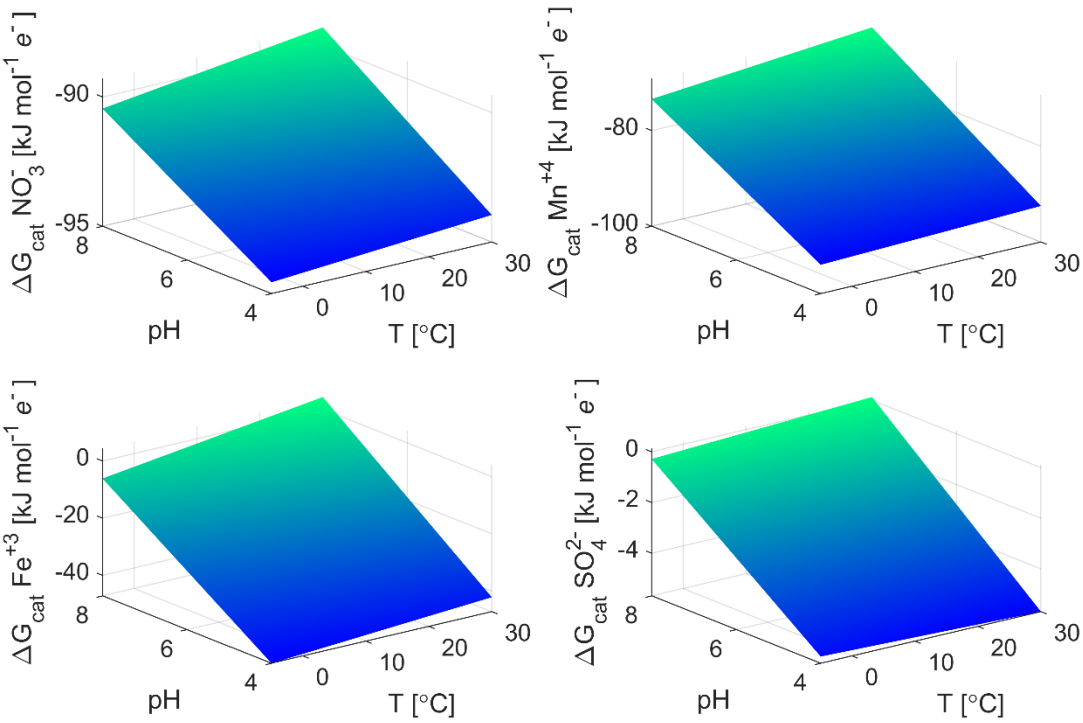

Figure 2.5: Surface area plots for the Gibbs Energy of catabolic anaerobic oxidation of methane reactions. Values are calculated using averaged activity data from each soil treatment's methane peak time-point.

2.5 Discussion

In this experiment, a closed incubation was used to simulate the hydrogeochemical conditions experienced by soils throughout the winter, where frozen soil may trap biogenic gases (van Bochove *et al*., 2001) and a lack of precipitation inputs may induce static hydraulic and geochemical conditions. We observed that the availability of e^- donors and acceptors exert an essential control on GHG emissions and water quality during the anoxic or "frozen" period.

2.5.1 Recycling of TEAs: Denitrification

In Phase I, NO_3^- consumption produced N_2O, which was further reduced to N_2 during Phase II (Figure 2.1). Headspace N_2O was consumed more slowly throughout Phase II for the treatments amended with e^- acceptors, sustaining high concentrations of the potent GHG as NO_3^- removal continued in soil porewater. Reduced rates of N_2O reduction can be attributed to the low temperature (5˚C) of the soil incubation (Phillips *et al.*, 2015) and change in pH to acidic conditions, which are less favourable for denitrification (Van Den Heuval *et al.*, 2011). Our observations of N_2O buildup and slowed consumption are consistent with winter observations of N_2O produced at depth under frozen soil (Burton and Beauchamp, 1994; Koponen *et al.*, 2004; Yanai *et al*., 2011). However, N_2O is often reduced before soil thaw, contributing less to the overall spring thaw N_2O efflux (Wagner-Riddle *et al.*, 2008).

Throughout the denitrification period (Phase I), organic acid consumption appeared steady, indicating a preference toward inorganic e^- donors, such as NH_4^+, Fe^{2+} and S. This effect is visible particularly in the +Electron Acceptor group whose net production rates of $C_2H_3O_2^-$ and NH_4^+ are close to zero despite increased NO_3^- and N_2O reduction between Days 1 and 14 (Figures 2.1 and

2.2). Under Phase I's experimental conditions, the reduction of NO_3^- paired to Fe^{2+} oxidation was determined to be less energetically favourable than $C_2H_3O_2^-$ oxidation (See Table S2 Appendix A). Yet, dissolved Fe^{2+} and sulfide (*i.e.*, H_2S and HS^-) oxidation by denitrification has been observed separately in the presence of $C_2H_3O_2^-$ in another study (Cardoso *et al*., 2006), leading to increased NH_4^+ concentrations resultant of DNRA (Burgin and Hamilton, 2008; Coby *et al.*, 2011). Additionally, the oxidation of FeS minerals has been observed in wetland environments, mobilizing S as SO_4^{2-} and recycling previously reduced TEA for future redox reactions involving C, N and S (Haaijer *et al.*, 2007). Although the apparent co-occurrence of NO_3^- and SO_4^{2-} reduction may mask the effects of DNRA, this reaction is most evident in the treatments which did not receive $C_6H_{12}O_6$ as an e^- donor where initial SO_4^{2-} concentrations were double the input level in the Natural Treatment, unlike in its +Glucose Treatment counterpart. Ultimately, chemolithotrophic denitrification may result in increased concentrations of e^- acceptors (Fe^{3+} and SO_4^{2-}) and donors (NH_4^+) for future reactions.

We hypothesized that this denitrification-based recycling of TEAs would continue into Phase III, stimulated by the cyclical creation of NH_4^+ from DNRA and consumption of NH_4^+ producing NO_2^- and NO_3^- for future Mn-oxide mediated anammox. This pathway may be further stimulated by the presence of reduced Fe and S, which promote DNRA (Zou *et al*., 2020). The recycled TEA from this network could then be utilized for future oxidation reactions, effectively masking their use and perpetuating “cryptic nutrient cycles”.

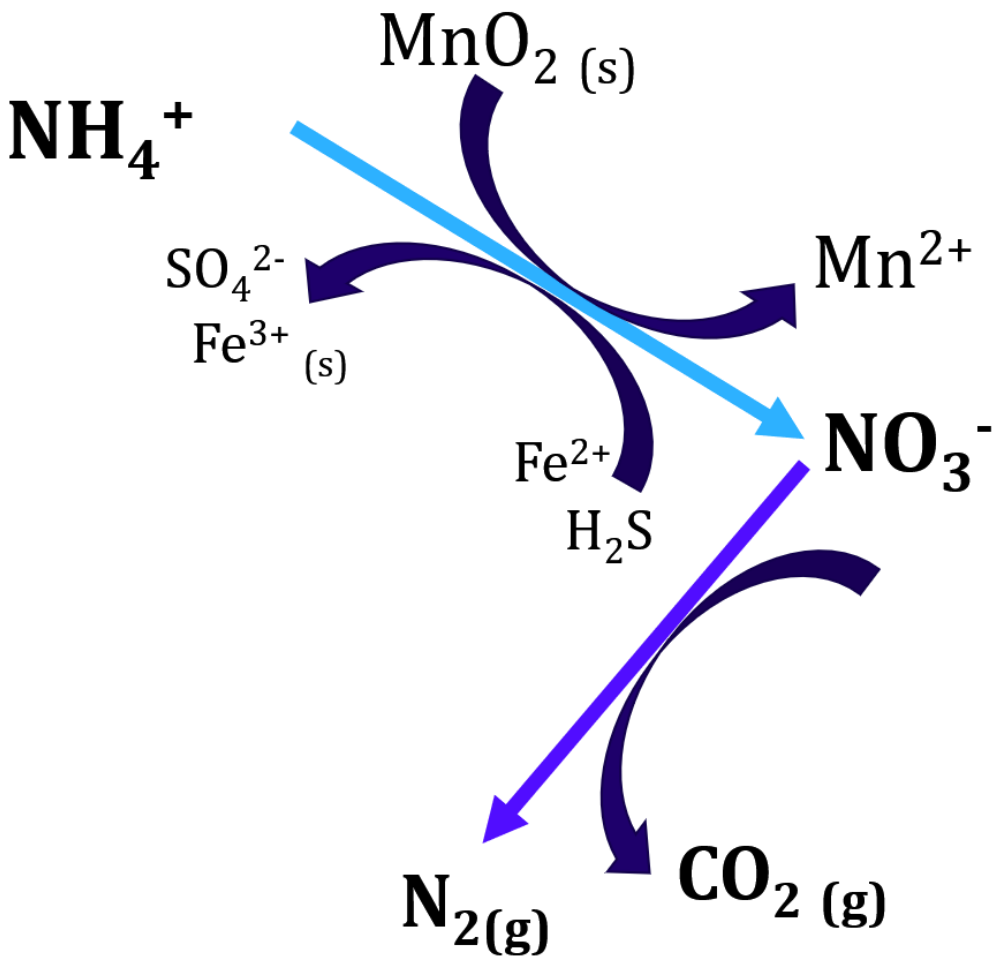

Figure 2.6: Conceptual understanding of coupled biogeochemical cycling occurring in the incubated soils. Chemical reactions involve anammox, anaerobic oxidation of methane (AOM) and dissimilatory nitrate reduction to ammonia.

2.5.2 Anammox: NO_3^- Regeneration

Initially high concentrations of NH_4^+ decreased throughout the incubation period and correlated with increasing concentrations of NO_3^- and NO_2^- as well as slowed rates of N_2O reduction during Phases II and III. Anammox is often paired to denitrification, wherein NH_4^+ is consumed alongside NO_2^- or N_2O, producing N_2 (Thamdrup, 2012). However, bioenergetic calculations support the anaerobic oxidation of NH_4^+ to NO_3^- during MnO_2 reduction throughout

the entirety of the incubation period (Table 2.3). This reaction pathway has been observed previously (Javanaud *et al*., 2011; Fernandes *et al*., 2014) and is substantiated by the presence of Mn-oxide minerals. As anammox occurs throughout the incubation, NO_3^- is consistently replenished as an e^- acceptor for denitrification, which may in-turn oxidize reduced Fe and S as discussed in *2.5.1*. The delayed consumption of N_2O may further reflect this, as NO_3^- reduction (produced from anammox) continues to produce N_2O, extending its tenure. Moreover, production of NH_4^+ via Fe- and S- driven denitrification has been observed to promote anammox in natural and wastewater- fed artificial wetlands due to increased NH_4^+ concentrations (Jones *et al.*, 2017; Zou *et al*., 2020).

Increased NO_3^- and NO_2^- concentrations related to anammox are a relatively new microbial metabolism carried out by distinct and slow-growing bacteria (Thamdrup, 2012). In this study, the anammox reaction network was sustained throughout the incubation, producing increasing or stable non-zero concentrations of NO_3^- and NO_2^- despite ongoing SO_4^{2-} reduction and CH_4 production and consumption. Our observations suggest that anammox can produce NO_3^- or NO_2^- when NH_4^+ concentrations are sufficiently high (Figures 2.1 and 2.2). Freshwater wetlands are already an ideal habitat for anammox-capable bacteria and archaea, where redox fluctuations are common (Zhu *et al.*, 2010). Hence, a closed environment, such as the winter soils, may promote inorganic e^- donors' consumption through relatively stagnant conditions and increased NH_4^+ availability and may also provide a suitable environment for slow-growing anammox organisms to thrive.

2.5.3 Syntrophic Anaerobic C and N Cycles

Chemical transformations of nutrients in the subsurface are strongly influenced by microbial activity and energetic needs (Thullner and Regnier, 2019). Microbial metabolisms are generally observed in sequential order, consuming e^- acceptors that yield the most energy first in the redox ladder (Bethke *et al.*, 2011). As a result, lower energy reactions such as SO_4^{2-} reduction or methanogenesis reactions are often suppressed in favour of more energetically favourable TEAs (*e.g.*, NO_3^-, Mn^{4+}). During this study, overlaps within the redox ladder were observed, including increasing NO_3^- concentrations alongside high CH_4 concentrations and potential methanogenesis. Traditionally, NO_3^- reduction yields more energy than CH_4 producing pathways (*e.g.*, $C_2H_3O_2^-$ fermentation or CO_2 reduction during hydrogen-based methanogenesis) and is predicted to occur before CH_4 generation. We posit that our observation of sustained or increasing concentrations of oxidized N species is not a contradiction to the TEA redox ladder. We attribute these results to reaction kinetics and an effective e^- donor preference under e^- acceptor limited conditions, complicated by long time steps (14 days) between some measurements. Utilizing both reaction kinetics and thermodynamics, the consumption of e^- donors appears to occur in a logical order.

During Phase I, suitably high concentrations of reduced Fe and S result in an exergonic DNRA favoured over microbial growth using $C_2H_3O_2^-$ oxidation. Although denitrification using $C_2H_3O_2^-$ yields more energy (Table S1 Appendix A), $C_2H_3O_2^-$ has been observed to build-up in the environment as other inorganic e^- donors are preferentially consumed (Duddlestone *et al.*, 2002). The DNRA oxidizes Fe and S, therefore removing its reactants while adding to existing concentrations of NH_4^+. Once DNRA concludes, a threshold concentration of CH_4 must be produced for AOM (Thullner *et al.*, 2007), thus $C_2H_3O_2^-$ oxidation and anammox prevail (Table 2.3). During Phase II, the observed increase in NO_3^- is driven by anammox, and CH_4

concentrations result from recently ceased methanogenesis, as evidenced by near-zero $C_2H_3O_2^-$ consumption in Phase III. The oxidative consumption of CH_4 follows closely until CH_4 concentrations are suitably low and kinetically unfavourable.

Although significant concentrations of NH_4^+ and organic acids were consumed throughout the experiment, less NO_3^-, NO_2^-, CO_2, and CH_4 were produced than what was estimated utilizing reaction stoichiometries (Appendix A). In Phase III, non-zero concentrations of the TEAs SO_4^{2-}, NO_3^-, and NO_2^- are sustained during AOM, suggesting that soil microbes shift between e^- donors as CH_4 availability declines. The elevated, non-zero concentrations of NO_3^-, NO_2^-, and SO_4^{2-} are resultant of anammox and prolonged DNRA behaving close to steady-state towards the end of the incubation. In contrast, during late Phase II and early Phase III, newly formed TEAs were consumed quickly to meet microbes' energetic needs during AOM. This unique reaction network is supported by MnO_2 reduction coupled to NH_4^+ oxidation, a thermodynamically favourable system within the context of the Mn species we considered (see Table 2.3). Within redox-fluctuating zones, Mn may be renewed on a seasonal basis when thaw occurs, and the water table eventually lowers, allowing the ingression of O_2 for abiotic Mn oxidation (Olivie-Lauquet *et al*., 2001; Rezanezhad et al., 2014; Pronk and Mellage *et al*., 2020). Organic matter, humic substances, and $C_2H_3O_2^-$ may also contribute to these reaction pathways by stimulating the biogeochemical network with e^- shuttling (Saxton *et al*., 2016; Valenzuela *et al*., 2017, 2019, 2020; He *et al*., 2019).

2.5.4 AOM and Anammox: Bioenergetics & Environmental Sensitivity

Sequential (or "coupled") anammox and AOM have been previously observed under controlled soil experiments (Haroon *et al*., 2013) but have often been dismissed in terms of real-world evidence and effect on a large scale (Smemo and Yavitt, 2011; Thamdrup, 2012). The slow

growth rates of the microbes capable of anammox or AOM have contributed to this idea (Kartal *et al*., 2013). However, wetlands have been deemed an ideal habitat for anammox microbes stemming from their relatively stagnant conditions and redox fluctuations (Zhu *et al.*, 2010). The static hydrology, trapping of biogenic gas, and anaerobic conditions experienced by wetlands throughout the winter may increase their habitability for anammox microbes in addition to the reaction networks' energetic favourability.

Under winter soil conditions, frozen soil limits the release of biogenic gases and plant nutrient uptake, enabling the accumulation of both CH_4 and NH_4^+. High NH_4^+ concentrations produced by freezing-induced cell lysis and reduced plant uptake may further increase the thermodynamic and kinetic favourability of anammox, facilitating NH_4^+ consumption as an e^- donor throughout the winter (Patel *et al*., 2018). We observed that under the extended closed system conditions (50 days), reactant concentrations (*e.g.*, pH, NH_4^+, Mn, CH_4) were sufficiently high to create thermodynamically favourable conditions. Furthermore, as CH_4 concentrations increase due to methanogenesis, the microbial community for AOM may grow as AOM becomes more kinetically favourable (Smemo and Yavitt, 2007).

Additionally, both AOM and anammox are potential autotrophic reactions, removing inorganic C as biomass in the overall metabolic reaction. Hence the winter (under-ice) conditions may also contribute a small CO_2 sink function to the soil system's reaction network. Within the soil incubation experiment, we observed a decrease in total inorganic carbon for the treatments with unmatched concentrations of e^- acceptors and donors and a plateau in DIC for the Natural and +Electron Acceptor +Glucose treatment (Figure S3 Appendix A). These observations are indicative of autotrophic reactions. However, this biogeochemical network's proposed role in the C cycle is susceptible to the duration of anoxia (*i.e.*, duration of soil freezing) in addition to the

effects of environmental factors on reaction thermodynamics. Therefore, while northern wetlands are one of the largest natural sources of atmospheric CH_4, combined anammox and AOM in wetlands may limit seasonal CH_4 release, despite anoxic conditions that limit aerobic CH_4 oxidation.

2.5.5 AOM and Annamox: Thermodynamic sensitivity

Our calculations demonstrate that environmental factors, pH and temperature, strongly influence the reaction network's thermodynamic favourability in addition to NH_4^+ and CH_4 concentrations. For most AOM and anammox pathways, hydrogen ions (H^+) are consumed as the reaction proceeds (Table 2.3), potentially increasing pH as the reactions proceed in poorly buffered systems, as was observed in Phase III of this soil incubation experiment (see Figure 2.1). Figures 2.4 and 2.5 demonstrate this relationship where the ΔG_r value is more negative for reactions that consume H^+. Similarly, the proposed reactions are exothermic, increasing in energetic favourability at lower temperatures. Hence, AOM and anammox are likely to have increased energetic favourability in northern wetlands, which are often cold and acidic (Dedysh, 2009). As the energetic favourability of a reaction increases (*i.e.*, as the Gibbs energies become more negative), reaction rates may increase as they become less thermodynamically limited (LaRowe *et al.*, 2012). However, temperature also exerts direct kinetic control on reaction rates and microbial activity, which are likely stronger influences on the reaction rate (Hobbs, 2013; Schipper *et al*., 2014; Alster *et al*., 2020).

The effect of pH on these reactions' Gibbs energies would impose an additional temporal constraint in poorly buffered systems, which may be unable to maintain a low pH as anammox and AOM continue to consume H^+ (Figure 2.1). We predict that in well-buffered soils (*e.g.*, enriched

in carbonates) AOM and anammox reactions may persist for a longer duration than in soils with a low pH buffering capacity. This thermodynamically-informed interpretation also provides a framework to predict how pH controls CH_4 and NH_4^+ oxidation rates.

2.5.6 Environmental Implications

Different biogeochemical processes throughout the soil incubation period produced peak concentrations of associated chemical end products at varying time points (Figure 2.1). Temporal fluctuations of dissolved NO_3^-, NO_2^-, NH_4^+, SO_4^{2-}, and DOC (*e.g.,* $C_2H_3O_2^-$), as well as headspace N_2O, CO_2, and CH_4, represent trade-offs to GHG emissions and water quality. For example, the consumption of NH_4^+ and subsequent production of toxic NO_2^- or the removal of CH_4 and NO_3^- through AOM. In the context of our experimental design, the observed concentrations of geochemical species would have been released to the atmosphere or neighbouring freshwater had the soil 'thawed' at that time, resulting in different pulse releases of headspace GHG and export of dissolved species (*e.g.,* Fe^{2+}, NO_2^-, $C_2H_3O_2^-$). Ultimately, these observed temporal trends emphasize the importance of the winter season duration under dynamic climate conditions in vulnerable cold region organic soils for GHG emissions and water quality.

The closed experiment system facilitated the buildup and eventual consumption of NH_4^+ and CH_4, which were traditionally considered to be anaerobic biogeochemical end products only exported from soil systems (Strous and Jetten, 2004). Our energetic calculations support these consumption trends and indicate that both consumption reactions, AOM and anammox, were energetically favourable. The production and accumulation of the two reactants, NH_4^+ and CH_4, would also make both reactions kinetically advantageous. The reproduction of NO_3^- and NO_2^- by anammox resulted in an extended period of denitrification and further recycling of these TEAs by

(chemo)lithoautotrophic reactions such as AOM. We identify that the oxidative consumption of CH_4 was driven by anammox wherein AOM occurs, in part, using NO_3^- produced by MnO_2-mediated anammox reactions (Fernandes *et al*., 2014). In natural systems, denitrification-driven AOM represents a "net good" for GHG emissions and water quality, resulting in a reduction of both CH_4 (and CO_2) emissions and dissolved NO_3^- and NO_2^- concentrations, which may otherwise have continued to increase in the soil porewater.

The observed coupling of anammox with AOM creates a unique and sensitive biogeochemical reaction network, where NO_3^- or NO_2^- produced by anammox are strong e^- acceptors capable of oxidizing CH_4 in the imposed environment. However, remnant concentrations of porewater NO_3^- and NO_2^- produced by anammox may detract from water quality if leached to groundwater and aquatic ecosystems. Additions of chemical energy (NO_3^- and SO_4^{2-} and glucose) to the soil impacts the potential chemistry of exported porewater through shifts in the timing of denitrification, methanogenesis, anammox, and AOM. The addition of a labile carbon source (e^- donor) to the +Glucose treatment resulted in larger and sustained CH_4 concentrations during Phase III without additional TEAs. In the treatment amended with labile carbon as well as NO_3^- and SO_4^{2-} (+Electron Acceptor + Glucose), a unique secondary CH_4 peak occurred at the last sampling time point, likely related to the steady pH value reached by this time (Figure 2.1). Overall, the addition of N, a redox-active element, to an anoxic soil system from natural and anthropogenic sources is likely to shift a soil system's natural equilibrium, driving a cascade of biogeochemical reactions and prolong the duration of N_2O and potentially CH_4.

2.6 Conclusions

Under conditions of restricted gas exchange between the atmosphere and organic soil and low temperature, we identified three phases in our experiments exhibiting distinct temporal trends in the dominant biogeochemical species and their associated processes throughout the winter. Under the imposed anoxic conditions, the progressive reductive consumption of the TEAs NO_3^- and SO_4^{2-} proceeded as expected through Phase I. Under the prolonged closed system conditions (Phases II & III), we observed the occurrence of anaerobic chemolithoautotrophic reactions, including AOM and anammox. Stable DOC concentrations reflect the favourability of AOM and anammox reactions over organic carbon oxidation despite high concentrations of $C_2H_3O_2^-$ persisting in porewater. Energetic calculations support the interpretation that the consumption (by oxidation) of CH_4 and NH_4^+, which accumulated under the imposed closed system conditions, could be coupled to NO_3^-, Fe^{3+}, Mn^{4+}, and SO_4^{2-} reduction. The energetic calculations also demonstrate that these reactions are especially favourable under the experiment's low temperature and acidic conditions. The presence of amorphous MnO_2 meaningfully supports this reaction network because of their ability to oxidize NH_4^+ to NO_3^- and H_2S to SO_4^{2-} for CH_4 consumption, another example of the tight coupling of C, N and S biogeochemistry in organic soils.

The identified AOM and anammox metabolisms have a negative feedback-type relationship with pH, where porewater becomes more alkaline and less conducive to AOM or anammox reactions as they proceed, eventually allowing a new CH_4 peak to develop. Our results suggest that CO_2 and CH_4 emissions from northern seasonally ice-covered organic soils are likely much lower than their production rates by respiration and methanogenesis despite the absence of oxygen to oxidize biogenic CH_4. Overall, these results highlight the importance of ice cover duration to winter soil processes, provide insight into their biogeochemical end products, and demonstrates a

need to further understanding of the coupled cycling of C, N, and S during the winter season where chemical energy-limited organic soils may have limited exchange with the atmosphere.

Acknowledgements

Funding was provided by the Canada Excellence Research Chair (CERC) program in Ecohydrology and Natural Sciences and Engineering Research Council Grants (Strategic Partnership Grant: STPGP494652-16 and Advancing Climate Change Science in Canada: ACCPJ 536050-18). We thank Mrs. Marianne VanderGriendt, Shuhuan Li, Carly Kemp, and Alison Mao for their assistance with sample analyses. We also thank Natural Resources Canada for access to the field site where the soil sample was collected.

3 Rates of Anaerobic Methane Oxidation in the Environment: An Energetic Approach

3.1 Introduction

In Chapter 2, the role of chemical energy availability was investigated to improve our understanding of how changes in e^- donor and acceptor availability (*e.g.*, from land-use management) may influence carbon (C) and nitrogen (N) dynamics in wetlands soils under seasonally frozen conditions. An observation of syntrophic C and N cycles resulted in the anaerobic oxidations of ammonium and methane (anammox and AOM, respectively). These observations were supported by thermodynamic calculations and extrapolated to compute the Gibbs Energy of the catabolic reaction ($\Delta G^{\circ}_{rT_{cat}}$) over a range of temperature and pH, highlighting AOM and anammox's dependencies on environmental factors. Although many observations of both anammox and AOM exist, these reactions' rates are necessary to understand how these geomicrobial networks may impact greenhouse gas emissions over time to limit CH_4 release. This chapter's main objective is to develop a bioenergetics informed framework capable of estimating the maximum rate of AOM reactions using the concentration of CH_4, the identity of the terminal electron acceptor (TEA) and temperature.

3.1.1 The Role of Soils in Methane Emissions

CH_4 is a potent greenhouse gas (GHG) with 25 times the global warming potential of carbon dioxide (CO_2) on a 100-year time scale (Forster *et al*., 2007). CH_4, the most reduced form of inorganic C and penultimate step of organic matter mineralization, is naturally produced by anaerobic reactions mediated by microorganisms who gain energy from its production. Wetlands are the single most significant contributor of atmospheric CH_4 globally, emitting an average of

164 Tg CH_4 each year from the anaerobic decomposition of organic matter (Bridgham *et al.*, 2013). An additional 103 Tg CH_4 per year is estimated to be released from organic C exported from soils into inland freshwater reservoirs (*e.g.*, lakes, impoundments, and rivers) (Bastviken *et al.*, 2011). Conversely, marine environments emit a combination of biogenic CH_4 and gas released from geologic deposits (*e.g.*, hydrocarbon seeps, methane hydrate reservoirs) (Saunois *et al.*, 2016). Weber *et al.* (2019) found that oceanic CH_4 emissions are driven by biogenic CH_4 ebullition in shallow coastal waters resulting in total oceanic CH_4 emissions between 6 and 12 Tg per annum. Amplified warming effects in mid- to high- latitude regions, dominated by wetland soils, are expected to mobilize C stores in perennially and seasonally frozen soils and further stimulate ongoing SOM degradation. The predicted increase in CH_4 emissions may have vital feedback to climate change mechanisms furthering warming effects (Dean *et al*., 2018); however, the quantity of CH_4 released to the atmosphere from terrestrial environments depends not only on its production but also its transport and consumption (See Figure 3.1).

The primary sink for CH_4 in the environment is methanotrophy, wherein CH_4 is oxidized to CO_2 by oxygen (O_2) as it diffuses out of the anoxic zone. However, as a robust e^- donor, CH_4 may be used as a reducing agent under O_2 limited conditions using an alternative TEA. AOM is an energy-yielding pathway (Gibbs Energy, $\Delta G^{\circ}_{r298} < 0$) for chemosynthetic organisms who derive their energy by catalyzing oxidation reactions using inorganic e^- donors. Under standard conditions, AOM is an exergonic reaction when paired with the reduction of common TEAs found in anoxic environments, including nitrate (NO_3^-), nitrite (NO_2^-), ferric iron (Fe^{3+}, *e.g.*, goethite, ferrihydrite), manganese (Mn^{4+}, *e.g.*, pyrolusite), and sulfate (SO_4^{2-}) (Bethke *et al.*, 2011) (Table 3.1). Intuitively, as CH_4 diffuses out of the subsurface, it crosses through these redox zonations and may be consumed for energy production (Figure 3.1). Yet, AOM has predominantly been

observed in marine environments and less frequently in freshwater ecosystems, contributing substantially more CH_4 to the atmosphere each year.

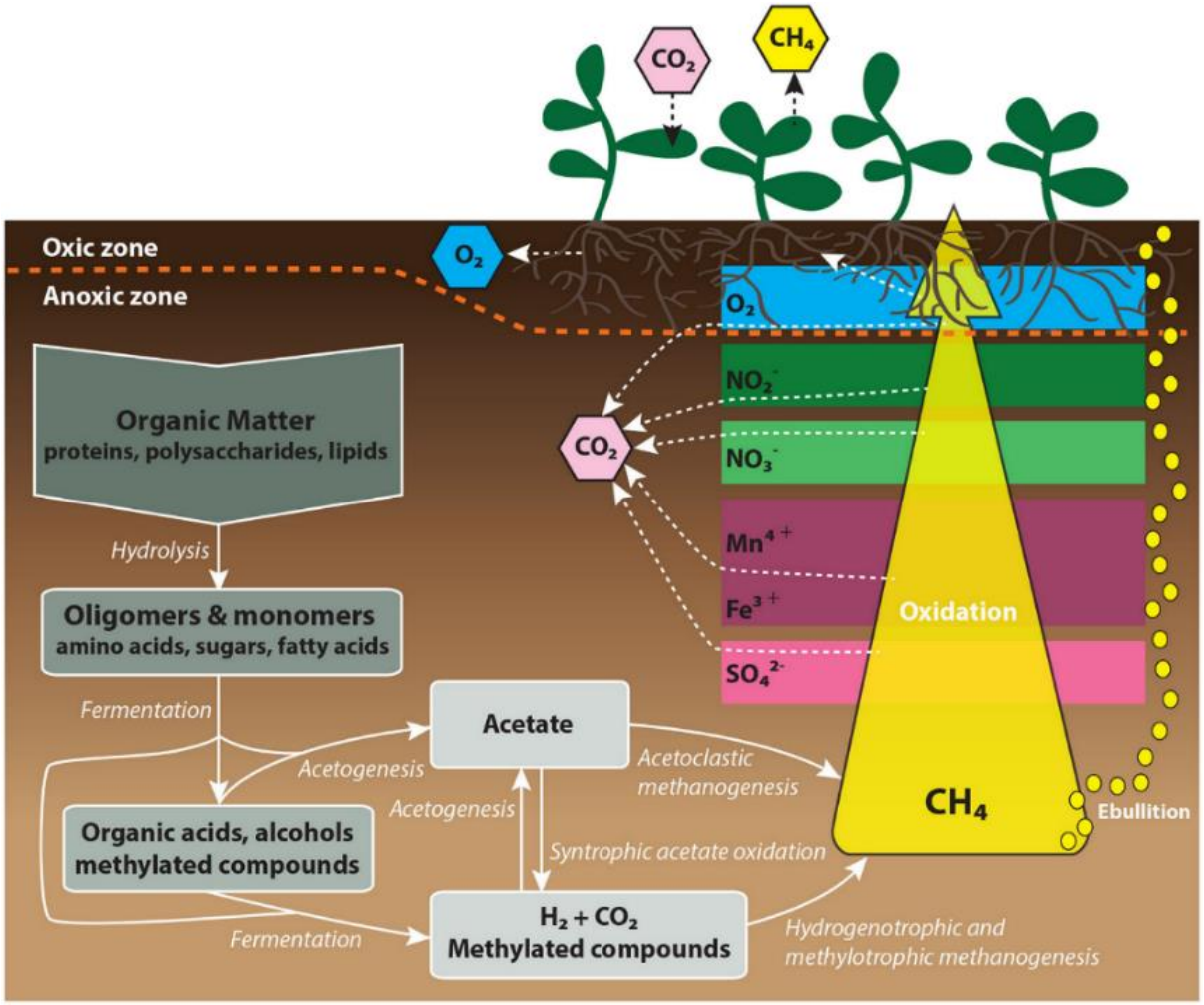

Figure 3.1: Conceptual understanding of CH_4 production, consumption and transport in terrestrial environments (Dean *et al*., 2018).

Table 3.1: Balanced catabolic CH_4 oxidation reactions and their associated Gibbs energy under standard conditions.

TEA	Reaction Number	Balanced Catabolic Reaction	ΔG°_{r298} [kJ / mol e^-]
O_2	1	$2O_{2_{(aq)}} + CH_{4_{(aq)}} + \rightarrow H_2CO_3 + H_2O$	-107.32
NO_2^-	1	$CH_{4_{(aq)}} + 2.67NO_2^- + 2.7H^+ \rightarrow H_2CO_3 + 1.33N_{2_{(g)}} + 2.3H_2O$	-130.63
NO_3^-	2	$CH_{4_{(aq)}} + 1.6NO_3^- + 1.6H^+ \rightarrow H_2CO_3 + 0.8N_{2_{(g)}} + 1.8H_2O$	-104.68
Mn^{4+}	3	$CH_{4_{(aq)}} + 4MnO_{2_{(s)}} + 8H^+ \rightarrow H_2CO_3 + 4Mn^{2+} + 5H_2O$	-103.27
Fe^{3+}	4	$CH_{4_{(aq)}} + 8Fe(OH)_{3_{(s)}} + 16H^+ \rightarrow H_2CO_3 + 8Fe^{2+} + 21H_2O$	-63.03
SO_4^{2-}	5	$CH_{4_{(aq)}} + SO_4^{2-} + 2H^+ \rightarrow H_2CO_3 + H_2S + H_2O$	-13.66

In marine environments, AOM is estimated to consume upwards of 90% of produced CH_4 (Dale *et al.*, 2006); and the reaction is most commonly observed along the SO_4^{2-} reduction and methanogenesis interface where high concentrations of SO_4^{2-} alongside upward diffusing CH_4 drive a syntrophic reaction pathway (Iverson and Jorgensen, 1985). More recently, AOM has also been observed in marine environments using other e^- acceptors, including Fe- and Mn-oxides within and above the methanogenic zone (Beal *et al.*, 2009; Aromokeye, *et al.*, 2020). Amendments of NO_2^- to marine sediments have also yielded AOM observations expanding the dynamic range in TEA capacity for AOM organisms (Shen *et al.*, 2016). The absence of high SO_4^{2-} concentrations in freshwater settings had long perpetuated the ideology that AOM pathways would not be sustainable in these environments (*e.g.*, wetlands, lakes, or rivers), resulting in their more considerable contribution of biogenic CH_4 to the atmosphere. The growing interest in AOM has debunked this theory, with >602 articles available on the Web of Science studying various environments and reactions using different TEA (Figure 3.2).

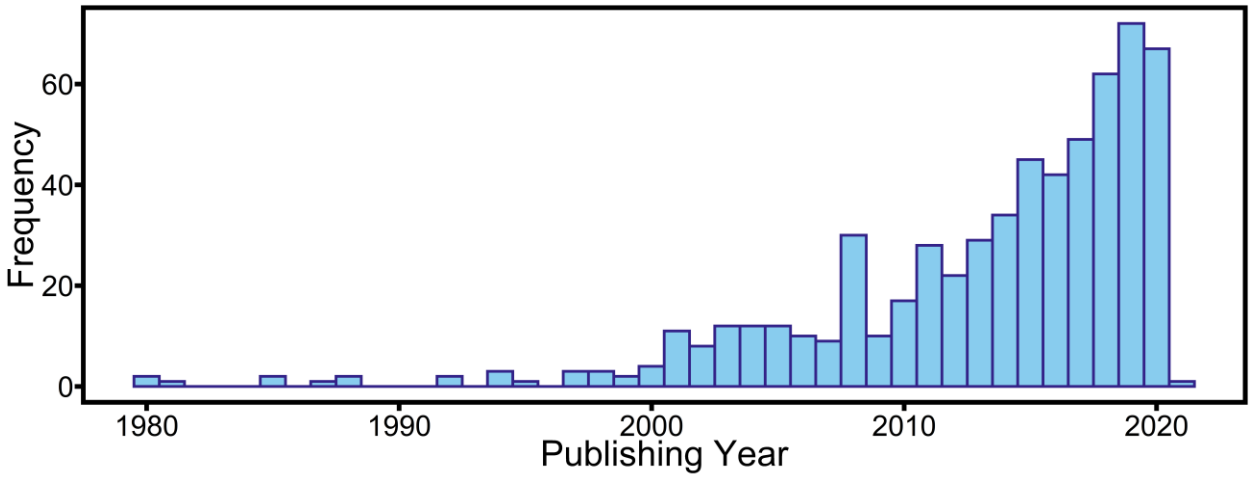

Figure 3.2: Publications in the Web of Science with "anaerobic oxidation of methane" included within the title or as a keyword.

Freshwater lakes have a demonstrated capacity for AOM (Martinez-Cruz *et al*., 2018), including a permanently frozen lake in Antarctica (Saxton *et al*., 2016). AOM in wetlands has been observed at high rates, up to 270 nmol cm^{-3} day^{-1} using Fe-oxides or SO_4^{2-} (Segarra *et al*., 2015) and at lower rates using natural organic matter as an e^- acceptor (Valenzuela *et al*., 2017). NO_3^- and NO_2^- additions to soil incubations have also been demonstrated to create favourable conditions for AOM (Noroi and Thamdrup, 2014; Shi *et al*., 2017), in some cases resulting in net-zero CH_4 emissions (Deutzmann *et al.*, 2014). A hidden link between anaerobic C and N cycles is recently hypothesized to provide NO_3^- and NO_2^- naturally for AOM through anammox (Hu *et al*., 2014), as discussed in Chapter 2 of this thesis. This phenomenon is masked by the proximity of the NO_3^- reducing zone to the aerobic layer and redox fluctuating zone where anammox bacteria thrive (Zhu *et al.*, 2010). The process of AOM paired to denitrification, or iron-oxide reduction (Hu *et al*., 2014; Segarra *et al*., 2015) is a previously overlooked CH_4 sink. Hence, Fe- and N-driven AOM rates should be considered a dynamic piece of the global C cycle, responding to environmental change (Zhu *et al.*, 2010).

3.1.2 Thermodynamic-Kinetic Models for AOM

The overall rate of reaction depends on the thermodynamic favourability and the availability of e^- donors and acceptors. In a biogeochemical system, the reaction rate can be predicted using Monod type kinetics with a thermodynamic factor for low energy environments, as discussed in Chapter 1 (Eq. 7). In the rate calculation, the substrate utilization rate is a fraction of the maximum rate determined by the thermodynamic and kinetic factors (F_T and F_K, respectively). The values of F_T and F_K range between 0 and 1, increasing as kinetic and thermodynamic limitations are removed. F_K is dependent on the availability of e^- donors and acceptors relative to their related

half-saturation constants K_S^{ED} and K_S^{EA}. Previously, the half-saturation constant for methane ($K_S^{CH_4}$) was unknown and assumed to be far greater than dissolved CH_4 concentrations (Dale *et al.*, 2006). In a kinetic simulation of marine AOM with SO_4^{2-} reduction by Dale *et al.* (2008) used a baseline K_S^{ED} equivalent to 1500 μM was used. The study yielded results similar to the expectation that AOM removes >90% of marine CH_4, determining that <1% of CH_4 from marine sediments reaches the water column. However, Yu *et al*. (2017) recently put forward a much smaller value for $K_S^{CH_4}$ of 83 μM determined from fitting experimental data using a kinetic model. The substantially lower value of $K_S^{CH_4}$ virtually eliminates the kinetic limitations derived from low dissolved CH_4 concentrations. This experiment was performed by incubating return activated sludge from North Middlessex, Ontario, Canada at 37˚C, and paired AOM with denitrification. Applying a singular K_S^{ED} to all environments may be difficult, as the substrate utilization can be organism-dependent and shaped by community composition and history (Pala-Ozkok *et al*., 2012).

3.1.3 Linear Free Energy Relationship

Thermodynamic calculations are not equivalent to the kinetic rate of reaction; however, they can be proportional. Marcus theory (Marcus, 1964) predicts a linear free energy relationship (LFER) between thermodynamic parameters and the kinetics of e^- transfer, including reduction-oxidation reactions catalyzed by microorganisms using similar reaction mechanisms and equilibrium fractionation factors (Silverstein, 2012; Joe-Wong *et al.*, 2019). In application, this produces a log-linear relationship between the reaction rate (r) and ΔG_r° predicting higher reaction rates for processes yielding the most energy. This relationship has been observed largely in abiotic reactions but has been applied for the microbially mediated reactions of Fe-oxide reduction (Bonneville *et al.*, 2009) and degradation of some organic compounds (Leffler and Grunwald,

1963; Luan *et al.*, 2015). The slope of the LFER best fit line typically has a value between 0 and 1 (Leffler and Grunwald, 1963). Although the relationship is empirical, LFERs are a powerful tool for estimating reaction rates and, by extension, the associated consumption and production of their chemical constituents (Bonneville *et al.*, 2009).

3.1.4 The Role of Temperature in Reaction Kinetics

The temperature of an environment (or experiment) may influence a microbially mediated reaction rate through the reactants' solubility and energy yield. Additionally, temperature exerts a significant influence over a microbial community's shape, growth, and activity level (Petterson and Baath, 2003; Sattley and Madigan, 2006; Robador *et al.*, 2009), in which microbial activity typically increases towards an optimal temperature and declines thereafter. Climate change-driven increases in temperature are also anticipated to enhance soil respiration (Kirschbaum, 1995, 2000; Davidson and Janssens, 2006). However, the optimum temperature for a microbial community can vary regionally, with annual and seasonal temperature regimes affecting community composition, as discussed by Petterson and Baath (2003). Microbial communities adapted to cooler climates may have optimal an optimal temperature for biomass growth below 30˚C. A study comparing SO_4^{2-} reduction rates in arctic and temperate marine sediments determined optimal temperatures of 22˚C and 33˚C for the arctic and temperate zone sediments, respectively (Sattley and Madigan, 2006).

A model developed by Rosso *et al*. (1993) linked the maximum microbial growth rate with cardinal temperature (minimum, optimum, and maximum) points for a microbial community (Eq. 3.1):

$$\mu_{max} = \begin{cases} T < T_{min},\ 0.0 \\ T_{min} < T < T_{max},\ \mu_{opt} f_{Temp} \\ T > T_{max},\ 0.0 \end{cases} \quad (3.1)$$

$$f_{Temp} = \frac{(T - T_{max})(T - T_{min})^2}{(T_{opt} - T_{min})[(T_{opt} - T_{min})(T - T_{opt}) - (T_{opt} - T_{max})(T_{opt} + T_{min} - 2T)]}$$

where μ_{max} [hr^{-1}] is the maximum specific growth rate, T [˚C] is the *in situ* or experimental temperature, T_{min}, T_{max}, and T_{opt} [˚C] are the minimum, maximum, and optimum temperatures for microbial growth, respectively, and f_{Temp} is the unitless temperature factor. This model was paired with an optimum pH for microbial growth, amplifying the temperature-dependency of microbial growth yields. Ultimately, maximal growth rates were predicted when microorganisms operate within their optimal temperature and pH ranges (Rosso *et al.*, 1995).

In this chapter, rates of AOM were investigated across various environments to construct a bioenergetics informed framework capable of estimating the rate of AOM as a function of CH_4 concentration, TEA, and temperature. AOM rates were collected from publications in addition to their associated environment, pH, temperature, identified TEA, and CH_4 concentration to compute the maximum reaction rate. Values for T_{min}, T_{max}, and T_{opt} were determined based on the AOM rates observed temperatures and applied to develop a LFER between maximum rate and energy yield at T_{opt}. Thus, reactions yielding more energy are anticipated to occur more rapidly, with the fastest reaction rates expected for the most thermodynamically favourable TEA (*i.e.*, NO_2^-). Overall, this chapter aims to review AOM rates from previous studies and construct a framework for predicting AOM, providing insight into how anaerobic CH_4 consumption limits emissions to the atmosphere.

3.2 Data Collection and Analyses

3.2.1 Data Collection

Data was collected from peer-reviewed articles reporting rates calculated from labelled or isotopic soil incubation experiments to develop a bioenergetics-informed framework for AOM rates. Articles were identified systematically by searching the Web of Science database and using cross-referencing. The methods used in each study were carefully screened to understand the experimental set-up, calculated rates and concentrations provided (*i.e.*, net rates, instantaneous rate, instantaneous concentration, etc.), and assess the suitability of the article. Data recorded from each article included the general environment type, field site and specific sample location (*e.g*, lake, depth), methods used for calculations, pH, incubation time and temperature, CH_4 concentration, CH_4 consumption rate, TEA identity, TEA concentration, TEA amendment, and any other relevant information or author observations (*e.g.*, thermodynamic computations completed by the author). From some studies, CH_4 concentrations and AOM rates were retrieved from plot digitization using the Plot Digitizer Java software. Digitized observations were noted during data collection, and values were rounded to have the same number of significant digits as the relevant axis. Overall, 23 papers were identified, providing 230 calculated AOM rates from isotopic or labelled carbon studies at 30 unique environments (Table 3.2); 122 of the identified AOM rates were appropriate to include in the $\bar{r}_{max}$ calculation.

Table 3.2: Selected papers for the rates study, including the number of points viable for the maximum rate calculations.

Publication	Number of Observations	
	Overall	**Included in $\bar{r}_{max}$ calculation**
Aromokeye *et al.* (2020)	1	1
Bar-Or *et al*. (2017)	1	1
Beal *et al.* (2009)	3	3
Bowles *et al.* (2019)	12	-
Egger *et al.* (2015)	1	1
Girguis *et al.* (2003)	7	-
Haroon *et al.* (2013)	1	1
Iverson *et al.* 1985	14	14
Iverson *et al.* 1987	11	-
Kip *et al.* (2012)	20	-
Martinez-Cruz *et al.* (2017)	1	1
Martinez-Cruz *et al.* (2018)	18	-
Noroi and Thamdrup (2014)	21	19
Raghoebarsing *et al.* (2006)	1	1
Saxton *et al.* (2016)	21	4
Segarra *et al.* (2015)	36	30
Shen *et al.* (2016)	28	23
Shi *et al*., (2017)	8	2
Sivan *et al*. (2011)	1	1
Valenzuela *et al*. (2017)	5	2
Valenzuela *et al*. (2020)	1	-
Weber *et al*. (2017)	12	12
Yu *et al.* (2017)	6	6
Total	***230***	***122***

3.2.2 Rate Calculations

The maximum rate of AOM was calculated using the collected data in a re-arranged and simplified version of Eq. 1.7, which utilizes the single-Monod equation and is independent of the biomass fraction (Eq. 3.2):

$$\bar{r}_{max} = R \cdot \left(\frac{[CH_4]_{(aq)}}{K_S^{CH_4} + [CH_4]_{(aq)}} \cdot F_T \right)^{-1} \tag{3.2}$$

where $[CH_4]_{(aq)}$ is the concentration of aqueous CH_4 calculated for articles reporting equilibrium headspace CH_4 concentrations. The factor F_T uses the $\Delta G^{\circ}_{R_{obs}}$ calculated for the catabolic reaction at the observation points temperature using the Gibbs-Helmholtz equation (Eq. 1.4). Three iterations of calculations were performed using $K_S^{CH_4}$ of 100 µM in the first iteration, 1500 µM in the second iteration, and a value of 100 and 1500 µM in the third iteration for freshwater and marine environments, respectively.

For studies reporting gaseous concentrations of headspace CH_4, the temperature-dependent dissolved fraction was computed using the Van't Hoff equation (Eq. 3.3) to determine the temperature-dependent equilibrium constant and Henry's Law (Eq. 3.4):

$$\ln K_{H_{obs}} = \ln K_{H_{298}} - \frac{\Delta H^{\circ}_R}{R} \left(\frac{1}{T_{obs}} - \frac{1}{298.15} \right) \tag{3.3}$$

$$[CH_4]_{(aq)} = K_{H_{obs}} \frac{[CH_4]_{(g)}}{R T_{obs}} \tag{3.4}$$

where $K_{H_{obs}}$ is the unitless equilibrium constant at the observation temperature, $K_{H_{298}}$ [mol L^{-1} atm^{-1}] is the equilibrium constant at 25˚C, ΔH°_R [kJ mol^{-1}] is the enthalpy of the reaction under standard conditions, T_{obs} [K] is the observation point's temperature, and R ([kJ mol^{-1} K^{-1}] and [L atm K^{-1} mol^{-1}] for equations 3.3 and 3.4, respectively) is the ideal gas constant. For articles

reporting dissolved CH_4 concentrations, the reported value was cross-checked with the temperature dependant CH_4 solubility ($K_{H_{298}}$= 1.29 × 10^{-3} M atm^{-1} at standard temperature and pressure (Stumm and Morgan, 1996)).

The AOM observation points occur across a variety of habitats with different temperature ranges. Hence, for comparison $\bar{r}_{max}$ is normalized by the f_{Temp} function (Eq. 8). Adding this function to Eq. 3.2 yields a final formula:

$$\bar{r}_{max} = R \cdot \left(\frac{[CH_4]_{(aq)}}{K_S^{CH_4} + [CH_4]_{(aq)}} \cdot F_T \cdot f_{Temp} \right)^{-1} \tag{3.5}$$

The values of T_{min}, T_{opt}, and T_{max} within the f_{Temp} function were determined using a non-linear optimization in R (nloptr package version 1.2.2.2; Ypma *et al*., 2020) to generate least-squares lines for the relationship between $\Delta G^{\circ}_{r_{opt}}$ and $\bar{r}_{max}$ (LFER). $\Delta G^{\circ}_{r_{opt}}$ was calculated using the Gibbs Helmholtz equation (Eq. 1.4) for the determined T_{opt} value. The constraints for optimization (presented in Table 3.3) were selected to maintain integrity for environmental conditions.

Table 3.3: Constraints applied to the optimization for f_{Temp} parameters. f_{Temp} values are always expected to be greater than zero for publications observing the reaction mechanism.

Variable	Constraint
T_{min}	$0℃ < T_{opt} < T_{obs_{min}}$
T_{opt}	$T_{min} < T_{opt} < T_{max}$
T_{max}	$T_{obs_{max}} < T_{max} < 45℃$
f_{Temp}	$0 < f_{Temp}$

To account for the various environments AOM rates collected from; the f_{Temp} optimization was computed in groups depending on the observation temperature. Up to five temperature groups were

used to produce T_{min}, T_{opt}, and T_{max} values tailored to the microbial community within an observation temperature range. This optimization was repeated for each of the three $K_S^{CH_4}$ iterations described earlier.

3.2.3 Assumptions

The AOM rates collected were retrieved from various publications using different methods, and the results were reported in different units. When appropriate data was unavailable from the methods section to compute between units, assumptions were made efficiently on an as-needed basis. These included assuming the porosity and particle density of the soil. For mineral soils, values of 0.5 and 2.6 g cm^{-3} were adopted for the porosity and particle density, respectively, and for organic soils, values of 0.85 and 1.3 g cm^{-3} were assumed (Ruhlmann *et al.*, 2006). For gas unit conversions, CH_4 was assumed to behave as an ideal gas at a pressure of 1 atm unless otherwise stated within the publication.

3.3 Results

3.3.1 Meta-data Synthesis

The collected data covers a wide range of freshwater and marine environments and temperatures (Figure 3.3), including AOM in freshwater and soda lakes, freshwater sediment, wetlands, and marine environments (*e.g.,* cold seeps, brackish wetlands). Observations of AOM from coastal wetlands containing saline water were classified as a marine environment. The freshwater sediment category is composed, primarily, of studies that amended sediment from lakes and ponds with wastewater sludge. Despite high concentrations of SO_4^{2-} driving AOM in marine

sediments, only one AOM rate study was produced for soda lake environments within the meta-data. No calculated rates of AOM in dammed reservoirs were obtained.

The most common TEA attributed to AOM was SO_4^{2-} followed by NO_3^-, NO_2^-, and Fe-oxides. Most NO_3^- and NO_2^- AOM observations were derived from studies amending sediment porewater with N regardless of environments. Additionally, a limited number of studies attributed the AOM reaction to natural organic matter (NOM), N_2O or Mn-oxides reduction, indicating their capacity to facilitate CH_4 oxidation when available. Without the amendment of TEA to the soil experiment, the e^- acceptor used for AOM was unclear using trends and stoichiometry for its identification. Roughly half (108) of the identified studies were unable to attribute the CH_4 oxidation to a singular TEA and could not be included in the AOM $\bar{r}_{max}$ calculation (Table 3.3). Additionally, in some studies, the author often attributed the AOM rate to a TEA with a disclaimer that the involvement of other TEAs could not be ruled out.

Of the collected 230 AOM data points, only 119 pH values were reported, limiting the ability to include pH as a function of AOM. Only seven publications (55 data points) reported both pH and a TEA and could be included in the $\bar{r}_{max}$ calculation. The energetic yield of AOM has a strong dependence on pH, as discussed in Chapter 2. Hence, the absence of pH data for AOM rate calculations is a short-coming for CH_4 oxidation due to its influence over the reaction's thermodynamic favourability and microbial growth rate.

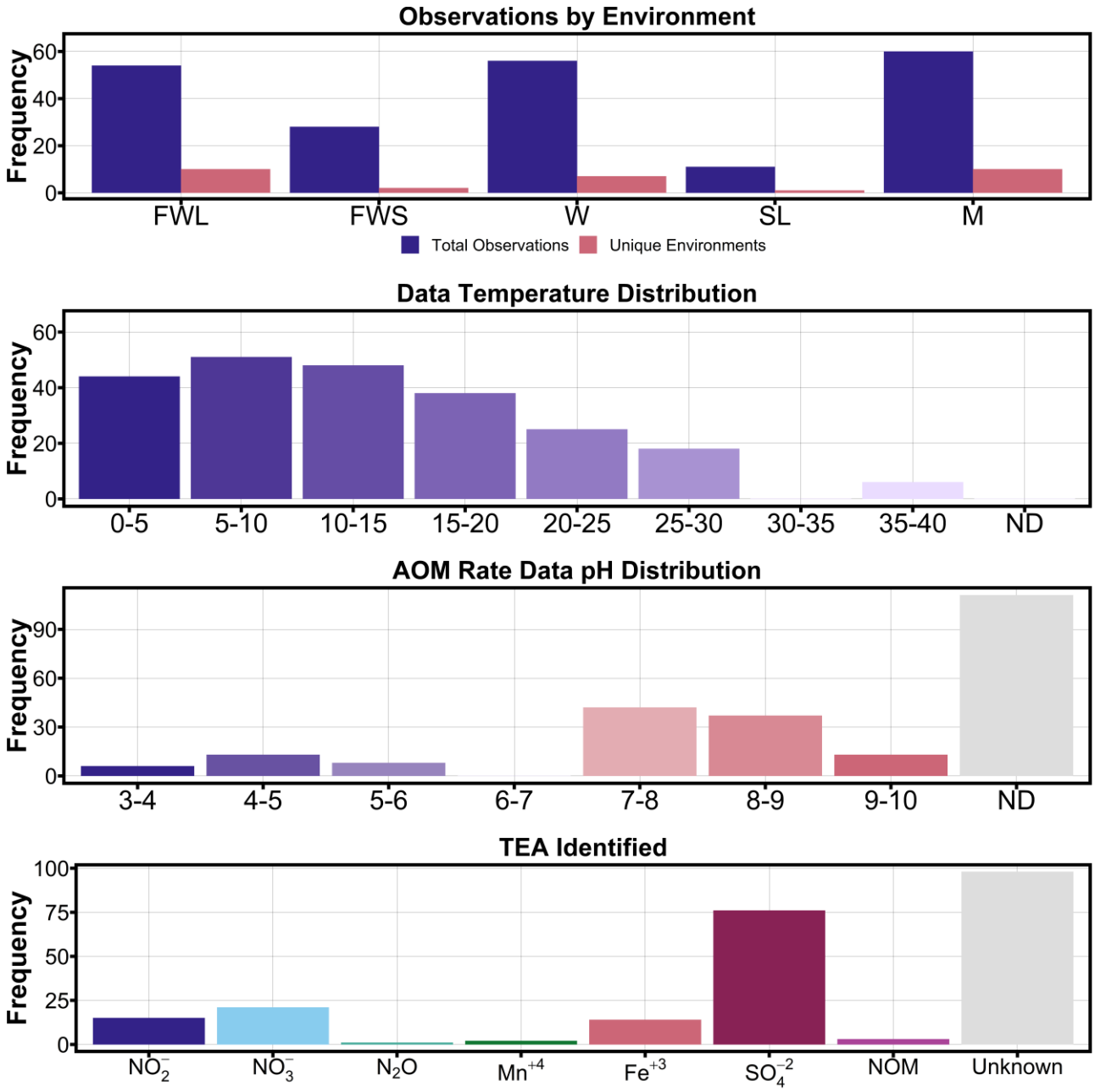

Figure 3.3: Metadata analysis of the collected anaerobic oxidation of methane rates demonstrating the data's distribution across environments, temperature, and pH as well as the e^- acceptor attributed to the reaction. FWL = freshwater lake, FWS = freshwater sediment, W = wetland, SL = soda lake, and M = marine.

3.3.2 AOM Rates in Different Environments

The reported rates of AOM in each publication demonstrate a universal capacity for CH_4 across freshwater and marine environments regardless of TEA amendment (Figure 3.4). Unamended freshwater environments (lakes, sediment and wetlands) appear to have a median rate of ~10^4 nmol L^{-1} day^{-1}, while unamended marine environments have a slightly higher AOM rate. The rate of AOM in soda lakes appears significantly lower at ~10^2 nmol L^{-1} day^{-1}. Notably, the observed rates were calculated using different methods and are not temperature corrected for their location within the classification. For instance, the unamended freshwater lake category contains a cluster of 16 points measured at Lake Fryxell, a perennially frozen lake in Antarctica. These AOM rates were measured at a temperature of 2.1˚C and ranged from ~$10^{-0.4}$ to ~$10^{1.3}$ nmol L^{-1} day^{-1}. In contrast, a study by Bowles *et al.* (2019) produced the highest known AOM rates (107 nmol L^{-1} day^{-1}) with the addition of up to 50 mM CH_4 to marine sediment incubated at 5˚C.

In the AOM rates reported for sediments amended with TEA, the largest rates appear in association with the energy level of the amended e^- acceptor (Figure 3.4). Overall, smaller ranges in AOM rates exist for sediments amended with TEA. Rates were highest in the freshwater sediment category where NO_3^-, a higher energy TEA, was added to the sediments from ponds and rivers. Although NO_2^- was amended to marine sediments for AOM, the average rate of AOM in the amended marine category was lower than that of either the freshwater lake or wetlands. Significantly fewer observations of wetland soils and soda lake sediments amended with TEA exist in contrast to the other environments.

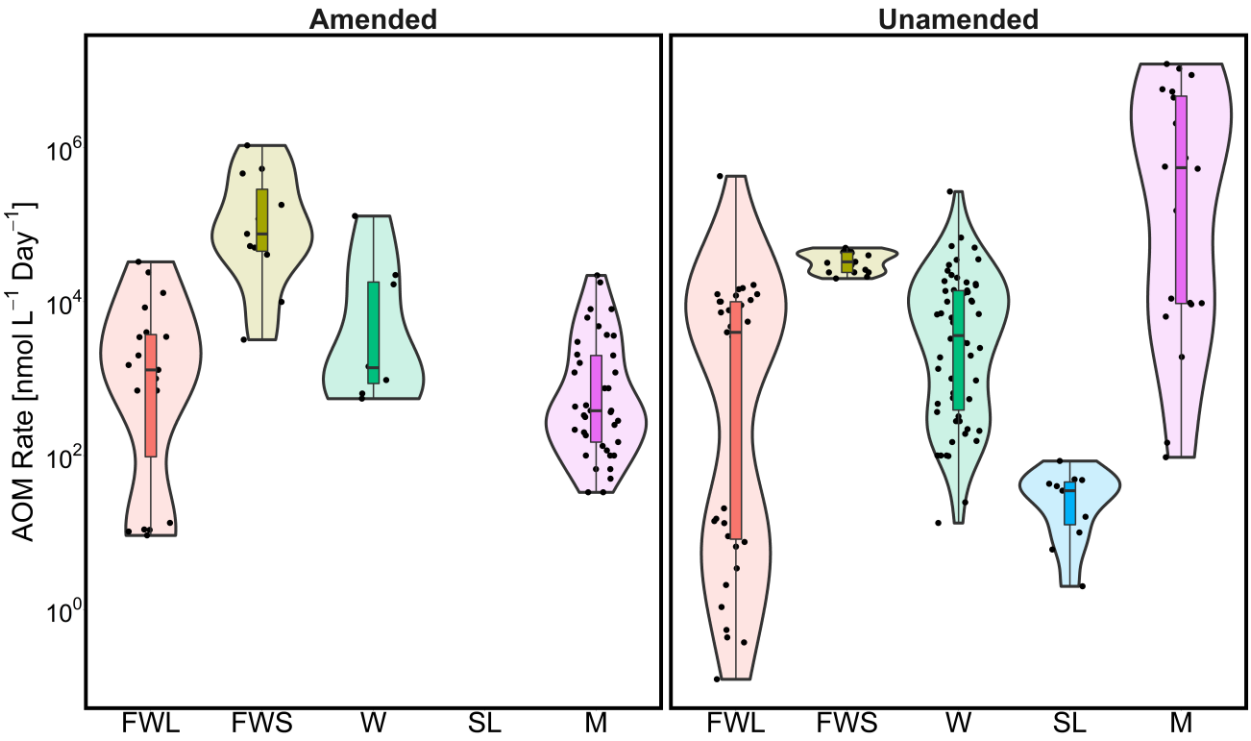

Figure 3.4: Ranges of anaerobic oxidation of methane rates observed across different environments using natural or amended concentrations of TEAs. FWL = freshwater lake, FWS = freshwater sediment, W = wetland, SL = soda lake, and M = marine.

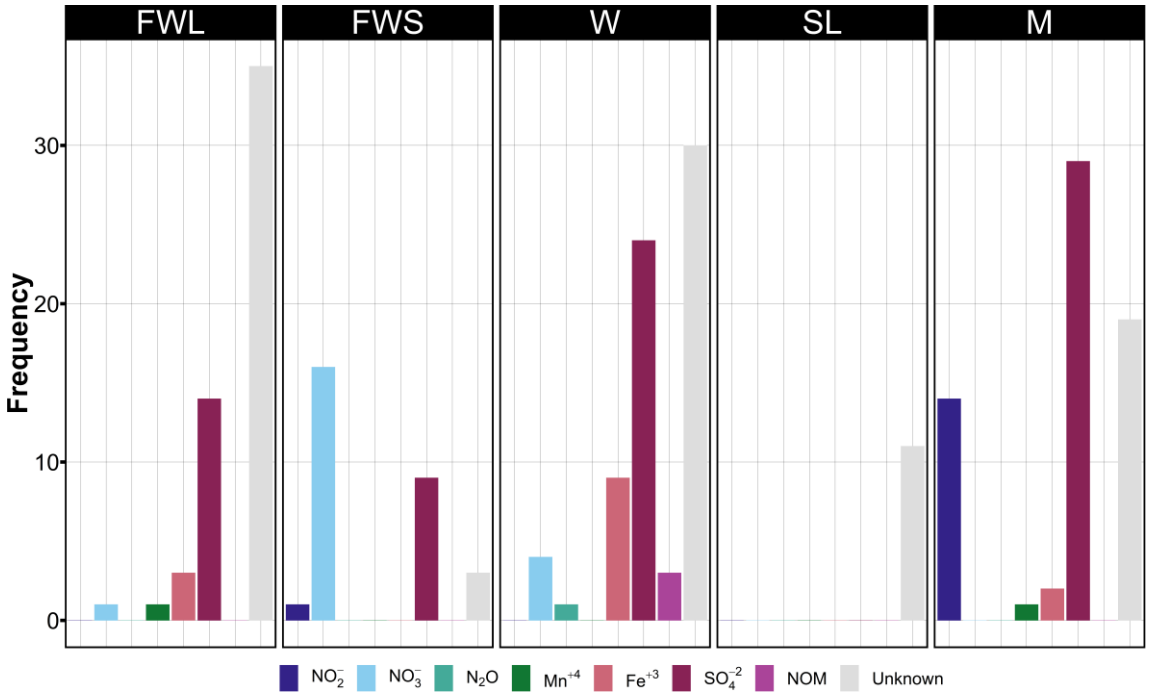

Figure 3.5: Identified e^- acceptors used in anaerobic oxidation of methane per environment. FWL = freshwater lake, FWS = freshwater sediment, W = wetland, SL = soda lake, and M = marine.

3.3.3 f_{Temp} Optimization and Maximum Rate Calculations

The f_{Temp} optimization resulted in a higher r^2 value for $\Delta G^{\circ}_{R_{opt}}$ and $\bar{r}_{max}$ in contrast to $\Delta G^{\circ}_{R_{obs}}$ and $\bar{r}_{max}$ with a *p*-value less than 0.005 for all runs with variable amounts of temperature bins (T-Bins) (Table 3.4). The r^2 value increased with an increasing number of temperature divisions for the f_{Temp} optimization. These increases in r^2 were small and ranged from 0.03 to 0.05 depending on the $K_S^{CH_4}$ value used to calculate $\bar{r}_{max}$. The lowest correlation between $\Delta G^{\circ}_{R_{opt}}$ and $\bar{r}_{max}$ occurs in the optimization using different $K_S^{CH_4}$ for freshwater and marine environments, while a higher $K_S^{CH_4}$ (1500 µM) resulted in a slightly better correlation overall (*i.e.*, regardless of the number of T-bins).

Optimal values of T_{min}, T_{max}, and T_{opt} vary with changes in the number of T-bins and $K_S^{CH_4}$ value(s) used (Table 3.5). Computed T_{min} values ranged from 0 to ~2.7˚C, the average T_{min} value computed between all $K_S^{CH_4}$ and T-bin runs is 1.34 ˚C with the highest T_{min} values occurring in the iteration with four T-Bins and a $K_S^{CH_4}$ equivalent to 1500 µM. Computed T_{max} ranged from ~12˚C to ~37˚C with an average value of ~26˚C overall. Similar trends occurred for the values of T_{opt} whose values ranged from ~2 to ~29˚C, and the average overall value was ~18.25˚C. The T_{opt} and T_{max} computed by the f_{Temp} optimization were lower than anticipated in most iterations and may not be representative of the environment with the chosen constraints.

Without the inclusion of the optimized f_{Temp} function, the initial log-linear relationship between $\Delta G^{\circ}_{R_{obs}}$ and $\bar{r}_{max}$ is low (Table 3.4). The standardization of the ΔG°_{R} and $\bar{r}_{max}$ values by an optimal temperature resulted in a better correlation and slightly elevated $\bar{r}_{max}$ values (Figure 3.3). Higher values of $K_S^{CH_4}$ result in a smaller F_K applied to the observed rates, and ultimately yield higher $\bar{r}_{max}$ for all TEAs. As hypothesized, $\bar{r}_{max}$ generally increases as ΔG°_{R} becomes more

negative; however, some outliers exist for all TEAs. Notably, with the inclusion of the f_{Temp} correction, $\bar{r}_{max}$ computed for AOM with NO_2^- reduction results in a cluster of low rates (Figure 3.4). The calculated range of $\bar{r}_{max}$ is large for all TEAs, ranging several orders of magnitude. Overall, NO_3^- has the highest average $\bar{r}_{max}$ computed (including all T-bin and $K_S^{CH_4}$ iterations; ~$10^{11.5}$ nmol L^{-1} day^{-1}) followed by Fe^{3+} (10^{10} nmol L^{-1} day^{-1}), SO_4^{2-} ($10^{9.5}$ nmol L^{-1} day^{-1}), and NO_2^- (10^9 nmol L^{-1} day^{-1}).

Table 3.4: Statistical results of the f_{Temp} optimization in comparison to the unstandardized relationship.

$K_S^{CH_4}[\mu M]$	f_{Temp} optimization				Without f_{Temp}		
	Number of T-Bins	r^2	p	Slope	r^2	p	Slope
1500	5	0.2586	3.05×10^{-9}	0.0650	0.0781	2×10^{-3}	0.0115
	4	0.2490	6.58×10^{-9}	0.0573			
	3	0.2525	4.98×10^{-9}	0.0637			
	2	0.2258	4.15×10^{-8}	0.0588			
	1	0.2278	3.56×10^{-8}	0.0610			
100	5	0.2576	3.29×10^{-9}	0.0619	0.0925	7.3×10^{-4}	0.010
	4	0.2575	3.33×10^{-9}	0.0588			
	3	0.2561	3.73×10^{-9}	0.0575			
	2	0.2440	9.90×10^{-9}	0.0580			
	1	0.2339	2.21×10^{-8}	0.0574			
$K_{S_{SW}}^{CH_4} = 100$ $K_{S_M}^{CH_4} = 1500$	5	0.2355	1.93×10^{-8}	0.0624	0.0681	4.0×10^{-3}	0.0104
	4	0.2289	3.26×10^{-8}	0.0615			
	3	0.2331	2.35×10^{-8}	0.0604			
	2	0.2094	1.44×10^{-7}	0.0552			
	1	0.1853	9.26×10^{-7}	0.05090			

Table 3.5: Calculated T_{min}, T_{opt}, and T_{max} values for the f_{Temp} optimization iterations.

# of T-Bins	Temperature Bin	Temperature Results								
		$K_S^{CH_4} = 100\ \mu M$			$K_S^{CH_4} = 1500\ \mu M$			$K_{S_{SW}}^{CH_4} = 100\ \mu M,\ K_{S_M}^{CH_4} = 1500 \mu M$		
		T_{min}[℃]	T_{opt}[℃]	T_{max}[℃]	T_{min}[℃]	T_{opt}[℃]	T_{max}[℃]	T_{min}[℃]	T_{opt}[℃]	T_{max}[℃]
5	$T_{obs} \leq 8$℃	1.0696	7.3225	11.8363	1.0247	6.8304	11.5503	1.0113	6.9199	11.8783
	8℃ $< T_{obs} \leq 16$℃	0.8321	1.9778	15.0100	0.9769	5.8739	15.0718	1.0091	6.1870	15.0100
	16℃ $< T_{obs} \leq 24$℃	1.0786	15.1783	22.2100	1.0059	17.1222	22.2552	0.9977	18.0157	22.2100
	24℃ $< T_{obs} \leq 32$℃	1.2567	29.2860	29.2993	1.0913	29.1097	29.1097	1.0548	29.02640	29.0265
	32℃ $< T_{obs}$	2.0070	23.5626	37.0100	1.3143	29.2673	37.0100	1.3190	29.1082	37.0100
4	$T_{obs} \leq 10$℃	1.0520	7.5730	12.4528	1.0275	7.8326	12.1143	1.0143	7.1960	13.0201
	10℃ $< T_{obs} \leq 20$℃	2.4716	20.9423	20.9477	1.3792	20.9788	20.9788	1.2532	21.2914	21.3041
	20℃ $< T_{obs} \leq 30$℃	2.6371	29.4850	29.4994	1.5298	29.7833	29.7841	1.5334	29.4484	29.4615
	30℃ $< T_{obs}$	2.6892	21.5508	37.0124	1.3974	28.5239	37.2614	1.5436	27.1720	37.0100
3	$T_{obs} \leq 15$℃	0.9825	8.1999	15.0100	0.9084	8.2903	15.0100	0.9735	8.3773	15.0100
	15℃ $< T_{obs} \leq 30$℃	0.6088	19.4586	29.9315	0.4089	14.4407	29.7527	0.6342	18.2358	29.7848
	30℃ $< T_{obs}$	1.6938	24.9058	37.0100	2.1502	21.9889	37.0100	1.8178	22.1616	37.0100
2	$T_{obs} \leq 19$℃	0.9923	9.370531	18.0100	0.75388	12.9114	18.0100	0.9365	9.2582	18.0100
	19℃ $< T_{obs}$	0.6290	27.1865	37.1608	0.1287	21.8329	37.0100	0.7446	28.5675	37.3975
1	$T_{obs} \leq 40$℃	0	17.4856	37.0100	0	18.3425	37.0100	0.3146	23.7534	37.0100

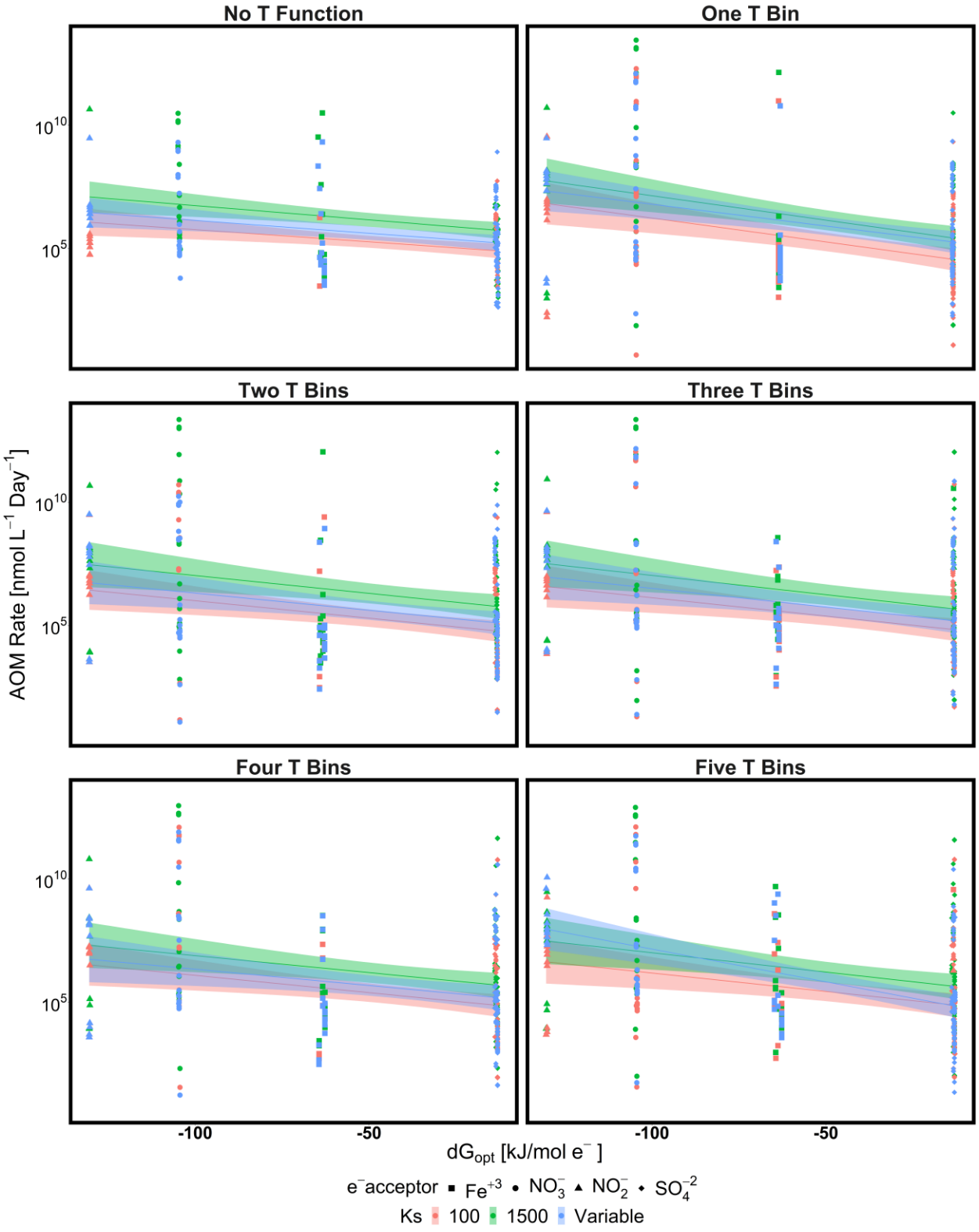

Figure 3.6: Graphical results of f_{Temp} optimization demonstrating the different slopes produced for *Ks* = 100 (red), 1500 (green), and var (blue). Variable K_S values used 1500 and 100 µM for marine and freshwater environments, respectively.

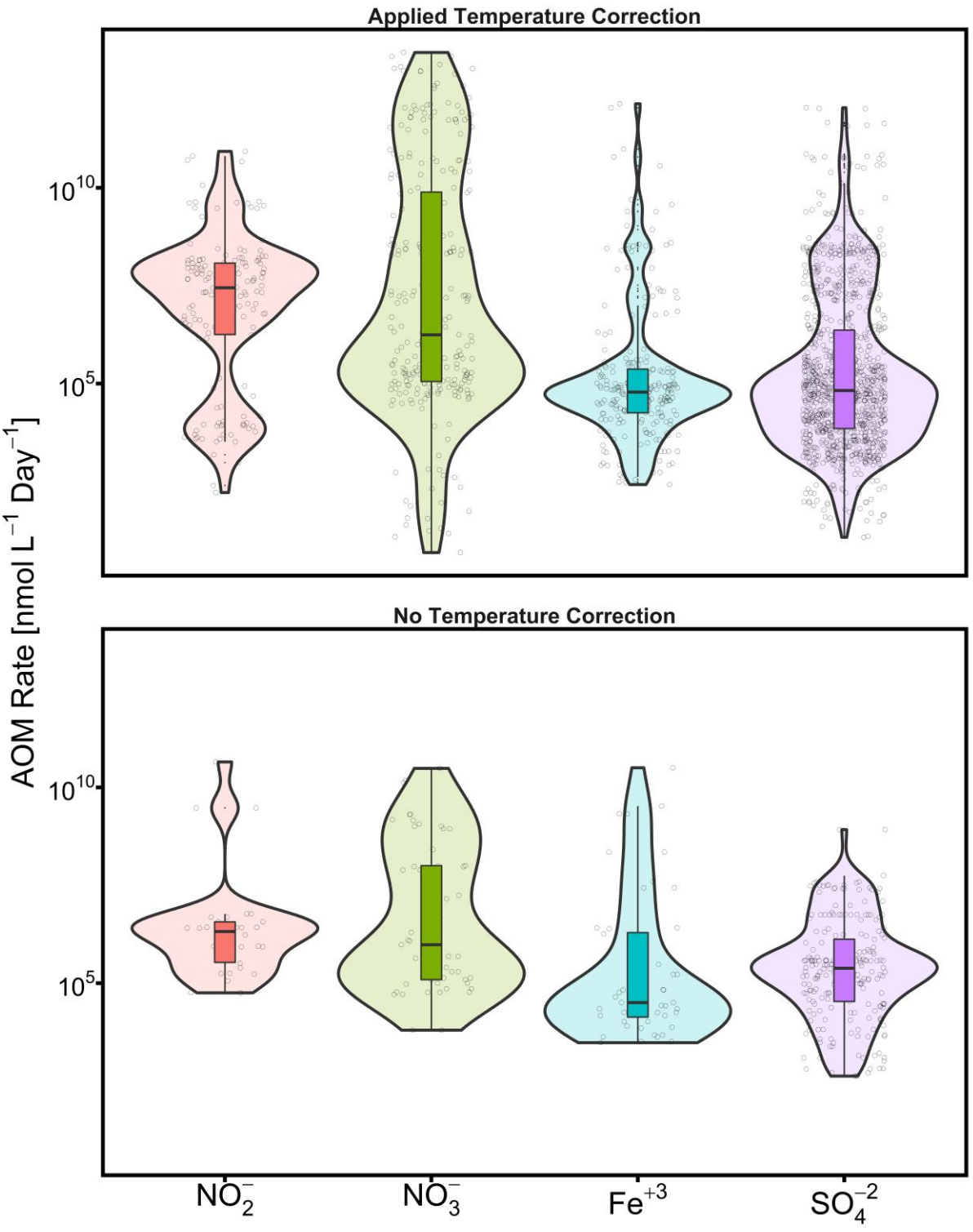

Figure 3.7: Ranges of anaerobic oxidation of methane rates calculated per e^- acceptor with and without the f_{Temp} optimization applied.

3.4 Discussion

3.4.1 Nitrite as a TEA

Marcus theory predicts that the rate of a reaction should increase log-linearly as the energy yield increases. Therefore, in the logarithmic $\Delta G^{\circ}_{R_{opt}}$ and $\bar{r}_{max}$, maximum rates of AOM are anticipated to occur when NO_2^- is utilized as the TEA, and the reaction is the most energetically favourable (Table 3.1). However, this relationship appears to be absent without applying the optimized f_{Temp} factor (Figure 3.7), which produced a least-squares line. Reduced rates of AOM driven by NO_2^- are likely resultant of its toxicity in the environment and ability to limit microbial activity rather than the temperature function (Zhang *et al*., 2013).

Within the metadata analysis, almost all the collected AOM observations attributing CH_4 consumption to NO_2^- are derived from one marine sediment incubation study by Shen *et al.* (2016), which treated sediment with either 100µM NO_2^- or 5mM SO_4^{2-} for AOM. The calculated rates of AOM from their experiment indicates that the SO_4^{2-} contributed significantly more to CH_4 consumption than NO_2^-, although AOM by SO_4^{2-} yielded less energy. Higher rates of NO_2^- driven AOM (~10^{10} nmol L^{-1} $day^{-}1$) were reported by (Raghoebarsing *et al*., 2006), who slowly fed the same concentration of NO_2^- into a bioreactor for 16 months and cultivated a NO_2^- consuming population at 25˚C. Additionally, anammox paired with AOM resulted in the production and subsequent consumption of NO_2^- as observed by Haroon *et al*. (2013), who attributed their calculated AOM rate to NO_3^- reduction. Anammox paired with AOM may produce NO_2^- in low enough concentration to reduce CH_4 emissions. To accurately calculate a maximum rate of AOM using NO_2^-, as an e^- acceptor, a toxicity correction proportional to NO_2^- concentration should be included as well as the tolerance of AOM organisms toward NO_2^-. The tolerance and rate at which

organisms can consume NO_2^- or NO_3^- as a TEA for AOM are influenced by several environmental parameters, including temperature (Ettwig *et al*., 2008; Hu *et al*., 2009; He *et al*., 2015).

3.4.2 Importance of Temperature to AOM

Temperature affects rates of AOM through both abiotic and biotic factors. Firstly, both CH_4 dissolution and oxidation are exothermic processes stimulated at lower temperatures enhancing CH_4 bubble formation (ebullition) and transport through the gas phase (Thornton *et al*., 2015; James *et al*., 2016). Therefore, climate change-derived temperature increases are anticipated to reduce aqueous CH_4 concentrations, limiting its availability for aerobic and anaerobic oxidation reactions (Dean *et al*., 2018). Reduced CH_4 concentrations from increased temperatures can be accounted for in their influence over the F_K and F_T factors within the AOM rate calculation. However, predictions of how increased air temperatures may affect soil respiration overall are more complex depending on an individual microbial community's adapted temperature range (Petterson and Baath, 2003). Here, the fitting of the f_{Temp} function significantly improved the relationship between $\Delta G^{\circ}_{R_{opt}}$ and $\bar{r}_{max}$, with correlation increasing using smaller T_{obs} optimization ranges.

The T_{min}, T_{max}, and T_{opt} temperatures for microbial activity are community dependant and change between environments. The steepness and shape of the temperature-microbial activity curve can be influenced by the pH and optimum pH of an environment relative to its microbial community (Rosso *et al.*, 1995). Most AOM mechanisms consume hydrogen ions and are less thermodynamically favourable at neutral and alkaline conditions, as discussed in Chapter 2. A study of NO_2^- as a TEA identified the highest reaction rates to occur at neutral pH and an optimal temperature of 35˚C (He *et al*., 2015).

Although the calculated values of T_{min}, T_{max}, and T_{opt} for f_{Temp} exhibit large ranges between the observational temperature bins, maximal and optimal temperatures of AOM organisms vary throughout the environment. For example, the observational temperature bin with the lowest range carried a cluster of points from an Antarctic Lake Fryxell where T_{opt} has been reportedly lower than usual in S-oxidizing bacteria (15˚C), and T_{min} has extended below freezing temperature (Sattley and Madigan, 2006). More variety has also been demonstrated amongst AOM catalyzing organisms specifically. A study by Hu *et al*. (2009) compared their archaea performing nitrogen-based AOM with a study conducted by Ettwig *et al*. (2008) using a pure culture of the NO_2^- reducers in the aforementioned high AOM rate bioreactor. Significantly different T_{max} values were observed corresponding to 45˚C by Hu *et al*. (2009) and a much lower temperature of 30˚C by Ettwig *et al*. (2008). Comparatively, in marine environments, AOM with SO_4^{2-} has been observed at significantly higher temperatures of 60˚C to 70˚C, and up to 90˚C in hydrothermal sediments at Guaymas Basin (Biddle *et al*., 2012) – where aforementioned Bowles *et al*. (2019) observed some of the highest known AOM rates (~4250 nmol cm^{-3} day^{-1}). As an exothermic reaction, AOM is likely driven by high CH_4 concentrations at elevated temperatures to overcome thermodynamic constraints pertaining to decreased energy yields occurring at high temperatures.

The heterogeneity of AOM temperature ranges indicates a need to include temperature as a function within the bioenergetics-based framework. To predict how AOM rates may respond to temperature change, an integrative f_{Temp} function for both the environment type and latitude or energy level is required. This function would normalize maximum rates to account for the low (*e.g.*, perennially frozen or subarctic lakes) and high energy environments (*e.g.*, Guaymas Basin) included within this study. Moreover, pH should be included as a critical thermodynamic and physiological control of microbially mediated reactions. Increases in microbial activity rates with

temperature and pH may stimulate AOM as optimal temperatures are approached (Rosso *et al.*, 1995); however, increased capacity for CH_4 production could overwhelm the slow-growing CH_4 reducing population, even in excess of SO_4^{2-} (Dean *et al*., 2018).

3.4.3 AOM in the Natural Environment

The amount of CH_4 produced and available for oxidation is dependant on a number of factors per environment, including climate, hydrology, chemical energy availability, and vegetation (Luo *et al.*, 2019). In all the selected studies for AOM rate calculations, labelled CH_4 was added as a tracer and may have occurred in concentrations abnormal to the natural subsurface environments (*e.g..*, 50 mM). Experimental rates of AOM are elevated under laboratory conditions rather than *in situ* experiments (Sivan *et al.*, 2007). The potentially low value of $K_S^{CH_4}$ cannot account for the wide range of aqueous CH_4 inputs as when $[CH_4] >> K_S^{CH_4}$ then the F_K term easily equals one. Elevated concentrations of CH_4 for experimental set-ups would increase the reactions thermodynamic favourability, an influence that could generally be captured using the reaction quotient within the F_T term of the $\bar{r}_{max}$. Within the data collected, insufficient porewater chemistry was available to calculate the activities of products and reactions for $\Delta G^{\circ}_{R_{opt}}$. The addition or selection of a TEA for the $\Delta G^{\circ}_{R_{opt}}$ term adds an additional layer of uncertainty, as many publications were unable to identify a singular TEA responsible for the AOM rate confidently.

NO_3^- and SO_4^{2-} have been identified as sinks of CH_4 in freshwater and marine settings as well as Fe-oxides (Dale *et al.*, 2006; Deutzmann *et al.*, 2014; Martinez-Cruz *et al*., 2018; Aromokeye *et al.*, 2020). While AOM using NO_3^- is notorious for removing both dissolved N and a potent GHG, CH_4 oxidation by Fe-oxides and SO_4^{2-} may shift sedimentary contributing to internal phosphorus loads as Fe-phosphates are converted to sulfidic minerals (Egger *et al*., 2016). In lakes

or reservoirs with long residency times, bioavailable phosphorus increases could harm water quality and promote harmful algal bloom formation.

Mn-oxides have received far less attention in AOM mechanisms and were the least recognized TEA for AOM within the collected data set. Redox-active Mn-oxides are present in many environments and are generally a more energetically favourable TEA than Fe-oxides or SO_4^{2-}, producing significant AOM rates in marine and freshwater environments (Beal *et al.*, 2009; Martinez-Cruz *et al*., 2017; Leu *et al*., 2020). Studies that specifically identified Mn^{4+} as the TEA added the element to their incubation as synthetic birnessite. Martinez-Cruz *et al*. (2017) narrowed the TEA of AOM to either Fe- or Mn-oxides in freshwater sediment using the total reactive pools but could not decipher which mineral was the dominant TEA. Mn-oxides are likely an under-explored sink for CH_4 in the environment and contribute to AOM when rates decouple from NO_3^- or SO_4^{2-} reduction, particularly in coastal regions where they are deposited each year (Leu *et al*., 2020), or in other cases when another responsible TEA can not be identified.

Wetland and freshwater lake environments had the largest percentage of unidentified TEAs. Low concentrations of SO_4^{2-} within these environments had previously led to the assumption that AOM was not a significant control of CH_4 in freshwater settings. Yet, in a soda lake and marine environments, inhibition of SO_4^{2-} reduction by tungstate did not reduce the soil's natural capacity for AOM (Iverson and Jorgensen, 1985; Iverson *et al.*, 1987), or similar rates were maintained regardless of the TEA added (Saxton *et al*., 2016). These observations support the use of multiple TEA for AOM and the flexibility of CH_4 oxidizers within an environment. Yet, even with ample TEAs, low rates of AOM have been observed in marine and soda lake environments. This discrepancy may occur as a function of salinity or a relatively overwhelming rate of methanogenesis.

3.4.4 Effects of Salinity

The retrieved AOM rates are derived from unique environments, each with its own water chemistry and environmental conditions. The $\bar{r}_{max}$ calculation does not take into account ionic strength and salinity, which differs greatly between freshwater and marine environments and soda lakes. These differences in water chemistry could affect AOM products, and reactants' activity influencing the energetic yields of AOM through the reaction quotient. Within the current proposed framework, these water chemistries are unaccounted for. Additionally, salinity may affect microbial activity, introducing a physiological constraint similar to NO_2^- toxicity. Changes in salinity and their effects on soil respiration and GHG emissions are a growing issue as climate change may influence microbial growth and reaction rates, including the AOM mechanism, in coastal wetlands affected by sea-level rise.

Increasing rates of sea-level rise (currently occurring at 3.3 mm yr^{-1} (Cazenave *et al*., 2014)) in combination with anthropogenic land subsidence, will inevitably result in elevated concentrations of SO_4^{2-} into coastal wetlands (Oppenheimer *et al*., 2019; Gosch *et al*., 2019), and decreasing availability of oxygen and other TEAs with inundation (Luo *et al.*, 2019). CH_4 production in tidal wetlands is strongly affected by atmospheric CO_2 levels and may increase in the future (Mueller *et al*., 2020), although a consensus on the effects of sea-level rise to organic C mineralization has not been reached (Luo *et al.*, 2019). Conceptually, changes in CH_4 emissions from salt-water intrusion result from the balance between methanogenesis and CH_4 oxidation. Several studies have shown varying effects of salinity on CH_4 emissions salt toxicity effects have scarcely been researched for methanotrophs. One study demonstrated decreasing NO_2^- driven AOM rates over a salinity range between 0 and 15 g NaCl L^{-1} with AOM ceasing at roughly ~20 g NaCl L^{-1} (He *et al*., 2015), less than the concentration of ocean water. In addition to salt toxicity,

sea-level rise may impact porewater pH and influence thermodynamic favourability of AOM, affecting *in situ* rates.

3.4 Conclusions

AOM reactions are ubiquitous to marine and freshwater environments, playing a dynamic role in climate change. Elevated air temperatures and sea-level rise may influence the AOM rates impacting GHG emissions globally through shifts in aqueous CH_4 availability and microbial activity. To understand the future role of AOM in the global C cycle, a bioenergetics informed framework is needed to estimate rates of CH_4 conversion to carbon dioxide CO_2. The TEA identity, optimum temperature, pH, and porewater chemistry exert strong controls over CH_4 oxidation rates and should be well quantified over various environments and latitudes to account for the gradient of T_{min}, T_{opt}, and T_{max} values across extreme environments (*e.g.,* perennially frozen lakes, permafrost regions, hydrothermal vents). Additionally, the introduction of a toxicity term for NO_2^- concentrations may be needed to correct experimental data in addition to changes in salinity for sea-level rise. To obtain this framework, AOM characterization should expand to determine optimum temperature values across different environments with latitude and include calculated rates for under-studied environments (arctic lakes, permafrost, dammed reservoirs, and soda lakes) and TEAs (Mn-oxides).

4 Conclusions

4.1 Summary of Key Findings

The overall objective of this thesis was to examine the effects of chemical energy availability on soil coupled biogeochemical cycles and reaction rates related to ongoing climate change, winter warming, and shifts in land-use management. In Chapter 2, a series of variable amounts of e^- donors and acceptors have been applied to closed soil treatments to measure their effect on GHG release and porewater nutrient concentrations. By pairing a factorial batch experiment design with sacrificial sampling, a novel experiment methodology was applied, enabling the collection of temporal data without removing products or reactants for future chemical reactions. Hence, biogeochemical data was collected over the incubation period without disturbance to the thermodynamic favourability of future nutrient transformations. Results of Chapter 2 indicate a preference towards inorganic e^- donors, including ammonium (NH_4^+) and methane (CH_4), over organoheterophic metabolisms (*e.g.*, acetate oxidation) under the experimental conditions. Using thermodynamics, the anaerobic oxidation of ammonium (anammox) was determined to be driven by manganese (Mn) oxide minerals, producing oxidized nitrogen (N) species and regenerating terminal electron acceptors (TEA) for future reactions. The resultant nitrate (NO_3^-) and nitrite (NO_2^-) were used to oxidize inorganic e^- donors producing oxidizing agents iron (Fe)-oxides and sulfate (SO_4^{2-}). Without new chemical energy inputs, the anaerobic oxidation of methane (AOM) experienced a syntrophic relationship to anammox and the re-cycling of Fe and S, consuming resultant NO_3^-, NO_2^-, Fe-oxides, and SO_4^{2-} to produce carbon dioxide (CO_2). These observed reactions are autotrophic, reducing CO_2 and CH_4 emissions from the soil under the experimental conditions while removing N from soil porewater.

Thermodynamic calculations indicated an environmental sensitivity towards the proposed reaction network in Chapter 2, resulting in less favourable conditions under the neutral-pH conditions developed as AOM and anammox proceeded consuming hydrogen ions. In turn, the proposed AOM reaction network may be cyclical in poorly buffered soils, allowing a new CH_4 peak to develop as porewater becomes less acidic. Conversely, in well-buffered soils (*e.g.*, limed, calcite enriched), AOM and anammox rates may be sustained longer, consuming more CH_4, NH_4^+, and CO_2. The novel temporal data presented in Chapter 2 demonstrates the importance of snow and ice-cover duration to limiting GHG release and solute export occurring during snowmelt. This sensitivity is furthered by these anaerobic metabolisms' exothermic nature producing less conducive conditions under the amplified warming effects to winter soil biogeochemical cycles.

In Chapter 3, a bioenergetics informed framework was constructed using a linear free energy relationship to examine the rate of AOM, and its thermodynamic favourability across different environments. The literature review results found AOM to be ubiquitous across freshwater and marine environments using naturally occurring concentrations of e^- acceptors. However, some environmental settings (*e.g.,* soda lakes, permafrost regions) were determined to be under-investigated. Temperature was observed as a vital influence in the maximum rate of AOM, with specific temperature functions required per microbial community. Thus, in a warming world, the effects of temperature and salinity are influential in future AOM changing with climate and sea-level rise. The results of Chapter 3 also indicate a complicated relationship between the energetic capacity of NO_2^- and the ability for microorganisms to perform AOM in its presence. As the most energetic TEA, NO_2^- was anticipated to produce the largest maximum AOM rates; however, when added to soil incubation experiments, its toxicity suppressed CH_4 consumption. As an intermediate of denitrification or anammox, low concentrations of NO_2^- produced more favourable conditions

for CH_4 consumption, indicting the role of coupled soil biogeochemical cycles to limit GHG release.

4.2 Recommendations for Future Research

Overall, this thesis highlights the importance of coupled biogeochemical cycles to GHG emissions and the sensitivity of microbially mediated redox reactions to changing environmental parameters such as temperature and pH. In Chapter 2, Mn-oxides were demonstrated to play a vital role in driving CH_4 consumption. The presence of Mn-oxides supported the observed reaction network by oxidizing NH_4^+ to NO_3^- and causing a syntrophic C and N relationship while renewing other TEAs. Although Mn-oxides' energetic yield rivals NO_3^-, observations of AOM in Chapter 3 were not attributed to Mn-oxides without its amendment. Like observations in Chapter 2, Mn-oxides likely support the AOM reaction network either directly or through the oxidation of inorganic e^- donors, such as NH_4^+ in anammox. Low concentrations of NO_2^- produced from anammox or denitrification could generate ideal conditions for AOM, reducing CH_4 release. Hence, the role of Mn-oxides in limiting CH_4 release from terrestrial ecosystems is likely understated and contributing to AOM without a mechanistic understanding.

The results of Chapters 2 and 3 stress the importance of changing temperature regimes for microbially mediated reaction networks in both freshwater and marine environments. Temperature increases may influence the solubility and energetic favourability of CH_4 oxidation; however, elevated temperatures could stimulate microbial activity if they approach a communities' optimum temperature range. To accurately predict net GHG emissions, consumption rates must be tailored to an environment, its chemical energy limitations (*i.e.*, reactant and product availability), and environmental parameters, including regional temperature averages and pH. Thus, a more

significant physiological understanding of AOM microorganisms and their diversity is needed to inform estimates of CH_4 oxidation rates on a larger scale under increased temperature.

The effects of temperature may be amplified by an environment's pH, determined to significantly influence the thermodynamic limits of the observed reaction network in Chapter 2. Yet, the results of Chapter 3's meta-data analysis for the reviewed literature revealed that pH was rarely reported alongside the observed AOM rate. The literature reviewed also revealed gaps of AOM observations in climate-sensitive cold regions (*e.g.*, arctic, sub-arctic, Antarctic lakes and permafrost), currently experiencing amplified warming effects jeopardizing C terrestrial stores. These effects are heightened throughout the winter season, which dominates the CH_4 budget in Arctic and sub-arctic regions. Thus, a focused effort should be applied to understand CH_4 transport and consumption throughout the winter season and ascertain a mechanistic understanding of AOM in cold low energy environments for net CH_4 fluxes.

Research into the physiological constraints of methanotrophs should also expand to include toxicity parameters. Within the maximum rate calculation, maximum rates of AOM using NO_2^- as a TEA were slower than anticipated without applying the optimized f_{Temp} function. Hence, NO_2^- toxicity was corrected within the f_{Temp} function rather than a TEA specific factor, which may account for its toxicity. Additionally, ongoing sea-level rise is anticipated to inundate coastal wetlands with seawater, exposing methanotrophs to elevated salt concentrations. Changes in salinity may be accounted for within the thermodynamic term; however, maximum AOM rate calculations could be improved with a better understanding of methanotrophs' tolerance of salt.

5 References

Aanderud, Zachary T., Stuart E. Jones, Donald R. Schoolmaster, Noah Fierer, and Jay T. Lennon. 2013. "Sensitivity of soil respiration and microbial communities to altered snowfall." *Soil Biology and Biochemistry* 217-227.

Alster, Charlotte J., Akihiro Koyama, Nels G. Johnson, Matthew D. Wallenstein, and Joseph C. von Fischer. 2016. "Temperature sensitivity of soil microbial communities: An application of macromolecular rate theory to microbial respiration." *Journal of Geophysical Research: Biogeosciences* 121: 1-14. doi:10.1002/2016JG003343.

Alster, Charlotte J., Joseph von Fischer, Steven D. Allison, and Kathleen K. Treseder. 2020. "Embracing a new paradigm for temperature sensitivity of soil microbes." *Global Change Biology* 26: 3221-3229. doi:10.1111/gcb.15053.

Aromokeye, David A., Ajinkya C. Kulkarni, Marcus Elvert, Gunter Wegener, Susan Henkel, Sarah Coffinet, Thilo Eickhorst, et al. 2020. "Rates and microbial players of iron-driven anaerobic oxidation of methane in methanic marine sediments." *Frontiers in Microbiology* 10: 3041. doi:10.3389/fmicb.2019.03041.

Bastviken, David, Lars J. Tranvik, John A. Downing, Patrick M. Crill, and Alex Enrichprast. 2011. "Freshwater Methane Emissions Offset the Continental Carbon Sink." *Science* 331: 50. doi:10.1126/science.1196808.

Beal, Emily J., Christopher H. House, and Victoria J. Orphan. 2009. "Manganese- and iron-dependent marine methane oxidation." *Science* 325: 184-187. doi:10.1126/science.1169984.

Bethke, Craig M., Robert A. Sanford, Matthew F. Kirk, Qusheng Jin, and Theodore M. Flynn. 2011. "The thermodynamic ladder in geomicrobiology." *American Journal of Soil Science* 311: 183-210. doi:10.2475/03.2011.01.

Biddle, J., Z. Carbman, H. Mendlovitz, and et al. 2012. "Anaerobic oxidation of methane at different temperature regimes in Guaymas Basin hydrothermal sediment." *ISME J* 6: 1018-1031. doi:10.1038/ismej.2011.164.

Bintanja, R. 2018. "The impact of arctic warming on increased rainfall." *Scientific Reports* 16001. doi:10.1038/s41598-018-34450-3.

Bonneville, S., T. Behrends, and P. Van Cappellen. 2009. "Solubility and dissimilatory reduction kinetics of iron(III) oxyhydroxides: A linear free energy relationship." *Geochemica et Cosmochimica Acta* 73: 5273-5282. doi:10.1016/j.gca.2009.06.006.

Bowles, M.W., V.A. Samarkin, K.S. Hunter, N. Finke, A.P. Teske, P.R. Girguis, and S.B. Joye. 2019. "Remarkable capacity for anaerobic oxidation of methane at high methane concentration." *Geophysical Research Letters* 46: 12,192-12,201. doi:10.1029/2019GL084375.

Bridgham, Scott D., Hinsby Cadillo-Quiroz, Jason K. Keller, and Qianlai Zhuang. 2013. "Methan emissions from wetlands: biogeochemical, microbial, and modeling perspectives from local to global scales." *Global Change Biology* 19: 1325-1346. doi:10.1111/gcb.12131.

Brin, Lindsay D., Claire Goyer, Bernie J. Zebarth, David L. Burton, and Martin H. Chantigny. 2018. "Changes in snow cover alter nitrogen cycling and gaseous emissions in agricultural soils." *Agriculture, Ecosystems and Environment* 91-103.

Brooks, Paul D., Diane McKnight, and Kelly Elder. 2004. "Carbon limitation of soil respiation under winter snowpacks: potential feedbacks between growing season and winter carbon fluxes." *Global Change Biology* 11: 231-238. doi:231-238.

Brooks, Paul D., Mark W. Williams, and Steven K. Schmidt. 1998. "Inorganic nitrogen and microbial biomass dynamics before and during spring snowmelt." *Biogeochemistry* 43: 1-15. doi:https://doi.org/10.1023/A:1005947511910.

Brooks, Paul D., Paul Grogan, Pamela H. Templer, Peter Groffman, Mats Oquist, and Josh Schimel. 2011. "Carbon and Nitrogen Cycling in Snow-Covered Environments." *Geography Compass* 682-699.

Burgin, Amy J., and Stephen K. Hamilton. 2008. "NO3- -Driven SO42- Proudction in Freshwater Ecosystems: Implications for N and S cycling." *Ecosystems* 11: 908-922. doi:10.1007/s10021-008-9169-5.

Burgin, Amy J., Wendy H. Yang, Stephen K. Hamilton, and Whendee L. Silver. 2011. "Beyond carbon and nitrogen: how the microbial energy economy couples elemental cycles in diverse ecosystems." *Fron. Ecol. Environ.* 9: 44-52. doi:10.1890/090227.

Burton, D.L., and E.G. Beauchamp. 1994. "Profile Nitrous Oxide and Carbon Dioxide Concentrations in a Soil Subject to Freezing." *Soil Science Society of America* 115-122.

Byun, Kyuhyun, and Alan F. Hamlet. 2018. "Projected changes in future climate over the Midwest and Great Lakes region using downscaled CMIP5 ensembles." *International Journal of Climatology* 531-553.

Callahan, B.J., P.J. McMurdie, M.J. Rosen, A.W. Han, A.J.A. Johnson, and S.P. Holmes. 581-583. "DADA2: High-resolution sample inference from Illumina amplicon data." *Nat Methods* 13: 2016. doi:10.1038/nmeth.3869.

Caporaso, J., J. Kuczynski, J Stombaugh, and et al. 2010. "QIIME allows analysis of high-throughput community sequencing data." *Nat Methods* 7: 335-336. doi:10.1038/nmeth.f.303.

Cardoso, Ricardo Beristain, Reyes Sierra-Alvarez, Pieter Rowlette, Elias Razo Flores, Jorge Gomez, and Jim A. Field. 2006. "Sulfide oxidation under chemolithoautotrophic denitrifying conditions." *Biotechnology and Bioengineering* 95: 1148-1157. doi:10.1002/bit.

Cazenave, A., H.B. Dieng, B Meyssignac, and et al. 2014. "The rate of sea-level rise." *Nature Climate Change* 4: 358-361. doi:10.1038/nclimate2159.

Ceglar, A., M. Zampieri, and F. Dentener. 2019. "Observed northward migration of agro-climate zones in Europe will further accelerate under climate change." *Earth's Future* 7: 1088-1101. doi:https://doi.org/10.1029/2019EF001178.

Chapman, Steve, Alexandre, Francez, Andre-Jean Buttler, Fatima Laggoun-Defarge, Harri Vasander, Michael Schloter, Jean Combe, Philippe Grozvernier, et al. 2003. "Exploitation of northern peatlands and biodiversity maintenance: a conflict between economy and ecology." *Frontiers in Ecology* 525-532.

Charlton, S.R., D.L. Parkhurst, and C.A.J. Appelo. 2020. "R Interface to Geochemical Modeling Software (Version 3.6.3)."

Coby, Aaron J., Flynn Picardal, Evgenya Shelobolina, Huifang Xu, and Eric Roden. 2011. "Repeated anaerobic microbial redox cycling of iron." *Applied and Environmental Microbiology* 77: 6036-6042. doi:10.1128/AEM.00276-11.

Cohen, Judah, James A. Screen, Jason S. Furtado, and et al. 2014. "Recent Arctic amplification and extreme mid-latitude weather." *Nature Geoscience* 7: 627-637. doi:10.1038/ngeo2234.

Cole, Martin, Mary Ann Augustin, Michael John Robertson, and John Michael Manners. 2018. "The Science of Food Security." *Nature* 1-8.

Creed, I. F., L. E. Band, N. W. Foster, I. K. Morrison, J. A. Nicolson, R. S. Semkin, and D. S. Jeffries. 1996. "Regulation of nitrate-N release from temperate forests: A test of the N flushing hypothesis." *Water Resources Research* 32: 3337-3354. doi: https://doi.org/10.1029/96WR02399.

Dale, A.W., P. Regnier, and P. Van Cappellen. 2006. "Bioenergetic controls on anaerobic oxidation of methane in coastal marine sediments: a theoretical analysis." *American Journal of Science* 306: 246-294. doi:10.2475/04.2006.02.

Dale, A.W., P. Van Cappellen, and P. Regnier. 2008. "Methane efflux from marine sediments in passive and active margins: Estimations from bioenergetic reaction-transport simulations." *EPSL* 265: 329-344. doi:10.1016/j.eosk.2007.09.026.

Davidson, Eric A., and Ivan A. Janssens. 2006. "Temperature sensitivity of soil carbon decomposition and feedbacks to climate change." *Nature* 165-173.

Davidson, Eric A., Emma C. Suddick, Charles W. Rice, and Linda S. Prokopy. 2015. "More food, low pollution (Mo Fo Lo Po): A grand challenge for the 21st century." *Journal of Environmental Quality* 44: 305–311. doi:10.2134/jeq2015.02.0078.

De Bruijn, A.M.G., K. Butterbach-Bahl, S. Blagodatsky, and R. Grote. 2009. "Model evaluation of different mechanisms driving freeze-thaw N2O emissions." *Agriculture, Ecosystems and Environment* 196-207.

Dean, J.F., J.J. Middleburg, T. Rockmann, R. Aerts, L.G. Blauw, M. Egger, and et al. 2018. "Methane feedbacks to the globalclimate system in a warmer world." *Reviews of Geophysics* 56: 207-250. doi:10.1002/2017RG0005599.

Dedysh, S.N. 2009. "Exploring methanotroph diversity in acidic northern wetlands: molecular and cultivation based studies." *Microbiology* 78: 655-669. doi:10.1134/S00262612709060010.

Denman, K.L., G. Brasseur, A. Chidthaisong, P. Clais, P.M. Cox, R.E. Dickinson, D. Hauglustaine, et al. 2007. *Couplings Between Changes in the Climate System and Biogeochemistry*. Cambridge, United Kingdom, and New York, NY, USA: Cambridge City Press.

Deutzmann, Joerg S., Peter Stief, Josephin Brandes, and Bernhard Schink. 2014. "Anaerobic methane oxidation coupled to denitrification is the dominant methane sink in a deep lake." *PNAS* 111: 18273-18278. doi:10.1073/pnas.1411617111.

Ding, B., Z. Li, and Y. Qin. 2017. "Nitrogen loss from anaerobic ammonium oxidation coupled to Iron(III) reduction in a riparian zone." *Environmental Pollution* 231: 379-386. doi:doi.org/10.1016/j.envpol.2017.08.027.

Duddlestone, K.N., M.A. Kinney, R.P. Kiene, and M.E. Hines. 2002. "Anaerobic microbial geochemistry in a northern bog: Acetate as a dominant metabolic end product." *Global Biogeochemical Cycles* 16: 11-19. doi:10.1029/2001GB001402.

Eberling, Bo, and Kristian K. Brandt. 2003. "Uncoupling of microbial CO2 production and release in frozen soils and its implications for field studies of arctic C cycling." *Soil Biology and Biochemistry* 35: 263-272. doi:10.1016/S0038-0717(02)00258-4.

Edwards, A.C., and M.S. Cresser. 1992. "Freezing and its effect on chemical and biological properties of soil." In *Advances in Soil Science*, 59-79.

Egger, Matthias, Olivia Rasigraf, Celia J. Sapart, Tom Jilbert, Mike S.M. Jetten, Thomas Rockmann, Carina van der Veen, et al. 2015. "Iron-mediated anaerobic oxidation of methane in brackish coastal sediments." *Environmental Science & Technology* 49: 277-283. doi:dx.doi.org/10.1021/es503663z |.

Egger, Matthias, Peter Kraal, Tom Jilbert, Fatimah Sulu-Gambari, Celia Sapart, Thomas Rockmann, and Caroline Slomp. 2016. "Anaerobic oxidation of methane alters sediment records of sulfur, iron, and phosphorus in the Black Sea." *Biogeosciences* 13: 5333-5355. doi:10.5194/bg-13-533-2016.

Environment and Climate Change Canada; Natural Resources Canada; Fisheries and Oceans Canada. 2014. "Characteristics of the Turkey Lakes Watershed Study Site." *Government of Canada.* 06 12. https://www.canada.ca/en/environment-climate-change/services/turkey-lakes-watershed-study/site.html.

Ettwig, K.F., S. Shima, K.T. van de Pas-Schoonen, J. Kahnt, M.H. Medema, J.M. op den Camp, M. S. M. Jetten, and M. Strous. 2008. "Denitrifying bacteria anaerobically oxidize methane inthe absence of Archaea." *Environmental Microbiology* 10: 3164-3173. doi:10.1111/j.1462-2920-2008.01724.x.

Fairbairn, L. 2020. *Linking soil moisture content and carbon dioxide fluxes: From batch experiments to process-based modelling.* Waterloo: University of Waterloo.

FAO. 2017. *World Fertilizer trends and outlook to 2020.* Summary Report, Rome: Food and Agriculture Organization of the United Nations.

Fernandes, Sheryl Oliveira, Cedric Javanaud, Axel Aigle, Valerie D. Michotey, Sophie Guasco, Jonathan Deborde, Bruno Deflandre, Pierre Anschutz, and Patricia C. Bonin. 2014. "Anaerobic nitrification-denitrification mediated by Mn-oxides in meso-tidal seediments: Implications for N2 and N2O production." *Journal of Marine Systems* 114: 1-8. doi:doi.org/10.1016/j.jmarsys.2014.11.011.

Finlay, J., J. Neff, S. Zimov, A. Davydova, and S. Davydov. 2006. "Snowmelt dominance of dissolved organic carbon in high-latitude watersheds: Implications for characterization and flux of river DOC." *Geophysical Research Letters* 33: L10401. doi:10.1029/2006GL025754.

Flerchinger, G.N., M.S. Seyfried, and Hardegree. 2006. "Using soil freezing characteristics to model multi-season water dynamics." *Vadose Zone Journal* 5: 1143-1153. doi:10.2136/vzj2006.0025.

Forster, P., V. Ramaswamy, P. Artaxo, T. Berntsen, R. Betts, D.W. Fahey, J. Haywood, et al. 2007. *Changes in Atmospheric Constituents and in Radiative Forcing. Contribution of Working Group I to the Fourth Assesment Report of the Intergovernmental Panel on Climate Change.* Cambridge, United Kingdom and New York, NY, USA: Cambridge University Press, 129-234.

Fouché, J., C.T. Christiansen, M.J. Lafrenière, and et al. 2020. "Canadian permafrost stores large pools of ammonium and optically distinct dissolved organic matter." *Nature Communications* 11: 4500. doi:10.1038/s41467-020-18331-w.

Gilbert, D., C. Amblard, G. Bourdier, and A.-J. Francez. 1998. "The microbial loop at the surface of a peatland: structure, function and impact of nutrient input." *Microbial Ecology* 83-93.

Gobel, Leonie, Heinz Coners, Dietrich Hertel, Sandra Willinghofer, and Christoph Leuschner. 2019. "The role of low soil temperature for photosynthesis and stomatal conductance of three graminoids from different elevations." *Frontiers in Plant Science* 10: 330. doi:10.3389/fpls.2019.00330.

Gorham, Eville. 1991. "Northern Peatlands: Role in the carbon cycle and probable response to climatic warming." *Ecological Applications* 182-195.

Gosch, L., H. Townsend, M. Kreuzburg, M. Janssen, F. Rezanezhad, and B. Lennartz. 2019. "Suldate mobility in fen peat and its impact on the release of solutes." *Fron. Environ. Sci.* 7: 189. doi:10.3389/fenvs.2019.00189.

Groffman, Peter M., Charles T. Driscoll, Timothy J. Fahey, Janet P. Hardy, Ross D. Fitzhugh, and Geraldine L. Tierney. 2001. "Colder soils in a warmer world: A snow manipulation study in a northern hardwood forest." *Biogeochemistry* 56: 135-150. doi:https://doi.org/10.1023/A:1013039830323.

Groffman, Peter M., Janet P. Hardy, Charles T. Driscoll, and Timothy J. Fahey. 2006. "Snow depth, soil freezing, and fluxes of carbon dioxide, nitrous oxide and methane in a northern hardwood forest." *Global Change Biology* 1748-1760.

Grogan, P., A. Michelsen, P. Ambus, and S. Jonasson. 2004. "Freeze-thaw regime effects on carbon and nitrogen dynamics in sub-arctic heath tundra mecocosms." *Soil Biology and Biochemistry* 641-654.

Haaijer, Suzanne C.M., Leon P.M. Lamers, Alfons J.P. Smolders, Mike S.M. Jetten, and Huub J.M. Op den Camp. 2007. "Iron Sulfide and Pyrite as Potential Electron Donors for Microbial Nitrate Reduction in Freshwater Wetlands." *Geomicrobiology* 24: 391-401. doi:10.1080/01490050701436489.

Handley, Kim M., Nathan C. VerBerkmoes, Carl I. Steefel, Kenneth F. Williams, Itai Sharon, Christopher S. Miller, Kyle R. Frischkorn, et al. 2013. "Biostimulation induces syntrophic interactions that impact C, S, and N cycling in a sediment microbial community." *ISME J* 7: 800-816. doi:10.1038/ismej.2012.148.

Haroon, Mohamed F., Shihu Hu, Ying Shi, Michael Imelfort, Jurg Keller, Philip Hugenholtz, and Zhiguo, Tyson, Gene W. Yuan. 2013. "Anaerobic oxidation of methane coupled to nitrate reduction in a novel archaeal lineage." *Nature* 500: 567-570. doi:https://doi.org/10.1038/nature12375.

Harryson Drotz, Stina, Emma L. Tilston, Tobias Sparrman, Jurgen Schleucher, Mats Nilsson, and Mats G. Oquist. 2009. "Contributions of matric and osmotic potentials to the unfrozen water content of frozen soils." *Geoderma* 392-398.

Hayashi, Masaki. 2013. "The Cold Vadose Zone: Hydrological and Ecological Significance of Frozen Soil Processes." *Vadose Zone Journal* 1-8.

Hayhoe, Katherine, Cameron P. Wake, Thomas G. Huntingtion, Lifeng Luo, Mark D. Schwartz, Justin Sheffield, Eric Wood, et al. 2007. "Past and future changes in climate and hydrological indicators in the US Northeast." *Climate Dynamics* 381-407.

He, Qiuxiang, Linpeng Yu, Jibing Li, Dan He, Cai Xixi, and Shungio Zhou. 2019. "Electron shuttles enhance anaerobic oxidation of methane coupled to iron (III) reduction." *Science of the Total Environment* 688: 664-672. doi:10.1016/j.scitoenv.2019.06.299.

He, Z., S. Geng, L. Shen, L. Lou, P. Zheng, X. Xu, and B. Hu. 2015. "The short- and long-term effects of environmental conditions on anaerobic methane oxidation coupled to nitrite reduction." *Water Research* 68: 554-562. doi:10.1016/j.watres.2014.09.055.

Hendershot, W.H., and M. Duquette. 1986. "A simple barium chloride method for determining cation exchange capacity and exchangeable cations." *Soil Sci. Soc. Am. J.* 50: 605-608.

Hendershot, W.H., H. Lalande, and M. Duquette. 2006. "Chapter 18: Ion Exchange and Exchangeable Cations 2nd Edition." In *Soil Sampling and Methods of Analysis*, by M.R. Carter and E.G. Gregorich. Boca Raton: Taylor and Francis Group.

Henry, Hugh A.L. 2007. "Soil freeze-thaw cycle experiments: Trends, methodological weaknesses and suggested improvements." *Soil Biology and Biochemistry* 977-986.

Heuer, Kristi, Paul D. Brooks, and Kathy A. Tonnessen. 1999. "Nitrogen dynamics in two high elevation catchments during spring snowmelt 1996, Rocky Mountains, Colorado." *Hydrological Processes* 13: 2203-2214. doi:https://doi.org/10.1002/(SICI)1099-1085(199910)13:14/15<2203::AID-HYP859>3.0.CO;2-K.

Hirota, T., M. Iwata, M. Hayashi, S. Suzuki, T Hamasaki, R Sameshima, and I. Takayabu. 2006. "Decreasingg soil frost depth and its relation to climate change in Tokachi, Hokkaido, Japan." *Journal of the Meteorlogical Society of Japan* 84: 791-802. doi:10.2151/jmsj.84.821.

Hobbs, Joanne K., Wanting Jiao, Ashley D. Easter, Emily J. Parker, Louis A. Schipper, and Vickery L. Arcus. 2013. "Change in heat capacity for enzyme catalysis determines temperature dependance of enzyme catalyzed rates." *ACS Chemical Biology* 8: 2388-2393. doi:10.1021/cb4005029.

Hu, Bao-Ian, Shen Li-dong, Xu Lian, Qun Zhu, Shuai Liu, Qian Huang, Zhan-fei He, et al. 2014. "Evidence for nitrite-dependent anaerobic methane." *PNAS* 111: 4495-4500. doi:doi.org/10.1073/pnas.1318393111.

Hu, S., R.J. Zeng, L.C. Burow, P. Lant, J. Keller, and Z. Yuan. 2009. "Enrichment of denitrifying anaerobic methane oxidizing microorganisms." *Environmental Microbiology Reports* 1: 377-384. doi:10.1111/j.1758-2229.2009.00083.x.

IPCC. 2014. *Climate Change 2014: Synthesis Report. Contribution of Working Groups I, II and III to the Fifth Assessment Report of the Intergovernmental Panel on Climate Change.* Geneva, Switzerland: IPCC, 1-151. doi:[Core Writing Team, R.K. Pachauri and L.A. Meyer (eds.)].

Ireson, A.M., G. van der Kamp, G. Ferguson, U. Nachshon, and H.S. Wheater. 2013. "Hydrogeological processes in seasonally frozen northern latitudes: understanding, gaps, and challenges." *Hydrogeology of Cold Regions* 21: 53-66. doi:10.1007/s10040-012-0916-5.

Irvine, Cameron, Merrin Macrae, Matthew Morison, and Richard Petrone. 2019. "Seasonal nutrient export dynamics in a mixed land use subwatershed of the Grand River, Ontario, Canada." *Journal of Great Lakes Research* 45: 1171-1181. doi:10.1016/j.jglr.2019.10.005.

Ivarson, K.C., and F.J. Sowden. 1970. "Effect of frost action and storage of soil at freezing temperatures on teh free amino acids, sugars and respiratory activity of soil." *Canadian Journal of Soil Science* 191-198.

Iverson, N., and B.B. Jorgensen. 1985. "Anaerobic methane oxidation rates at the sulfate-methane transition in marine sediments from Kattegat and Skagerrak." *Limnology Oceanography* 30: 944-955.

Iverson, N., R. S. Oremland, and M.J. Klug. 1987. "Big Soda Lake (Nevada). 3. Pelagic methanogenesis and anaerobic methane oxidation." *Limnology Oceanography* 32: 804-814.

Jackson, Bradley E., and Michael J. McInerney. 2002. "Anaerobic microbial metabolisms can proceed close to thermodynamic limits." *Nature* 416: 454-456. doi:10.1038/415454a.

James, Rachael H., P. Bousquet, I. Bussman, M. Haeckel, R. Kipfer, and I. Leifer. 2016. "Effects of climate change on methane emissions from seafloor sediments in the Arctic Ocean: A review." *Limnology and Oceanography* 61: 283-299. doi:10.1002/lno.10307.

Javanaud, Cedric, Valerie Michotey, Sophie Guasco, Nicole Garcia, Pierre Anschutz, Mathieu Canton, and Patricia Bonin. 2011. "Anaerobic ammonium oxidation mediate by Mn-

oxides: from sediment to strain level." *Research in Microbiology* 162: 848-857. doi:10.1016/j.resmic.2011.01.011.

Jia, G., E. Shevliakova, P. Artaxo, N. De Noblet-Ducoudré, R. Houghton, J. House, K Kitajima, C. Lennard, and A. Popp. 2019. "Climate Change and Land: an IPCC special report on climate change, desertification, land degradation, sustainable land management, food security, and greenhouse gas fluxes in terrestrial ecosystems." 131-247.

Jiang, Shenghua, Sunhwa Park, Younggun Yoon, Ji-Hoon Lee, Wei-Min Wu, Nguyen Phuoc Dan, Michael J. Sadowsky, and Hor-Gil Hur. 2013. "Methanogenesis Facilitated by Geobiochemical Iron Cycle in a Novel Syntrophic Methanogenic Microbial Community." *Environmental Science and Technology* 47: 10078-10084. doi:10.1021/es40241c.

Jin, Qusheng, and Craig M. Bethke. 2003. "A New Rate Law Describing Microbial Respiration." *Applied and Environmental Microbiology* 69: 2340-2348. doi:10.1128/AEM.69.4.2340-2348.2003.

Jin, Qusheng, and Craig M. Bethke. 2002. "Kinetics of Electron Transfer through the Respiratory Chain." *Biophysical Journal* 83: 1797-1808. doi:10.1016/S0006-3495(02)73945-3.

Jin, Qusheng, and Craig M. Bethke. 2005. "Predicting the rate of microbial respiration in geochemical environments." *Geochemica et Cosmochimica* 69: 1133-1143. doi:10.1016/j.gca.2004.08.010.

Joe-Wong, C., K.L. Weaver, S.T. Brown, and K. Maher. 2019. "Thermodynamic controls on redox-driven kinetic stable isotope fractionation." *Geochemical Perscpectives Letters* 10: 20-25. doi:10.7185/geochemlet.I909.

Jonasson, Sven, and Gaius R. Shaver. 1999. "Within-stand nutrient cycling in arctic and boreal wetlands." *Ecology* 2139-2150.

Jones, Zackary L., Justin T. Jasper, David L. Sedlak, and Jonathan O. Sharp. 2017. "Sulfide-Induced Dissimilatory Nitrate Reduction to Ammonium Supports Anaerobic Ammonium Oxidation (Anammox) in an Open-Water Unit Process Wetland." *Applied and Environmental Microbiology* 83: 1-14. doi:10.1128/AEM.00782-17.

Joosten, H., M.L. Tapio-Bistrom, and S. Tol. 2012. *Peatlands -- Guidance for climate change mitigation through conservation, rehabiliation, and sustainable use (second edition).* The Food and Agriculture Organization of the United Nations and Wetlands International.

Joseph, G., and H.A.L. Henry. 2008. "Soil nitrogen leaching losses in response to freeze–thaw cycles and pulsed warming in a temperate old field." *Soil Biology and Biochemistry* 40: 1947-1953. doi:10.1016/j.soilbio.2008.04.007.

Kartal, Boran, Naomdi M.de Almeida, Wouter J. Maalcke, Hubb J.M. Op den Camp, Mike S.M. Jetten, and Jan T. Keltjens. 2013. "How to make a living from anaerobic ammonium oxidation." *FEMS Microbiology Reviews* 37: 428-461. doi:10.1111/1574-6976.12014.

King, Myron, Daniel Altdorff, Pengei Li, Galagedara Lakshman, Joseph Holden, and Adrian Unc. 2018. "Northward shift of the agricultural climate zone under 21st-century global climate change." *Scientific Reports* 8: 7904. doi:https://doi.org/10.1038/s41598-018-26321-8.

Kirschbaum, Miko U.F. 1995. "The temperature dependance of soil organic matter decomposition and the effect of global warming on soil organic C." *Soil Biology and Biochemistry* 27: 753-760. doi:10.1016/00385-0717(94)00242-S.

Kirschbaum, Miko U.F. 2000. "Will changes in soil organic carbon act as a positive or negative feedback on global warming?" *Biogeochemistry* 48: 21-51. doi:10.1023/A:1006238902976.

Koponen, Hannu, Laura Flojt, and Pertti J. Martikainen. 2004. "Nitrous oxide emissions from agriculture soil at low temperatures; a laboratory microcosm study." *Soil Biology and Biochemistry* 6: 757-766. doi:10.1016/j.soilbio.2003.12.011.

Kozlowski, Tomasz. 2009. "Some factors affecting supercooling and the equilibrium freezing point in soil-water systems." *Cold Regions Science and Technology* 25-33.

Kurylyk, Barret L., Kerry T.B. MacQuarrie, and Clifford I. Voss. 2014. "Climate change impacts on the temperature and magnitude of groundwater discharge from shallow, unconfied aquifers." *Water Resources Research* 3253-3274.

Lai, D.Y.F. 2009. "Methane dynamics in northern peatlands: a review." *Pedosphere* 409-421.

LaRowe, Douglas E., Andrew W. Dale, Jan P. Amend, and Philippe Van Cappellen. 2012. "Thermodynamic limitations on microbially catalyzed reaction rates." *Geochemica et Cosmochimica Acta* 90: 96-109. doi:10.1016/j.gca.2012.05.011.

Lee, S.Y., M.C. Maniquiz, J.Y. Choi, S.M. Jeong, and L.H. Kim. 2013. "Seasonal nutrient uptake of plant biomass in a constructed wetland treating piggery waste effluent." *Water Science & Technology* 67: 1317-1323. doi:10.2166/wst.2013.002.

Leffler, J.E., and E. Grunwald. 1963. *Rates and Equilibria of Organic Reactions.* New York: Dover Publications.

Leu, Andy O., Chen Cai, G.S. McIlroy, G. Southam, V.J. Orphan, Z. Yuan, S. Hu, and G.W. Tyson. 2020. "Anaerobic methane oxidation coupled to manganese reduction by members of Methanoperedenaceae." *ISME J* 14: 1030-1041. doi:10.1038/s41396-020-0590-x.

Liu, Haojie, Jonathan Price, Fereidoun Rezanezhad, and Bernd Lennartz. 2020. "Centennial-scale shifts in hydrophysical properties of peat induced by drainage." *Water Resources Research* 56: 1-14. doi:10.1029/2020WR027538.

Liu, Jian, Helen M. Baulch, Merrin L. Macrae, Henry F. Wilson, Jane A. Elliott, Lars Bergstrom, Aaron J. Glenn, and Peter A. Vada. 2019. "Agricultural Water Quality in Cold Climates: Processes, Drivers, Management Options, and Research Needs." *Journal of Environmental Quality* 48: 792-802. doi:10.2134/jeq2019.05.0220.

Liu, L.-Y., G.-J Xie, Xing, D.-F., B.-F. Liu, J. Ding, G.-L. Cao, and N.-Q. Ren. 2021. "Sulfate dependent ammonium oxidation: A microbial process linked nitrogen with sulfur cycle and potential application." *Environmental Research* 192: 110282. doi:doi.org/10.1016/j.envres.2020.110282.

Luan, F., C.A. Gorski, and W.D. Burgos. 2015. "Linear Free Energy Relationships for the Biotic and Abiotic Reduction of Nitroaromatic Compounds." *Environmental Science & Technology* 49: 3557-3565. doi:10.1021/es5060918.

Luan, Junwei, Wu Jianghua, Shirong Liu, Nigel Roulet, and Mei Wang. 2019. "Soil nitrogen determines greenhouse gas emissions from northern peatlands under concurrent warming and vegetation shift." *Nature* 1-10.

Luo, Min, Jia-Fang Huang, Wen-Feng Zhu, and Chuan Tong. 2019. "Impacts of increasing salinity and inundation on rates and pathways of organic carbon mineralization in tidal wetlands: a review." *Hydrobiologia* 827: 31-49. doi:10.1007/s10750-017-3416-8.

Maracchi, Gianpiero, Oleg Sirotenko, and Marco Bindi. 2005. "Impacts of present and future climate variability on agriculture and foresty in the temperate regions: Europe." *Climate Change* 117-135.

Marcus, R.A. 1964. "Chemical and electrochemical electron-transfer theory." *Annual Review of Physical Chemistry* 15: 155-196. doi:10.1146/annurev.pc.15.100164.001103.

Marquarat, K.A., B.R. Haller, J.M. Paper, T.M. Flynn, M.I. Boyanov, G. Shodunke, C. Guara, Q. Jin, and M.F. Kirk. 2018. "Influence of pH on the balance between methanogenesis and iron reduction." *Geobiology* 17: 185-198. doi:10.1111/gbi.12320.

Martinez-Cruz, Karla, Armando Sepulveda-Jauregui, Peter Casper, Walter Katey Anthony, Kurt A. Smemo, and Frederic Thalasso. 2018. "Ubiquitous and significant anaerobic oxidation of methane in freshwater lake sediments." *Water Research* 144: 332-340. doi:10.1016/j.watres.2018.07.053.

Martinez-Cruz, Karla, Mary-Catherine Leewis, Ian Charold Herriott, Armando Sepulveda-Jauregui, Katey Walter Anthony, Frederic Thalasso, and Mary Beth Leigh. 2017. "Anaerobic oxidation of methane by aerobic methanotrophs in sub-Arctic." *Science of the Total Environment* 607-608: 23-31. doi:https://doi.org/10.1016/j.scitotenv.2017.06.187.

Matzner, E., and W. Borken. 2008. "Do freeze-thaw events enhance C and N losses from soils of different ecosystems? A review." *European Journal of Soil Science* 274-284.

Mohammed, Aaron A., Barret L. Kurylyk, Edwin E. Cey, and Masaki Hayashi. 2018. "Snowmelt Infiltration and Macropore Flow in Frozen Soils: Overview, Knowledge Gaps, and a Conceptual Framework." *Vadose Zone Journal* 1-15.

Moore, T.R. 1987. "Thermal regime of peatlands in subarctic eastern Canada." *Can. J. Earth Sci.* 24: 1352-1359. doi:10.1139/e87-129.

Moyano, F.E., S. Manzoni, and C. Chenu. 2013. "Responses of soil heterotrophic respiration to moisture availability: An exploration of processes and models." *Soil Biology & Biochemistry* 59: 72-85. doi:10.1016/j.soilbio.2013.01.002.

Mueller, Peter, Thomas J. Mozdar, A. Langley, L.R. Aoki, G.L. Noyce, and P. Megonigal. 2020. "Plant species determine tidal wetland methane response to sea level rise." *Nature Communications* 11: 5154. doi:10.1038/s.41467-020-18763-4.

Munoz, Cristina, Leandro Paulino, Carlos Monreal, and Erick Zagal. 2010. "Greenhouse gas (CO2 and N2O) emissions from soil: a review." *Chilean Journal of Soil Science* (Chilean Journal of Soil Science) 70: 485-497.

Nagare, R.M., R.A. Schincariol, W.L. Quinton, and M. Hayashi. 2011. "Effects of freezing on soil temperature, frost propagation and moisture redistribution in peat." *Hydrology and Earth System Sciences Discussions* 8: 5387-5426. doi:10.5194/hessd-8-5387-2011.

Natali, S.M., J.D. Watts, B.M. Rogers, and et al. 2019. "Large loss of CO2 in winter observed across the northern permafrost region." *Nat. Clim. Chang.* 9: 852-857. doi:10.1038/s41558-019-0592-8.

Noroi, Katrin a, and Bo Thamdrup. 2014. "Nitrate-dependant anaerobic methane oxidation in a freshwater sediment." *Geochemica et Cosmochimica Acta* 141-150. doi:10.1016/j.gca.2014.01.032.

Nyameogo, Gretta Fabienne Toudanaba, Mamert Mbonimpa, Bruno Bussiere, and Akue-Sylvette Awoh. 2018. "Influence of frozen conditions on the oxygen diffusion coefficient." *Acta Geotechnica* 15: 409-421. doi:10.1007/s11440-018-0690-1.

Olesen, J.E., T.R. Carter, C.H. Diaz-Ambrona, S. Fronzek, T. Heidmann, T. Hickler, T. Holt, et al. 2007. "Uncertainties in projected impacts of climate change on European agriculture and terrestrial ecosystems based on scenarios from regional climate models." *Climate Change* 123-143.

Olivie-Lauquet, Gwenaelle, Gerard Gruau, Aline Dia, Christine Riou, Anne Jafrezic, and Odile Henin. 2001. "Release of trace elements in wetlands: role of seasonal variability." *Water Research* 35: 943-952. doi:10.1016/S0043-1354(00)00328-6.

Oppenheimer, M., B.C. Glavovic, J. Hinkel, R. van de Wal, A.K. Magnan, A. Abd-Elgawad, R. Cai, et al. 2019. "Sea Level Rise and Implication for Low Lying Islands, Coasts and Communities." *IPCC Special Report on the Ocean and Cryosphere in a Changing Climate.* Edited by D.C. Roberts, V. Masson-Delmotte, P. Zhai, M. Tignor, E. Poloczanska, K. Mintenbeck, A. Alegría, M. Nicolai, A. Okem, J. Petzold, B. Rama, N.M. Weyer (eds.)] [H.-O. Pörtner.

Oquist, Mats G., Kevin Petrone, Mats Nilsson, and Leif Klemedtsson. 2007. "Nitrification controls N2O production rates in a frozen boreal forest soil." *Soil Biology & Biochemistry* 39: 1809-1811. doi:10.1016/j.soilbio.2007.01.010.

Oquist, Mats G., Mats Nilsson, Fred Sorensson, Asa Kasimir-Klemedtsson, Tryggve Persson, Per Weslien, and Leif Klemedtsson. 2004. "Nitrous oxide production in a forest soil at low temperatures -- processes and envrionmental records." *FEMS Microbiology Ecology* 49: 371-378. doi:10.1016/j.femsec.2004.04.006.

Oquist, Mats G., Tobias Sparrman, Leif Klemedtsson, Stine Harrysson Drotz, Harald Grip, Jurgen Schleucher, and Mats Nilsson. 2009. "Water availability controls microbial temperature responses in frozen soil CO2 production." *Global Change Biology* 2715-2722.

Pala-Ozkok, Ilke, Ateequr Rehman, Nevin Yagci, Emine Ubay-Cokgor, Daniel Jonas, and Derin Orhon. 2012. "Characteristics of mixed microbial culture at different sludge ages: Effect on variable kinetics for substrate utilization." *Bioresource Technology* 126: 274-282. doi:10.1016/j.biortech.2012.08.115.

Patel, Kaizad F., Corianne Tatariw, Jean D. MacRae, Tsutomu Ohno, Sarah J. Nelson, and Ivan J. Fernandez. 2018. "Soil carbon and nitrogen responses to snow removal and concrete frost in a northern coniferous forest." *Canadian Journal of Soil Science* 98: 436-447. doi:dx.doi.org/10.1139/cjss-2017-0132 .

Peppin, Stephen S.L., and Robert W. Style. 2012. "The Physics of Frost Heave and Ice Lens Growth." *Vadose Zone Journal* 1-12.

Pernthaler, Annelie, Anne Dekas, C. Titus Brown, Shana K. Goffredi, Tsegereda Embaye, and Victoria J. Orphan. 2008. "Diverse syntrophic partnerships from deep-sea methane vents revealed by direct cell capture and metagenomics." *Proceedings of the National Academy of Sciences* 105: 7052-7057. doi:10.1073/pnas.0711303105.

Perovich, Donald K. 2007. "Light reflection and transmission by a temperate snowcover." *Journal of Glaciology* 53: 201-210. doi:10.3189/171756507782202919.

Petterson, Marie, and Erland Baath. 2003. "Temperature-dependant changes in the soil bacterial community in limed and unlimed soil." *FEMS Microbiology Ecology* 45: 13-21. doi:10.1016/S0168-6496(03)00106-5.

Phillips, R.L., A.M.S. McMillan, T. Palmada, J. Dando, and D. Giltrap. 2015. "Temperature effects on N2O and N2 denitrification end-products for a New Zealand pasture soil." *New Zealand Journal of Agricultural Research* 58: 89-95. doi:https://doi.org/10.1080/00288233.2014.969380.

Price, D.T., D.W. McKenney, L.A. Joyce, R.M. Siltanen, P. Papadopol, and K. Lawrence. 2011. *High-Resolution Interpolation of Climate Scenarios for Canada Derived from General Circulation Model Simulations.* Canadian Forest Service Northern Forestry Center, Edmonton, Alberta: Natural Resources Canada.

Pronk, G.J., A. Mellage, T. Milojevic, C.M. Smeaton, K. Engel, J.D. Neufeld, F. Rezanezhad, and P. Van Cappellen. 2020. "Carbon turnover and microbial activity in an artificial soil under

imposed cyclic drainage and imbibition." *Vadose Zone Journal* 19: e20021. doi:10.1002/vzj2.20021.

Raghoebarsing, A., Ashna, A. Pol, K. van de Pas-Schoonen, and et al. 2006. "A microbial consortium couples anaerobic methane oxidation to denitrification." *Nature* 440: 918-921. doi:10.1038/nature04617.

Raich, J. W., and C.S. Potter. 1995. "Global patterns of carbon-dioxide emissions." *Biogeochemical Cycles* 23-26.

Raymond, Peter A., James E. Saiers, and Sobczak. 2016. "Hydrological and biogeochemical controls non watershed dissolved organic matter transport: pulse-shunt concept." *Concepts & Synthesis* 97: 5-16. doi:10.1890/14-1684.1.

Rempel, Alan W. 2012. "Hydromechanical Processes in Freezing Soils." *Vadose Zone Journal* 1-10.

Reyes, Francisco R., and Vanessa Lougheed. 2015. "Rapid nutrient release from permafrost thaw in arctic aquatic ecosystems." *Arctic, Antarctic, and Alpine Research* 47: 35-48. doi:10.1657/AAAR0013-099.

Rezanezhad, F., J.S. Price, W.L. Quintion, B. Lennartz, T. Milojevic, and P. Van Cappellen. 2016. "Structure of peat soils and implications for water storage, flow, and solute transport: A review update for geochemists." *Chemical Geology* 429: 75-84. doi:https://doi.org/10.1016/j.chemgeo.2016.03.010.

Rezanezhad, F., R.-M. Couture, R. Kovac, D. O'Connell, and P. Van Cappellen. 2014. "Water table fluctuations and soil biogeochemistry: An experimental approach using an automated soil column system." *Journal of Hydrology* 509: 245-256. doi:10.1016/j.jhydrol.2013.11.036.

Ringuet, Stephanie, Lara Sassano, and Zackary I Johnson. 2011. "A Suite of Microplate Reader-Based Colorimetric Methods to Quantify Ammonium, Nitrate, Orthophosphate and SIlicate Concentrations for Aquatic Nutrient Monitoring." *Journal of Environmental Monitoring* 13: 370-376. doi:10.1039/c0em00290a.

Rios-Del Toro, E.E., E. Valenzuela, N. Lopez-Lozano, M. Cortes-Martinez, M.A. Sanchez-Rodriguez, O. Calvario-Martinez, S. Sanchez-Carrillo, and F.J. Cervantes. 2018. "Anaerobic ammonium oxidation linked to sulfate and ferric iron reduction fuels nitrogen loss in marine sediments." *Biodegredation* 29: 429-442. doi:10.1007/s10532-018-9839-8.

Risk, Neil, Claudia Wagner-Riddle, Adriana Furon, Jon Warland, and Christian Blodau. 2014. "Comparison of simultaneous soil profile N2O concenrtation and surface N2O flux measurements overwinter and at spring thaw in agricultural soil." *Soil Biology & Biochemistry* 180-193.

Robador, A., V. Bruchert, and B.B. Jorgensen. 2009. "The impact of temperature change on the activity and community composition of sulfate-reducing bacteria in arctic versus temperatre marine sediments." *Environmental Microbiology* 11: 1692-1703. doi:10.1111/j.1462-2920.2009.01896.x.

Rosso, G.J., C. Wang, and P.A. Schuppli. 1985. "Hydroxylamine and ammonium oxalate solutions as extractants for Fe and Al from soil." *Soil Sci. Soc. Am. J.* 49: 783-785.

Rosso, L., J.R. Lobry, S. Bajard, and J.P. Flandrois. 1995. "Convenient model to describe the combined effects of temperature and pH on microbial growth." *American Society for Microbiology* 61: 610-616. doi:0099-2240/95/$04.00+0.

Ruhlmann, Jorg, Martin Korschens, and Jan Graefe. 2006. "A new approach to calculate the particle density of soils considering properties of soil organic matter and the mineral matrix." *Geoderma* 130: 272-283. doi:10.1016/j.geoderma.2005.01.024.

Rydin, H., and J. Jeglum. 2006. *The Biology of Peatlands.* New York: Oxford University Press.

Sattley, W.M., and M.T. Madigan. 2006. "Isolation, Characterization, and Ecology of Cold-Active, Chemolithotrophic, Sulfur-Oxidizing Bacteria from Perenially Ice-Covered Lake Fryxell, Antartica." *Applied and Environmental Microbiology* 72: 5562-5568. doi:10.1128/AEM.00702-06.

Saunois, M. et al. 2016. "The global methane budget: 2000-2012." *Earth System Science Data Discussion* 8: 697-751. doi:10.5194/essd-8-697-2016.

Saxton, Matthew A., Vladimir A. Samarkin, Charles A. Schutte, Marshall W. Bowles, Michael T. Madigan, Sarah B. Cadieux, Lisa M. Pratt, and Samantha B. Joye. 2016. "Biogeochemicl and 16S rRNA gene sequence evidence supports a nodel mode of anaerobic methanotrophy in permanently ice-covered Lake Fryxell, Antartica." *Limnology and Oceanography* 61: 119-130. doi:10.1002/lno.10320.

Saxton, Matthew A., Vladmir A. Samarkin, Charles A. Schutte, Marshall W. Bowles, Michael T. Madigan, Sarah B. Cadieux, Lisa M. Pratt, and Samantha B. Joye. 2016. "Biogeochemical and 16S rRNA gene sequence evidence supports a novel mode of anaerobic methanotrophy in permanently ice-covered Lake Fryxell, Antartica." *Limnology and Oceanography* 61: 119-130. doi:10.1002/lno.10320.

Schelker, J., D.A. Burns, M. Weiler, and H. Laudon. 2011. "Hydrological mobilization of mercury and dissolved organic carbon in a snow-dominated, forested watershed: Conceptualization and modeling." *Biogeosciences* 116: 1-17. doi:10.1029/2010JG001330.

Schink, Bernhard. 1997. "Energetics of Syntrophic Cooperation in Methanogenic Degredation." *Microbiology and Molecular Biology Reviews* 61: 262-280.

Schipper, Louis A., Joanne K. Hobbs, Susanna Rutledge, and Vickery L. Arcus. 2014. "Thermodynamic theory explains the temperature optima of soil microbial processes and high Q10 values at low temperatures." *Global Change Biology* 20: 3578-3586. doi:10.1111/gcb.12596.

Schlesinger, W. H. 1977. "Carbon balance in terrestrial detritus." *Annual Review of Ecology and Systematics* 8: 51-81.

Schlesinger, W., and J. Andrews. 2000. "Soil respiration and the global carbon cycle." *Biogeochemistry* 7-20.

Schlindlbacher, Andreas, Steve Wunderlich, Werner Borken, Barbara Kitzler, Sophie Zechmeister-Boltenstern, and Robert Jandl. 2012. "Soil respiration under climate change: prolonged summer drought offsets soil warming effects." *Global Change Biology* 18: 2270-2279. doi:10.1111/j.1365-2486.2012.02696.x.

Schmidt, S. K., E. K. Costello, D. R. Nemergut, Cory C. Cleveland, S. C. Reed, M. N. Weintraub, A. F. Meyer, and A. M. Martin. 2007. "Biogeochemical Consequences of Rapid Microbial Turnover and Seasonal." *Ecology* 88: 1379-1385. doi:https://doi.org/10.1890/06-0164.

Scott-Denton, Laura E., Todd N. Rosenstiel, and Russell K. Monson. 2005. "Differential controls by climate and substrate over the heterotrophic and rhizospheric components of soil respiration." *Global Change Biology* 205-216.

Screen, J.A. 2014. "Arctic amplification decreases temperature variance in northern mid- to high-latitudes." *Nature Climate Change* 4: 577-582. doi:10.1038/nclimate2268.

Segarra, K.E.A, F. Schubotz, V. Samarkin, M.Y. Yoshinaga, K.-U. Hinrichs, and S.B. Joye. 2015. "High rates of anaerobic methane oxidation in freshwater wetlands reduce potential atmospheric methane emissions." *Nature Communications* 6: 7477. doi:10.1038/ncomms8477.

Segarra, K.E.A., F. Schubotz, V. Samarkin, M.Y. Yoshinaga, K-U Hinrichs, and S.B. Joye. 2015. "High rates of anaerobic methane oxidation in freshwater wetlands reduce potential atmospheric methane emissions." *Nature Communications* 7477. doi:https://doi.org/10.1038/ncomms8477.

Semkin, R.G., D.S. Jeffries, R. Neureuther, G. Lahaie, and M. McAulay. 2012. *Summary of hydrological and meteorological measurements in the Turkey Lakes Watershed, Algoma, Ontario, 1980-2010.* Water Science and Technology Directorate Contribution No. 11-145., Burlington, ON: Environment Canada, National Water Research Institute, 1-85.

Shen, Li-dong, Bao-Ian Hu, Shuai Liu, Xiao-ping Chai, Zhan-fei He, Hong-xing Ren, Yan Liu, et al. 2016. "Anaerobic methane oxidation coupled to nitrite reduction can be a potential methane sink in coastal environments." *Applied genetics and molecular biotechnology* 100: 7171-7180. doi:10.1007/s00253-016-7627-0.

Shi, Yao, Zhongqiang Wang, Chunguang He, Xinyu Zhang, Lianxi Sheng, and Xiaodong Ren. 2017. "Using 13C isotopes to explore denitrification-dependant anaerobic methane oxidation in a paddy peatland." *Scientific Reports* 7: 40848. doi:10.1038/srep40848.

Silverstein, T.P. 2012. "Marcus Theory: Thermodynamics CAN control the kinetics of electron transfer reactions." *Journal of Chemical Education* 89: 1159-1167. doi:10.1021/ed1007712.

Sivan, O., P. Schrag, and W. Murray. 2007. "Rates of methanogenesis and methanotrophy in deep-sea sediments." *Geobiology* 5: 141-151. doi:10.111/j.1472-4669-2007.00098.x.

Sivan, Orit, Gilad Antler, Alexandra V. Turchyn, Jeffrey L. Marlow, and Victoria J. Orphan. 2014. "Iron oxides stimular sulfate-driven anaerobic methane oxidation in seeps." *Proceedings of the National Academy of Sciences* 111: E4139-E4147. doi:10.1073/pnas.1412269111.

Smemo, K.A., and J.B. Yavitt. 2011. "Anaerobic oxidation of methane: an underappreciated aspect of." *Biogeosciences* 8: 779-793. doi:doi:10.5194/bg-8-779-2011.

Smemo, Kurt A., and Joseph B. Yavitt. 2007. "Evidence for anaerobic CH4 oxidation in freshwater peatlands." *Geomicrobiology Journal* 24: 583-597. doi:doi.org/10.1080/01490450701672083.

Sorenson, P. O., H. R. Bill, M. Beller, N. J. Bouskill, S. S. Hubbard, U. Karaoz, A. Polussa, H. Steltzer, et al. 2020. "The snowmelt niche differentiates three microbial life strategies that influence soil nitrogen availability during and after winter." *Frontiers in Microbiology* 11: 1-18. doi:https://doi.org/10.3389/fmicb.2020.00871.

Strous, Marc, and Mike S.M. Jetten. 2004. "Anaerobic Oxidation of Methane and Ammonium." *Annual Review Microbiology* 58: 99-117. doi:10.1146/annurev.micro.58.030603.123605.

Stumm, Werner, and James J. Morgan. 1996. *Aquatic Chemistry: Chemical Equilbria and Rates in Natural Waters.* Vol. 3rd Edition. New York, United States of America: John Wiley & Sons, Inc. doi:ISBN 978-0-47-51185-4.

Sturm, Matthew, Jon Holmgren, Max Konig, and Kim Morris. 1997. "The thermal conductivity of seasonal snow." *Journal of Glaciology* 43: 26-41. doi:10.3189/S0022143000002781.

Tarnocai, Charles. 2006. "The effect of climate change on carbon in Canadian peatlands." *Global and Planetary Change* 222-232.

Tarnocai, Charles. 2009. "The Impact of Climate Change on Canadian Peatlands." *Canadian Water Resources* 453-466.

Thamdrup, Bo. 2012. "New Pathways and Processes in the Global Nitrogen Cycle." *Annual Reviews* 43: 407-428. doi:10.1146/annurev-ecolsys-102710-145048.

Thornton, Brett F., Martin Wik, and Patrick M. Crill. 2015. "Climate-forced changes in available energy and methane bubbling from subarctic lakes." *Geophysical Research Letters* 42: 1936-1942. doi:10.1002/2015GL063189.

Thullner, M., and P. Regnier. 2019. "Microbial Controls on the Biogeochemical Dynamics in the Subsurface." *Reviews in Mineralogy and Geochemistry* 85: 265-302. doi:10.2138/rmg.2019.85.9.

Thullner, M., P. Regnier, and P. Van Cappellen. 2007. "Modeling Microbially Induced Carbon Degradation in Redox-Stratified Subsurface Environments: Concepts and Open Questions." *Geomicrobiology* 24: 139-155. doi:10.1080/01490450701459275.

Tian, H., Xu, R., Canadell, J.G. et al. 2020. "A comprehensive quantification of global nitrous oxide sources and sinks." *Nature* 586: 248-256. doi:10.1038/s41586-020-2780-0.

Tian, Huihui, Wei Changfu, Houzhen Wei, and Jiazuo Zhou. 2014. "Freezing and thawing characteristics of frozen soils: Bound water content and hysteresis phenomenon." *Cold Regions Science and Technology* 74-81.

Trumbore, Susan. 2006. "Carbon respired by terrestrial ecosystems -- recent progress and challenges." *Global Change Biology* 141-153.

Tuck, Gill, Margaret J. Glendining, Pete Smith, Jo I. House, and Martin Wattenbach. 2006. "The potential distribution of bioenergy crops in Europe under present and future climate." *Biomass & Bioenergy* 183-197.

Valentine, David L. 2002. "Biogeochemistry and microbial ecology of methane oxidation in anoxic environments: a review." *Antonie van Leeuwenhoek* 81: 271-282. doi:10.1023/A:1020587206351.

Valenzuela, Edgardo I., Alejandra Prieto-Davo, Nguyen E. Lopez-Lozano, Alberto Hernandez-Eligio, Leticia Vega-Alvarado, Katy Juarez, Ana Sarahi Garcia-Gonzalez, Mercedes G. Lopez, and Francisco J. Cervantes. 2017. "Anaerobic Methane Oxidation Driven by Reduction of Natural Organic Matter in a Tropical Wetland." *Applied and Environmental Microbiology* 83: 1-15. doi:10.1128/AEM.00645-17.

Valenzuela, Edgardo I., Karen A. Avendano, Nagamani Balagurusamy, Sona Arriaga, Cesar Nieto-Delgado, Frederic Thalasso, and Francisco J. Cervantes. 2019. "Electron shuttling by humic substances fuels anaerobic methane oxidation and carbon burial in wetland sediments." *Science of the Total Environment* 650: 2674-2684. doi:10.1016/j.scitotenv.2018.09.388.

Valenzuela, Edgardo, Claudia Padilla-Loma, Nicolas Gomez-Hernandez, Nguyn E. Lopez-Lozano, Sergio Casas-Flores, and Francisco J. Cervantes. 2020. "Humic substances mediate anaerobic methane oxidation link to nitrous oxide in wetland sediments." *Frontiers in Microbiology* 11: 587. doi:10.3389/fmicb.2020.00587.

van Bochove, E., G. Theriault, and P. Rochette. 2001. "Thick ice layers in snow and frozen soil affecting gas emissions from agriultural soils during the winter." *Journal of Geophysical Research* 106: 23061-23071.

Van Den Heuval, R.N., S.E. Bakker, M.S.M. Jetten, and M.M. Hefting. 2011. "Decreased N2O reduction by low soil pH causes high N2O emissions in a riparian ecosystem." *Geobiology* 9: 294-300. doi:10.1111/j.1472-4669.2011.00276.x.

Van Esbroeck, Chris J., Merrin L. Macrae, Richard I. Brunke, and Kevin McKague. 2016. "Annual and seasonal phosphorus export in surface runoff and tile drainage from agricultural fields with cold temperate climates." *Journal of Great Lakes Research* 42: 1271-1280. doi:10.1016/j.jglr.2015.12.014.

Voigt, C., M.E. Marushchak, B.W Abbott, and et al. 2020. "Nitrous oxide emissions from permafrost-affected soils." *Nature Reviews Earth & Environment* 1: 420-434. doi:10.1038/s43017-020-0063-9.

Wagner-Riddle, C, Q. C. Hu, E. van Bochove, and S. Jayasundara. 2008. "Linking Nitrous Oxide Flux During Spring Thaw to Nitrate Denitrification in the Soil Profile." *Soil Physics* 72: 908-916. doi:10.2136/sssaj2007.0353.

Wagner-Riddle, Claudia, Katelyn A. Congreves, Diego Abalos, Aaron Berg, Shannon E. Brown, Jaison T. Ambadan, Xiaopeng Gao, and Mario Tenuta. 2017. "Globally important nitrous oxide emissions from croplands induced by freezing and thawing cycles." *Nature Geoscience* 279-292.

Wang, C., P.A. Schuppli, and G.J. Ross. 1987. "A comparison of hydroxylamine and ammonium oxalate solutions as extractants of Al, Fe, and Si from Spodosols and Spodosol-like soils in Canada." *Geoderma* 40: 345-355.

Warren, S. G. 1982. "Optical properties of snow." *Phil. Trans. R. Soc.* 20: 67-89. doi:10.1029/RG020i001p00067.

Weber, Thomas, Nicola A. Wiseman, and Anette Kock. 2019. "Global ocean methane emissions dominated by shallow coastal waters." *Nature Communications* 10: 4584. doi:10.1038/s41467-019-12541-7.

Webster, K.L., I.F. Creed, R.A. Bourbonniere, and F.D. Beall. 2008. "Controls on the heterogeneity of soil respiration in a tolerant hardwood forest." *Journal of Geophysical Research* 113: G03018. doi:10.1029/2008JG000706.

Wertz, S, C Goyer, D.L. Burton, E Tatti, M.H. Chantigny, and M Fillion. 2013. "Effects of temperature near the freezing point on N2O emissions, denitrification and on the abundance of nitrifying soil communities." *FEMS. Microbiol. Ecol.* 242-254.

Winter, Thomas C. 2000. "The vulnerability of wetlands to climate change: a hydrologic landscape perspective." *Journal of American Water Resources Association* 36: 305-311.

Wuebbles, Donald J., Katharine Hayhoe, and Julia Parzen. 2010. "Introduction: Assessing the effects of climate change on Chicago and the Great Lakes." *Journal of Great Lakes Research* 1-6.

Yanai, Yosuke, Tomoyoshi Hirota, Yukiyoshi Iwata, Manabu Nemoto, Osamu Nagata, and Nobuhisa Koga. 2011. "Accumulation of nitrous oxide and depletion of oxygen in seasonally frozen soils in northern Japan -- Snow cover manipulation experiments." *Soil Biology and Biochemistry* 1779-1786.

Ypma, J., S.G. Johnson, H.W. Borchers, D. Eddelbuettel, B. Ripley, K. Hornik, J. Chiquet, and A. Adler. 2020. "'nloptr'." *Package 'nloptr'.* CRAN, July 2.

Yu, Hou, Hiroyuki Kashima, John M. Regan, Abid Hussian, Elsayed Elbeshbishy, and Hyung-Sool Lee Lee. 2017. "Kinetic study of anaerobic oxidation of methane coupled to denitrification." 104: 47-55. doi:10.1016/j.enzmictec.2017.05.005.

Yu, Zicheng. 2011. "Holocene carbon flux histories of the world's peatlands: Global carbon-cycle implications." *The Holocene* 761-771.

Yu, Zicheng, Julie Loisel, Daniel P. Brosseau, and David W. Beilman. 2010. "Global peatland dynamics since the Last Glacial Maximum." *Geophysical Research Letters* 1-5.

Zhang, Haiyan, Huihui Fu, Jixuan Wang, Linlin Sun, Yaoming Jiang, Lili Zhang, and Haichun Gao. 2013. "Impacts of Nitrate and Nitrite on Physiology of Shewanella oneidensis." *PLoS One* 8: e62629.

Zhu, Guibing, Mike S.M. Jetten, Peter Kushk, Katharina F. Ettwig, and Chengqing Yin. 2010. "Potential roles of anaerobic ammonium and methane oxidation in the nitrogen cycle of wetland ecosystems." *Applied Microbial Biotechnology* 86: 1043-1055. doi:10.1007/s00253-010-2451-4.

Zou, C., B. Guo, X. Zhuang, and et al. 2020. "Achieving fast start-up of anammox process by promoting the growth of anammox bacteria with FeS addition." *npj Clean Water* 3: 1-10. doi:10.1038/s41545-020-00088-w.

6 Appendix A: Chapter 2 Supplementary Materials

Supplementary Figures 1 and 2 (Figures S1 and S2, respectively) add the abiotic control group to initial Figures 1 and 2 (Section 2.4.1) for comparison with the biotic treatment groups. Additionally, Supplementary Figure 2 includes calculated net production rates from the measured concentrations of H_2. Supplementary Figure 3 (Figure S3) contains measured concentrations and calculated speciation of DIC throughout the incubation. Concentrations of carbonic acid (H_2CO_3) and bicarbonate (HCO_3^-) were calculated in PHREEQC using the methods outlined in Section *2.3*. Supplementary Table 1 provides the standard and calculated Gibbs energy of reaction for the experimental conditions determined using the methods outlined in Section *2.3.3*.

6.1 Supplementary Results: Abiotic Control

The abiotic control group was composed of soil dried, sieved, and rewetted using the methods outlined in Sections *2.3.1* and *2.3.2*. Prior to re-wetting (24 hours), the soil was removed from the anaerobic chamber in a sealed plastic bag and autoclaved for 1 hour (Tuttnauer Electronic Tabletop Autoclave) alongside its input solution, which had identical chemistry content as the Natural treatment group, containing relatively low quantities of NO_3^- and SO_4^{2-} as well as no additional labile C.

Porewater pH, concentrations of SO_4^{2-} , NH_4^+ and headspace CH_4 and N_2O concentrations are relatively constant throughout the abiotic control group's incubation period. Some changes in DOC, NO_3^- and NO_2^- species were observed during Phases II and III, where NO_3^- and NO_2^- were consumed. Changes to oxidized-N, DOC, and DIC concentrations (Figures S1, S2, and S3, respectively) under the anaerobic incubation conditions suggest that soil microbes were present in

the latter stage of incubation despite the autoclaving of the soil. These microbes were likely able to re-emerge from heat-tolerant spores, which survived the single autoclave treatment.

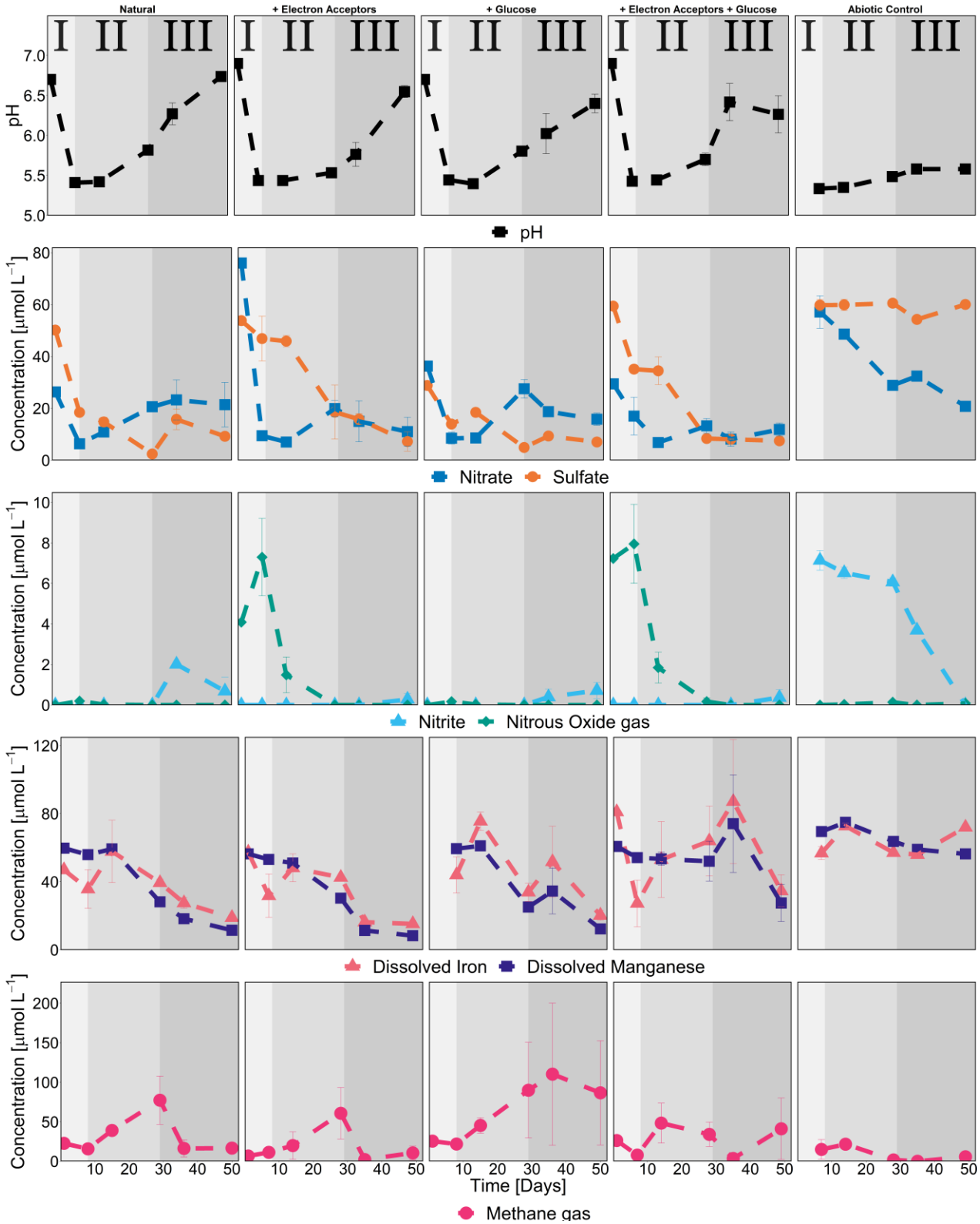

Figure S1: Concentrations of biogeochemical species with the addition of the Abiotic Control treatment group.

6.2 Supplementary Results: Additional e^- donors

Non-zero H_2 concentrations were detected in the jars' headspaces during the experiment by gas chromatography, which indicates that an additional inorganic e^- donor in addition to those considered in the main text was present for the microbial community to use. The anaerobic chamber in which the soil jars were assembled contains 2% H_2 gas, measured at ~6650 ppm (~270 µM) by gas chromatography (using the TCD Section *2.3.2*). Concentrations of H_2 are below this value in all soil treatments, excluding the abiotic control group, demonstrating the biotic consumption and production of H_2. Bioenergetic calculations, which incorporate these H_2 concentrations, indicate that H_2-methanogenesis and reverse acetogenesis are thermodynamically favourable reactions, which supports both the production and consumption of headspace H_2 were possible during the incubation (Table S1 Appendix A).

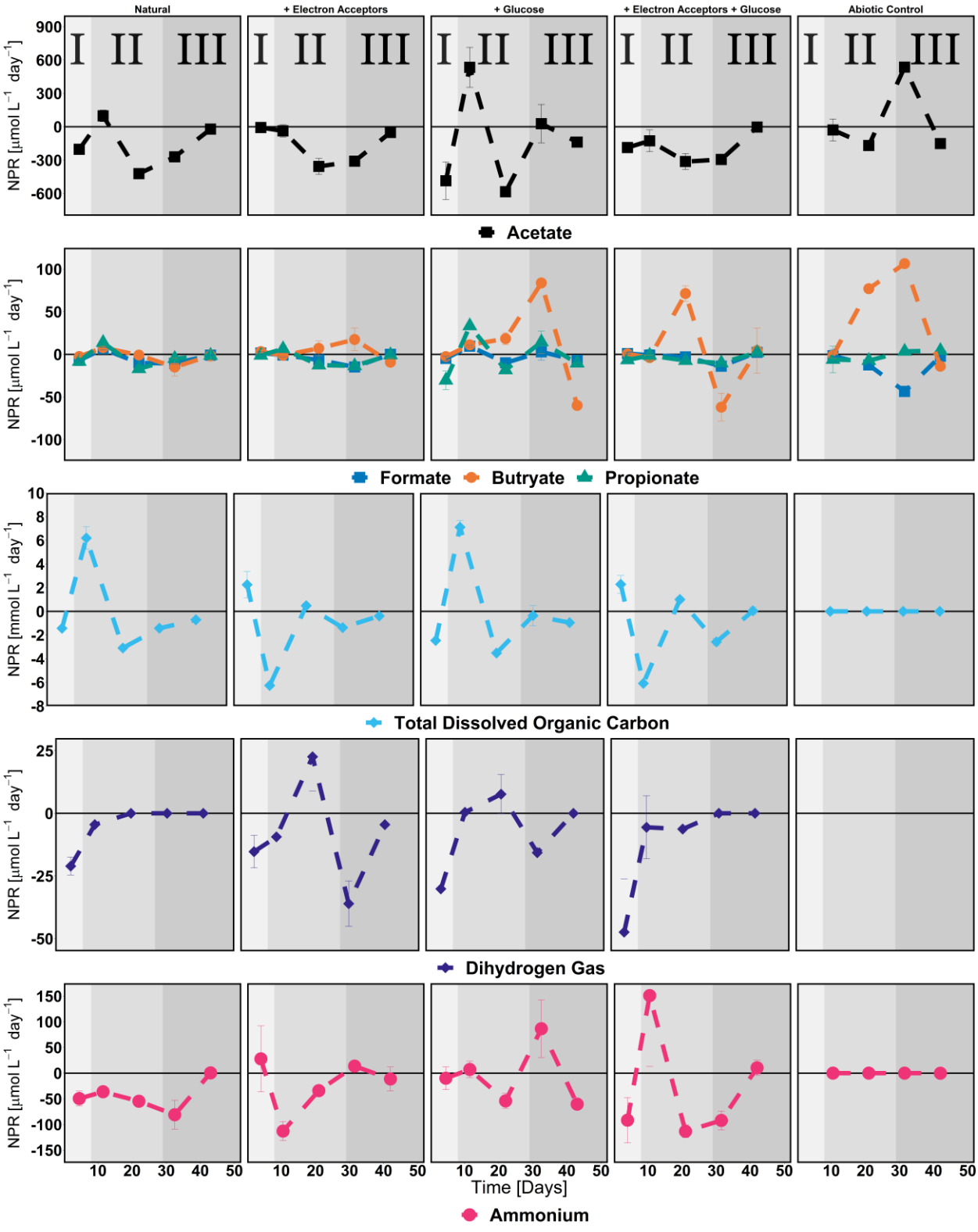

Figure S2: Net production rates (NPR) of all treatments for organic and inorganic (NH_4^+ and H_2) e^- donors as well as total dissolved organic carbon.

6.3 Supplementary Results: Dissolved Inorganic Carbon

TIC concentrations initially increased exponentially in all treatment groups, except for the abiotic control (Supplementary Figure 3). However, after day 28, DIC concentrations appear to decline or plateau despite ongoing soil respiration and microbial activity. The observed change in TIC coincided with a significant increase in pH, which approached the pK_{a1} value of H_2CO_3 (pK_{a1} = 6.35 @ 25˚C), causing a decrease in headspace CO_2 and an increase in the dissolved fraction. Anticipated concentrations of DIC were largely below the threshold MDL at the required dilution for the sample volume. We believe that the pH change ultimately influenced the measured TIC and created a more dramatic plateau or decrease than what we expected. The observed decreases in inorganic carbon production signify the potential uptake of DIC for biomass growth through the hypothesized chemoautotrophic reactions, supported by the 16S RNA data.

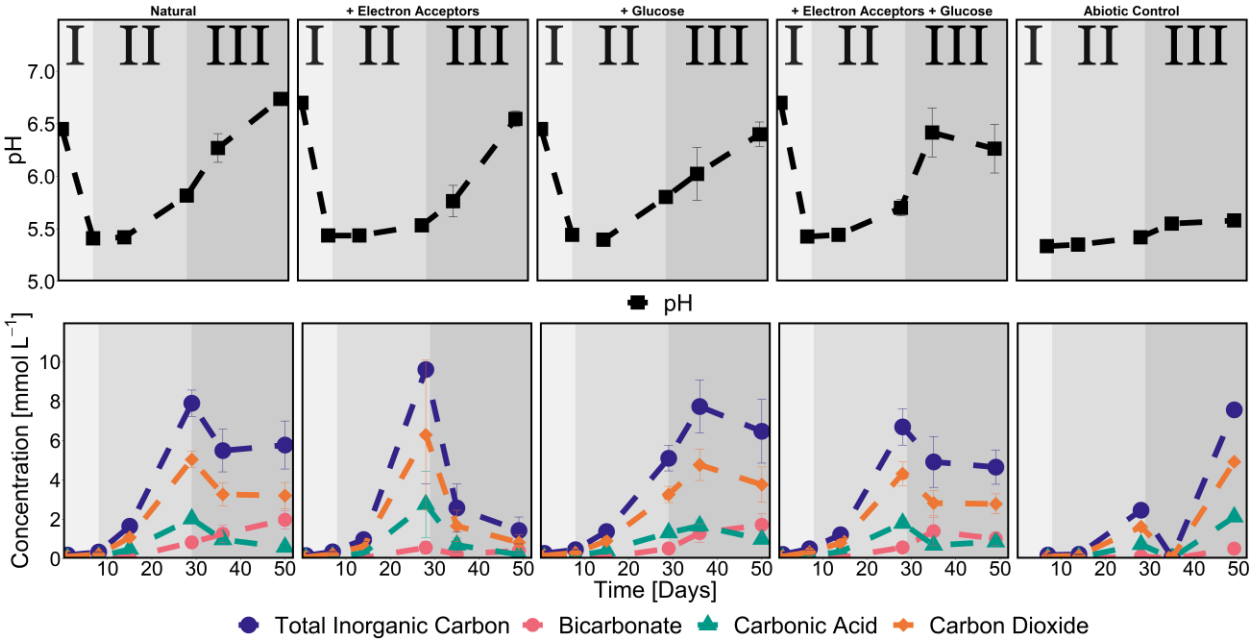

Figure S3: Measured concentrations of non-methanogenic inorganic carbon for all treatment groups.

6.4 Supplementary Results: Major Cations and Cation Exchange Capacity

A cation exchange capacity (CEC) of 0.7331 meq g-1 dry soil was determined using the methods outlined in Section *2.2.2* at a pH of ~4.8. However, porewater pH, particularly in organic soil, can be influence the CEC, potentially increasing CEC by a magnitude as pH becomes neutral (Hendershot *et al.*, 2006). These results are reflected in the observed decrease in major cation concentrations during late-Phase II and Phase III when pH began to increase. Divalent cations calcium and magnesium observe the largest change. This effect is not observed in the abiotic control group, whose pH remains stable throughout the incubation.

Changes in pH and the associated increase in CEC may mask the reduction of Fe- and Mn-oxides throughout the incubation period. However, decreases in total sulfur (118.2 µM ± 28.6) provide indirect evidence of Fe reduction as FeS minerals are supersaturated in solution and anticipated to precipitate. The removal of S from the soil porewater is not observed in the abiotic control group and is likely linked to microbial Fe-oxide reduction (at least 100 µM). Calculations of the non-crystalline Fe pool support this (Section *2.3.2*), providing roughly 503.8 µmol ± 66.43 Fe^{3+} per soil jar.

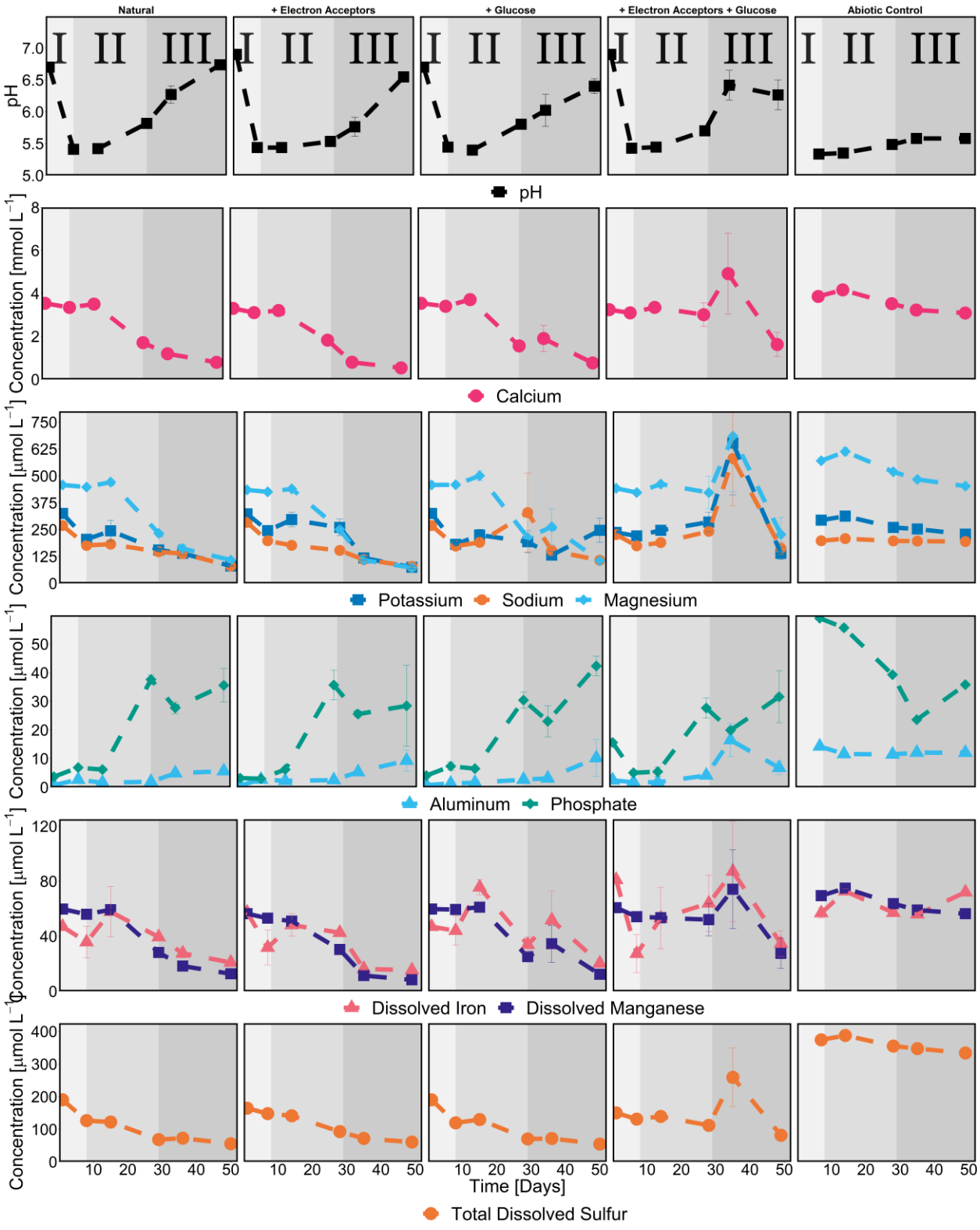

Figure S4: Temporal concentration profiles of major cations in solution changing with pH, phosphate, and dissolved total sulfur.

6.5 Supplementary Results: Additional Thermodynamic Calculations

Table S1: Additional balanced catabolic reactions for anoxic conditions with their associated standard and calculated Gibbs energy values (ΔG°_{r298} and ΔG_r, respectively).

e^- **Donor**	**Balanced Catabolic Reaction**	ΔG°_{r298} [kJ / mol e^-]	$\overline{\Delta G_r}$ [kJ / mol e^-]
$C_2H_3O_2^-$	$0.5C_2H_3O_2^- + 1.3H^+ + 0.8NO_3^- \rightarrow H_2CO_3 + 0.4N_2 + 0.4H_2O$	-111.06	-96 to -101
	$0.5C_2H_3O_2^- + 2MnO_{2(s)} + 4.5H^+ \rightarrow H_2CO_3 + 2Mn^{2+} + 2H_2O$	-109.64	-87.13 to –92.40
	$0.5C_2H_3O_2^- + 4FeOOH_{(s)} + 8.5H^+ \rightarrow H_2CO_3 + 4Fe^{2+} + 6H_2O$	-57.63	-10.75 to -26.41
	$0.5C_2H_3O_2^- + 0.5SO_4^{2-} + 1.5H^+ \rightarrow H_2CO_3 + 0.5H_2S$	-20.04	-8.27 to -11.56
$H_{2(aq)}$	$H_{2(aq)} + 0.25H_2CO_3 \rightarrow 0.25CH_{4(aq)} + 0.75H_2O$	-17.76	-2.10 to -4.63

6.6 Supplementary Results: Stoichiometric Calculations

Table S2: Maximum estimates of oxidation capacity of terminal electron acceptor (TEA) using stoichiometric ratios.

e^- Donor	Reaction Number	Balanced Catabolic Reaction	TEA [µM]	Max Product / e^- donor consumption
$\boldsymbol{Fe^{2+}}$	1	$0.2NO_3^- + Fe^{2+} + 2.4H_2O \rightarrow 0.1N_2 + Fe(OH)_3 + 1.7H^+$	600	3000 µM $Fe(OH)_3$
$\boldsymbol{S^{2-}}$	2	$NO_3^- + 0.25H_2S + 3.5H^+ \rightarrow 0.5N_2 + 0.25SO_4^{2-} + 2H_2O$	600	150 µM SO_4^{2-}
$\boldsymbol{NH_4^+}$	3	$NH_4^+ + 4MnO_{2(s)} + 6H^+ \rightarrow NO_3^- + 4Mn^{2+} + 5H_2O$	200	50 µM NO_3^-
$\boldsymbol{CH_{4(aq)}}$	4	$CH_{4(aq)} + 1.6NO_3^- + 1.6H^+ \rightarrow H_2CO_3 + 0.8N_{2(g)} + 1.8H_2O$	50	31.25 µM H_2CO_3
	5	$CH_{4(aq)} + 4MnO_{2(s)} + 8H^+ \rightarrow H_2CO_3 + 4Mn^{2+} + 5H_2O$	200	50 µM H_2CO_3
	6	$CH_{4(aq)} + 8Fe(OH)_{3(s)} + 16H^+ \rightarrow H_2CO_3 + 8Fe^{2+} + 21H_2O$	500	62.5 µM H_2CO_3
	7	$CH_{4(aq)} + SO_4^{2-} + 2H^+ \rightarrow H_2CO_3 + H_2S + H_2O$	60	60 µM H_2CO_3
$\boldsymbol{H_{2(aq)}}$	8	$H_{2(aq)} + 0.25H_2CO_3 \rightarrow 0.25CH_{4(aq)} + 0.75H_2O$	1000	250 µM CH_4
$\boldsymbol{C_2H_3O_2^-}$	9*	$0.5C_2H_3O_2^- + 1.3H^+ + 0.8NO_3^- \rightarrow H_2CO_3 + 0.4N_2 + 0.4H_2O$	600	750 µM H_2CO_3
	10*	$0.5C_2H_3O_2^- + 2MnO_{2(s)} + 4.5H^+ \rightarrow H_2CO_3 + 2Mn^{2+} + 2H_2O$	200	100 µM H_2CO_3
	11*	$0.5C_2H_3O_2^- + 4FeOOH_{(s)} + 8.5H^+ \rightarrow H_2CO_3 + 4Fe^{2+} + 6H_2O$	500	125 µM H_2CO_3

Table S2 continued.

e^- Donor	Reaction Number	Balanced Catabolic Reaction	TEA [µM]	Max Product / e^- donor consumption
$\boldsymbol{C_2H_3O_2^-}$	12*	$0.5C_2H_3O_2^- + 0.5SO_4^{2-} + 1.5H^+ \rightarrow H_2CO_3 + 0.5H_2S$	60	30 µM H_2CO_3
	13**	$C_2H_3O_2^- + H^+ + H_2O \rightarrow H_2CO_3 + CH_{4(aq)}$	7000	7000 µM H_2CO_3/CH_4

*Reaction 9 to 12 $C_2H_3O_2^-$ consumption is equivalent to half of the concentration of the estimated H_2CO_3 produced

**Reaction 13 TEA concentration is equal to observed change in net molar $C_2H_3O_2^-$ concentration throughout the experiment